Multivalently binding antagonists for the neurokinin-1 receptor

DISSERTATION ZUR ERLANGUNG DES DOKTORGRADES DER NATURWISSENSCHAFTEN (DR. RER. NAT.) DER FAKULTÄT CHEMIE UND PHARMAZIE

DER UNIVERSITÄT REGENSBURG

vorgelegt von

Anika Veser

aus Ravensburg

im Jahr 2018

This work was carried out from November 2012 until November 2018 at the Department of Pharmaceutical Technology of the University of Regensburg.

The thesis was prepared under supervision of Prof. Dr. Achim Göpferich.

Submission of the PhD application:		26.11.2018
Date of examination		01.02.2019
Examination board:	Chairman:	Prof. Dr. Jens Schlossmann
	1. Expert:	Prof. Dr. Achim Göpferich
	2. Expert:	Prof. Dr. Joachim Wegener
	3. Expert:	Prof. Dr. Rainer Müller

To my family

Ohne Begeisterung schlafen die besten Kräfte unseres Gemütes. Es ist ein Zunder in uns, der Funken will.

Johann Gottfried von Herder

Table of Contents

Multivalently binding antagonists for the neurokinin-1 receptor

Chapter 1

Introduction

The interrelation of inflammation and pain

The body´s homeostasis is regulated by three well-connected systems: the nervous system, the endocrine system, and the immune system. Direct cell-to-cell contact, soluble signaling molecules like neuropeptides, hormones, and cytokines together provide effective and rapid channels for mutual communication [1]. For this reason, inflammation and pain are closely related and the severity of both correlate to each other (Figure 1).
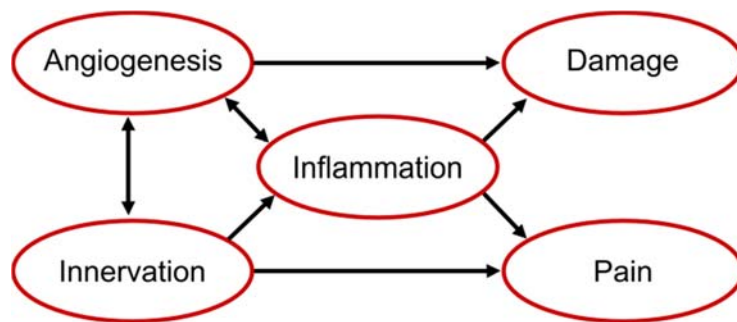

Figure 1: Relationship between innervation, inflammation, vascularization, damage, and pain. This neuroimmune interplay is bidirectional.

Based on this relationship, if inflammation regresses, pain symptoms should also be relieved. In contrast, in autoimmune diseases, the state of inflammation and pain is ongoing. This phenomenon which is attributed to neuroinflammation, also called neurogenic inflammation. This kind of inflammation is characterized by the release of inflammatory substances from peripheral endings of primary afferent nerve fibers, which seem to be responsible for preserving the status of inflammation and pain in an unending cycle. These inflammatory substances are categorized as neuropeptides [2]. These peptides are able to interfere between the central nervous system (CNS) and the periphery because they are released from nerves in the CNS and from peripheral nerves, endothelial tissues, and various immune cells, including T and B lymphocytes, monocytes/macrophages, neutrophils, and mast cells [3, 4]. The combination of up-regulation of expression of these substances and their receptors in the pathophysiological state of an autoimmune disease, together with further factors like the release of cytokines, appears to cause an inflammatory state. Inflammation may include

clinical symptoms such as heat, redness, swelling, pain, and decreased function, symptoms that significantly reduce the quality of life of affected patients [5]. Neuropeptides, like substance P, bradykinin, or calcitonin gene-related peptide (CGRP) induce vasodilatation and plasma extravasation of proteins to the site of injury, which causes swelling. Substance P is a sensory neuropeptide. Ulf von Euler and John Gaddum identified substance P in 1931; they concentrated it in a powdered form and therefore named it substance P [6].

In the case of rheumatoid arthritis (RA), the volume of synovial fluid in the joint cavity is increased compared to the unaffected joint, due to the presence of neuropeptides. Osteoarthritis (OA) may develop in later stages, which is characterized by cartilage breakdown, the outgrowth of bone, bone sclerosis, and synovitis [5]. In contrast to RA, OA is not defined as an inflammatory disorder because the leukocyte number in the synovial fluid is below the typical threshold of 2000 cells/mm^3 [7]. However, in both disease states, patients feel pain because of the activation of primary afferent nociceptors, which innervate the joint´s synovial membrane and are connected to the spinal cord for transmitting the received stimuli to higher brain centers where the perception of pain occurs. In contrast to the synovium, healthy cartilage does not contain blood vessels and is therefore a hostile area for a deep innervation by nerve fibers. The perivascular localization of nerves implies that vascularization is the driver behind innervation [8]. With increasing cartilage destruction, vascularization and innervation increase and is therefore an indicator for severity and may be a potential source of pain, particularly in patients with OA.

Arthritic pain affects millions of people worldwide, but understanding of the origin of the painful sensation is still limited. Current understanding is that during inflammation, the joint nerves become sensitized to mechanical stimuli through the actions of neuropeptides, eicosanoids, activated receptors, and ion channel ligands [9].

That neuropeptide antagonists have anti-inflammatory characteristics is well proven, but whether they can act as analgesics is controversial and has only be confirmed in experiments with animals, not with humans. It is suggested that in particular pain states, antagonists against the neurokinin-1 receptor (NK$_1$R) may be effective analgesics or at least may be used as adjuvants to existing analgesics [10]. Many NK$_1$R antagonists have failed trials of a variety of clinical pain states, although they have shown in preclinical studies that they can

attenuate nociceptive responses. However, they have not reached the efficacy of typical nonsteroidal anti-inflammatory drugs, or NSAIDs, which are directed against the biosynthesis of prostaglandins by cyclooxygenase, or COX inhibition [10, 11]. In rats, it has been shown that the presence of NK_1R in the knee joint cavity contributes to the induction of pain response, but seems not to be involved in the maintenance of arthritic pain [12]. It is also not clear which neuropeptides are involved in immune response and pain enhancement. Some believe that it is not substance P that increases inflammation and hyperalgesia, but hemokinin-1, which is also able to bind to several neurokinin receptors with very high affinity to NK_1Rs [13, 14]. Because of its low receptor selectivity compared to substance P, this aspect could be a further reason that selective NK_1R blockers do not reach the desired anti-inflammatory and analgesic effects. In contrast, substance P and glutamate together have been found to contribute to arthritic pain and joint swelling. This concept was proven in an arthritic rat model by co-administration of respective substance P and glutamate antagonists to common dexamethasone therapy [15]. It seems that NK_1R is one component, but not the only key component at the interface of immune and pain responses.

Peripheral targeting of substance p/ NK₁R interactions

The therapeutic potential of targeting substance P and NK_1R interactions in peripheral inflammatory and CNS-associated disorders and their impact on the pharmacology of pain are a focus of research [16, 17]. One cornerstone is the observation that NK_1Rs are expressed on common immune cells and cells of the brain with immune cell-like properties, known as glia cells and astrocytes. The major ligand of NK_1R, substance P, is mainly stored together with CGRP and other transmitters in dorsal root ganglion cells of the spinal cord. Upon depolarization, sensory nerve fiber terminals can quickly and ubiquitously release both neuropeptides throughout the body´s peripheral tissues. This release is triggered by various proinflammatory factors [18]. Substance P and CGRP are responsible for either peripheral neurogenic inflammatory responses or equivalent responses in the CNS by cell activation via their respective surface receptors. The NK_1R target cells can be either vascular or non-vascular endothelial cells, various immune cells, or other cell types. Together with cytokines, overexcited substance P/NK_1R interactions can initiate and promote some autoimmune diseases, e.g., RA and inflammatory bowel disease, as well as pathogen derived or sterile neuroinflammatory disorders, e.g., meningitis or multiple sclerosis [17]. The impact of

NK_1R activation is also discussed in studies for a variety of psychiatric disorders, including anxiety and depression [19]. Since substance P crosses the blood-brain barrier (BBB) and is responsible for BBB permeabilization, it seems to be a key factor in the transmission of peripheral inflammatory response to the CNS and therefore a main trigger of autoimmune diseases by activating monocyte-like parenchymal microglia [20]. Like systemic macrophages, microglia cells also express innate immune receptors and have the ability for phagocytosis and therefore represent the brain´s own immune system. However, not only substance P but also cytokines, like interleukins and growth factors, modulate the actions in both defense systems, because they are also produced by microglia [21]. Besides increased cytokine concentrations in the blood and liquor, which is evident during inflammation, it could be found that sensory nerves also have higher neuropeptide content [22]. In parallel, the presence of cytokines regulates NK_1Rs. Figure 2 shows the cross-talk between the CNS and peripheral systems by blood-derived immune cells and peripheral nerve fibers.
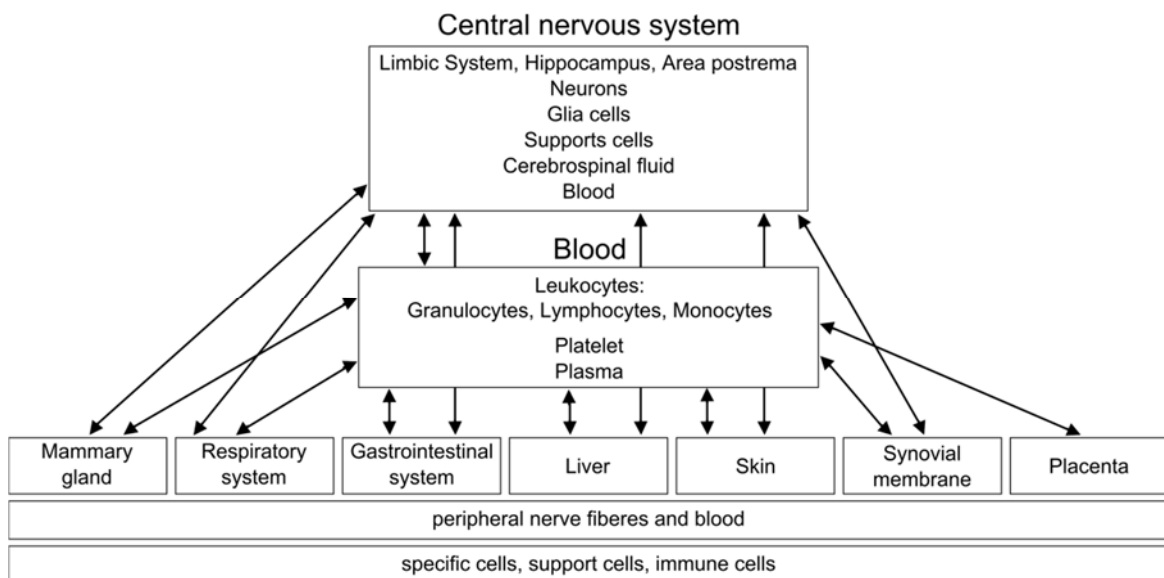

Figure 2: Cross-talk between the CNS and various peripheral systems in which the NK_1R is upregulated under pathological conditions. Substance P binds to the NK_1R by autocrine, paracrine, and/or endocrine mechanisms, and is released from nerve terminals. The neuropeptide reaches the whole body through the bloodstream. This figure is adapted from [23].

Implication of NK₁R expression in cancer and rheumatoid arthritis

The recruitment of immune cells into the joint space is one similarity of RA to the pathology of cancer caused by increased angiogenesis and higher permeability of blood vessels. Therefore, common strategies for RA treatment exactly pick up regulatory mechanisms in the context of angiogenesis or inflammation for selective interruption. For cancer, some well-known examples are the antibody treatments with bevacizumab or trastuzumab, which both have antiangiogenic, anti-inflammatory, and growth inhibitory effects. In RA, the treatment of choice is also anti-inflammatory, e.g., with etanercept or infliximab to reduce the action of cytokines like TNF-α [24]. Its neutralization leads to the subsequent inhibition of other proinflammatory cytokines. Besides increased cytokine levels, a second similarity between cancer and RA is increased levels of substance P in the blood and in the CNS, and for RA in particular, in the synovial fluid within the joint space. In cancer, substance P is considered a mitogen because it has been associated with tumor growth and metastasis [25]. High cytokine and substance P concentrations are synergistically linked to each other since the release of substance P from local peripheral nerve fiber terminals is a result of cytokine stimulation. Substance P then significantly contributes on the one hand to the production of further cytokines, such as IL-1β, TNF-α and the neutrophil chemoattractant IL-6 by direct NK₁R interaction on present immune cells. On the other hand, NK₁R interaction on vascular endothelial cells involves substance P in the recruitment of further immune cells, which causes higher permeability and vasodilatation [26]. Other proinflammatory effects are the release of lysosomal enzymes, nitric oxide, and prostaglandin E₂ [5, 12]. This increasing inflammation leads in later stages to tissue destruction and hyperalgesia. There is also strong evidence that angiogenesis and inflammation are two major driving forces for the progress of early and later OA stages. Both are closely integrated perpetuating processes, such that inflammation can trigger angiogenesis, and angiogenesis can speed up inflammation, rather than cause it, by facilitating the immigration of more inflammatory cells that generate angiogenic factors [27, 28]. In arthritis, vascular proliferation contributes to the pathogenesis of synovitis, pannus growth, bone and cartilage destruction, and the formation of osteophytes [29]. Beside substance P, many more substances are localized or released within osteoarthritic human synovium, synovial fluid, and articular chondrocytes [30]. One of those

is angiotensin II, which is released from the synovium into the synovial fluid and seems to join with substance P. Several other factors, like various cytokines such as IL-1, IL-4, IL-8, IL-18, and TNF-α are responsible for angiogenesis and may exacerbate inflammation. However, IL-10 and TGF-β, as well as cytokine inhibitors such as IL-1ra and soluble TNF-R, are also produced as anti-inflammatory counterparts [26]. All these factors were found in increased levels in the synovial fluid from patients with arthritis [29].

Function of different NK$_1$R isoforms

Accumulating evidence has suggested that NK$_1$R is closely related to immune responses and may be recognized as a key factor in neuroinflammation. Therefore, NK$_1$R may represent a potential therapeutic target in the neuro-immune axis. For a better understanding of NK$_1$R-ligand interactions it is important to know that other neurokinin receptor types exist (NK2R and NK3R) [31], two different isoforms with different intracellular pathways. The broad spectrum of different receptors and their distinct selectivity for certain ligands makes the topic of specific receptor ligand interaction even more complex. The exact functional pathways and the reason for different neurokinin receptor types, different expression profiles, and different ligand affinities, in addition to different NK$_1$R isoforms with distinct molecular masses is still not clarified. Differences in lengths arise from a lack of 96 amino acids at the intracellular C-terminal end of the receptor, which vary from 407 amino acids for the full-length receptor isoform to 311 amino acids for the truncated receptor isoform [3]. These isoforms originate from two differently spliced mRNAs. It is suggested that the different receptor versions may have a regulatory role in receptor desensitization, since the short form has a 10-fold lowered affinity for substance P and is not able to elicit intracellular G-protein binding, which induces the activation of NFκB via kinase-cascade activation and eventually results in the production of proinflammatory cytokines [32, 33]. After repeated induction of these intracellular mechanisms by binding agonists, the full-length receptor becomes internalized by endosomes. This is not the case for the truncated receptor version because of the loss of C-terminal Ser/Thr residues, which are essential for receptor internalization upon G-protein-coupled receptor kinase interaction and β-arrestin recruitment [34]. The prevalence of different splice variants seems to be distributed into brain and peripheral tissues, where the full-length form is mostly found in the brain and the truncated form is mostly found in peripheral tissues [35]. There is evidence that, especially

in cancer, the short receptor form is over-expressed and offers a potential target site for anti-substance P and NK_1R treatment [36]. It has been shown recently that the truncated NK_1R also has important functional roles concerning the modulation of immune responses by cytokines and the chemotaxis of macrophages [37].

Multivalent antagonistic NK₁R targeting

Antagonistic treatment of neuropeptide receptors, especially NK_1R, could be a promising approach to anti-inflammatory pharmacotherapy [1]. The main benefit arises from using a multivalent technique such as coupling antagonists on the surface of nanoparticles where an increased effectiveness of treatment by the blockade of multiple receptors at the same time is expected. This aspect depends on high receptor densities on cell surfaces, which is the case in neurogenic inflammatory states, where NK_1Rs are over-expressed. The generation of a spatial proximity of multiple ligands on the surface of the nanoparticle to a highly receptor crowded cell surface determines whether a receptor blockade is sustained. Keeping several ligands close to receptors after the initial binding of the first ligand preserves this proximity. The likelihood for a second ligand binding is relatively high. This state, when several ligands bind several receptors at the same time, is called multivalency, and the effect—that an initial receptor binding promotes the binding of a second one—is called cooperativity. This potent docking principle to cells´ surfaces was found for various viruses [38]. Other approaches focus on hetero-multivalent binding drugs since single drug treatments often suffer from limited efficacy and/or high toxicity. Depending on the nanoparticles´ core material for the design of multivalently acting drugs, cell and organ toxicity are an issue. For experimental studies, the visibility of particles, homogeneity in size, and charge are major demands. Quantum dots offer all these benefits and are therefore a perfect tool to investigate multivalent interactions. Although quantum dots perfectly meet the specifications for experimental studies, strong evidence suggests cell toxicity in higher concentrations because of their bright fluorescent cadmium core, and little is known about QD metabolism [39]. In addition, dense surface PEGylation might increase blood half-life, and precludes elimination from the body. This results in a large area under the exposure-time curve and increases the likelihood of toxicity [40]. However, if the concept of multivalent receptor targeting is proven for a target receptor, there are several possibilities for exchanging the nanoparticle species.

Peptide and non-peptide NK₁R antagonists

There are two fundamental parameters that determine the binding quality of a drug to its receptor binding site: the affinity and the efficacy. The affinity specifies the propensity of a ligand to form a reversible complex with its receptor. The efficacy describes the intrinsic activity of the ligand, which is the ability to produce a functional response in the form of a signaling cascade in cells and tissues [41, 42]. A full agonist can generate a maximal response and tends to stabilize the active state of the G-protein-coupled receptors, whereas full antagonists have no functional effect. The typical stabilized receptor conformation plays an important role for the resulting intracellular signaling or determining if the receptor is simply blocked [43]. For example, substance P binds to the extracellular loops of the NK₁R, whereas small hydrophobic molecular antagonists like aprepitant bind more deeply between the transmembrane segments III–VII [44] (see Figure 3). Partial agonists induce only a submaximal effect and seem to reduce the rate of G-protein turnover, relative to a full agonist, by strongly stabilizing the ternary complex [45]. In general, partial and full agonists share a certain binding topography, but stabilize distinct receptor conformations [46].
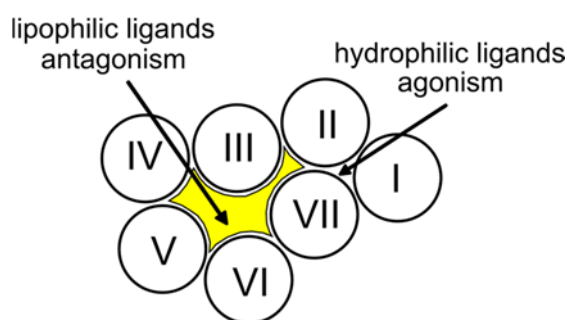

Figure 3: Pattern of 7-transmembrane segments of NK₁R. The arrows indicate different binding sites for small molecular lipophilic antagonists and more hydrophilic peptide agonists.

In the case of NK₁R downstream signaling, a full and potent agonist, such as substance P, would result in intrinsic activity in the form of a great calcium influx into the cytosol even in picomolar concentrations. Aprepitant is known to act as a full antagonist, which does not trigger intrinsic activity and can be seen as a receptor blocker. Most full antagonists are

synthetic compounds and therefore do not appear in nature, unlike full agonists like substance P. However, the assumption that synthetic compounds produce no functional response is false. On the contrary, most known synthetic drugs exhibit a range of responses between full agonism and full antagonism and are termed *partial agonists* because their intrinsic response is reduced compared to their full agonistic analogs. Partial agonists can elicit different receptor responses depending on their environment: In the presence of agonists with higher intrinsic activity, partial agonists can demonstrate antagonist properties by blocking access to the receptor, but on their own they will act as agonists [41]. The design of peptide NK_1R antagonists has focused on the introduction of D-amino acids [47]. However, there are several drawbacks; for example, binding affinities are several orders of magnitude lower than their natural agonists and therefore exhibit poor potency. In addition, partial residual agonist activity and mast cell degranulation activity and neurotoxicity have been observed. Another disadvantage is the inability to discriminate between different tachykinin receptor types [48, 49]. In addition, these peptides are not able to gain access to the CNS through the BBB [50]. Depending on the desired application, though, this aspect may not be a limiting factor except for drugs that explicitly address the brain, such as neurotherapeutics [51]. It can be concluded that peptide as well as non-peptide antagonists are useful for peripheral NK_1R targeting. In the context of this work, both species were selected for *in vitro* multivalent binding experiments. Spantide I was chosen as the peptide antagonist, and the influence of PEGylation on binding affinity was checked prior to coupling to PEG-coated quantum dots. As the non-peptide antagonist, aprepitant was modified by a short alkyl linker to make it accessible for polyethylene glycol (PEG) coupling.

Cost-benefit balancing of drug PEGylation

Up-to-date PEGylation is one post-synthetic strategy of choice with the aim of increasing the solubility and circulatory half-lives of sparely soluble and/or enzymatically unstable drugs. The PEG coatings on the surface of nanoparticles have an additional shielding effect, which prevents them from aggregation, opsonization, and phagocytosis [52]. The reasons for the popularity of PEG are simple. Polyethylene glycol is a water-soluble, non-toxic, non-immunogenic, and commercially available polymer that is approved by the United States Food and Drug Administration and sold with various functional groups at the polymer chain

endings for individual arbitrary chemical modification by customers [53, 54]. But the challenges for drug PEGylation are many: degree of PEGylation, determination of an ideal position within the molecule for PEG-linkage, evaluation of an ideal PEG type and PEG length, choice of PEGylation chemistry, preservation of the drug´s affinity, control of loss in specificity and selectivity, and the avoidance of the gain of unwanted binding effects. Altogether, an extensive chemical and biological analysis of the PEGylated drug cannot be avoided. In the context of hydrophobic ligands on the surface of PEG-coated nanoparticles, the existence of individual PEG and ligand configurations comes into question, depending on the PEG density and ligand properties. This aspect is important since the behavior of the ligand in proximity to a dense PEG shell significantly influences the characteristics of the particle in respect to its charge and its impact on cell binding and uptake. Two possible configurations are known for PEG: brush and mushroom, differentiated by PEG chain density. As a high PEG density is expected to yield a brush conformation with good shielding properties and high particle mobility, this conformation is favored for PEG in nanoparticle targeting in respect to ligand coupling. However, a high PEG density implies the risk for hydrophobic ligand shielding, which could drastically minimize the exposure of the ligands to the outer nanoparticle surface and therefore reduce the potential for multivalent receptor binding.

Mechanistic concept of enzymatic nanoparticle activation in the context of diabetic nephropathy and rheumatoid arthritis

The concept of enzyme-based nanoparticle activation at the site of the disease as a further strategy for active targeting is discussed in the literature. In particular, metalloproteinases, which are expressed ubiquitously, are the focus of nanoparticle shell conversion to make underlying ligands available [55]. But no concept currently focuses on the induction of multivalency by enzyme driven ligand conversion on the surface of nanoparticles.

For earlier disease stages in RA, David A. Walsh and colleagues found that increased levels of angiotensin-converting enzyme (ACE), a membrane metallopeptidase are present in the synovial fluid of patients because of the increasing density of ACE-bearing stromal cells and not because of an increase in vascular delivered ACE [29, 56]. Angiotensin-converting enzyme primarily converts angiotensin I to the vasoactive angiotensin II and can therefore be one reason for the progress of disease with respect to the formation of new small blood vessels in the synovium [29]. Especially in the acute inflammation phase of arthritis, bradykinin, substance P, CGRP, angiotensin II, prostaglandin E2, nitric oxide, histamine, and hyaluronic acid (low molecular weight) contribute to angiogenesis. In the chronic phase, other influences like vascular endothelial growth factor and other growth factors, such as interleukins, TNF-α, TGF-β, and the platelet-derived endothelial cell growth factor play a role. All these factors can be designated as angiogenic factors, and subclassified in acute and chronic inflammation [29]. The inhibition of angiogenesis may be of therapeutic interest to stop the progress of arthritic diseases. Angiotensin I-modified quantum dots may be useful for further investigation of the influence of ACE in the progression of RA and for the identification of target cells for enzymatically processed quantum dots. Moreover, these quantum dots may be used as a diagnostic marker for different disease states. Since it is known that, in addition to synovium derived cells, bovine chondrocytes in a 2D cell culture express AT1 receptors for angiotensin II, cartilage cells could also be a potential target for antiangiogenic drugs. Nanoparticles would reach these cells by simple diffusion, especially in a pathological condition where the extracellular matrix is leaky because of cartilage destruction. In preclinical research, such quantum dots could aid understanding of the

mechanism of action of ACE in RA after local administration into either inflamed or healthy joint space. In general, the selective inhibition of undesired angiogenesis is challenging because angiogenesis itself also has a physiological function and occurs in the absence of inflammation. Therefore, for the development of angiostatic therapeutics it is necessary to understand and distinguish among different regulatory mechanisms in both the healthy state and the disease state. In the healthy state, articular cartilage is avascular, and its nutrition is dependent from factors released from the synovium into the fluid-filled joint cavity. The normal synovium must be well supplied with capillaries to fulfill this function. This status is profoundly changed in the presence of inflammation because the morphology of the synovium is altered in respect to number, density, and spatial distribution of the vasculature [28]. In contrast to the healthy state, there is more vasculature in the disease state, but paradoxically the blood supply is inadequate. The consequences are hypoxia, hypercapnia, and acidosis [28]. If angiogenesis inhibitors reach off-targets, they could have potentially detrimental effects on wound healing or on the female reproductive capacity, for example [28]. Along with angiotensin I, substance P and bradykinin are also susceptible to ACEs. Compared to angiotensin, these proinflammatory kinins become inactive [57]. Substance P and bradykinin are known to induce plasma extravasation and to increase blood flow [56, 58]. Therefore, it is therapeutically beneficial to stimulate ACE in the inflamed joint, rather than to inhibit it.

References

[1] Pintér E, Pozsgai G, Hajna Z, Helyes Z, Szolcsányi J. Neuropeptide receptors as potential drug targets in the treatment of inflammatory conditions. Br J Clin Pharmacol 2014; 77: 5–20.

[2] Firestein GS, Kelley WN. Kelley's textbook of rheumatology: Neurologic Regulation of Inflammation. 9th ed. Philadelphia, PA [etc.]: Elsevier Saunders op. 2013 [i.e. 2012.

[3] Lai JP. Full-length and truncated neurokinin-1 receptor expression and function during monocyte/macrophage differentiation. Proceedings of the National Academy of Sciences 2006; 103: 7771–7776.

[4] Sabatino F, Di Zazzo A, Simone L de, Bonini S. The Intriguing Role of Neuropeptides at the Ocular Surface. The Ocular Surface 2017; 15: 2–14.

[5] Sellam J, Berenbaum F. The role of synovitis in pathophysiology and clinical symptoms of osteoarthritis. Nat Rev Rheumatol 2010; 6: 625–635.

[6] v. Euler, U. S., Gaddum JH. An unidentified depressor substance in certain tissue extracts. The Journal of Physiology 1931; 72: 74–87.

[7] Dougados M. Synovial fluid cell analysis. Baillière's Clinical Rheumatology 1996; 10: 519–534.

[8] Grässel S. The role of peripheral nerve fibers and their neurotransmitters in cartilage and bone physiology and pathophysiology. Arthritis Res Ther 2014; 16: 521.

[9] McDougall JJ. Arthritis and Pain. Neurogenic origin of joint pain. Arthritis Res Ther 2006; 8: 220.

[10] Hill R. NK1 (substance P) receptor antagonists--why are they not analgesic in humans? Trends Pharmacol. Sci. 2000; 21: 244–246.

[11] Ricciotti E, FitzGerald GA. Prostaglandins and Inflammation. Arteriosclerosis, Thrombosis, and Vascular Biology 2011; 31: 986–1000.

[12] Hong SK, Han JS, Min SS, et al. Local neurokinin-1 receptor in the knee joint contributes to the induction, but not maintenance, of arthritic pain in the rat. Neurosci. Lett. 2002; 322: 21–24.

[13] Borbély É, Hajna Z, Sándor K, et al. Role of Tachykinin 1 and 4 Gene-Derived Neuropeptides and the Neurokinin 1 Receptor in Adjuvant-Induced Chronic Arthritis of the Mouse. PLoS ONE 2013; 8: e61684.

[14] Berger A, Paige CJ. Hemokinin-1 has Substance P-like function in U-251 MG astrocytoma cells: A pharmacological and functional study. Journal of Neuroimmunology 2005; 164: 48–56.

[15] Lam FFY. Substance P and glutamate receptor antagonists improve the anti-arthritic actions of dexamethasone in rats. British Journal of Pharmacology 2010; 159: 958–969.

[16] Dickenson AH. Spinal cord pharmacology of pain. British Journal of Anaesthesia 1995; 75: 193–200.

[17] Johnson MB, Young AD, Marriott I. The Therapeutic Potential of Targeting Substance P/NK-1R Interactions in Inflammatory CNS Disorders. Front. Cell. Neurosci. 2017; 10: 450.

[18] Richardson JD. Cellular Mechanisms of Neurogenic Inflammation. Journal of Pharmacology and Experimental Therapeutics 2002; 302: 839–845.

[19] Kramer MS, Cutler N, Feighner J, et al. Distinct mechanism for antidepressant activity by blockade of central substance P receptors. Science (New York, N.Y.) 1998; 281: 1640–1645.

[20] Becher B, Prat A, Antel JP. Brain-immune connection: immuno-regulatory properties of CNS-resident cells. GLIA 2000; 29: 293–304.

[21] Banks WA, Kastin AJ. Blood to brain transport of interleukin links the immune and central nervous systems. Life Sciences 1991; 48: PL117-PL121.

[22] Dray A. Inflammatory mediators of pain. British Journal of Anaesthesia 1995; 75: 125–131.

[23] Muñoz M, Coveñas R. Involvement of substance P and the NK-1 receptor in human pathology. Amino Acids 2014; 46: 1727–1750.

[24] Schaible H-G, Banchet GS von, Boettger MK, et al. The role of proinflammatory cytokines in the generation and maintenance of joint pain. Annals of the New York Academy of Sciences 2010; 1193: 60–69.

[25] Garcia-Recio S, Gascón P. Biological and Pharmacological Aspects of the NK1-Receptor. BioMed research international 2015; 2015: 495704.

[26] Feldmann M, Brennan FM, Maini RN. Role of cytokines in rheumatoid arthritis. Annual review of immunology 1996; 14: 397–440.

[27] Bonnet CS. Osteoarthritis, angiogenesis and inflammation. Rheumatology 2005; 44: 7–16.

[28] Stevens CR, Blake DR, Merry P, Revell PA, Levick JR. A comparative study by morphometry of the microvasculature in normal and rheumatoid synovium. Arthritis and rheumatism 1991; 34: 1508–1513.

[29] Walsh D. Angiogenesis and arthritis. Rheumatology 1999; 38: 103–112.

[30] Millward-Sadler SJ, Mackenzie A, Wright MO, et al. Tachykinin expression in cartilage and function in human articular chondrocyte mechanotransduction. Arthritis & Rheumatism 2003; 48: 146–156.

[31] Vanderah T, Sandweiss A. The pharmacology of neurokinin receptors in addiction: prospects for therapy. SAR 2015: 93.

[32] Douglas SD. Neurokinin-1 receptor: functional significance in the immune system in reference to selected infections and inflammation. Annals of the New York Academy of Sciences 2011; 1217: 83–95.

[33] Fong TM. Differential activation of intracellular effector by two isoforms of human neurokinin-1 receptor. Molecular Pharmacology 1992; 41: 24–30.

[34] DeFea KA, Vaughn ZD, O'Bryan EM, Nishijima D, Déry O, Bunnett NW. The proliferative and antiapoptotic effects of substance P are facilitated by formation of a beta -arrestin-dependent scaffolding complex. Proceedings of the National Academy of Sciences of the United States of America 2000; 97: 11086–11091.

[35] Caberlotto L, Hurd YL, Murdock P, et al. Neurokinin 1 receptor and relative abundance of the short and long isoforms in the human brain. Eur J Neurosci 2003; 17: 1736–1746.

[36] Patel HJ, Ramkissoon SH, Patel PS, Rameshwar P. Transformation of breast cells by truncated neurokinin-1 receptor is secondary to activation by preprotachykinin-A peptides. Proceedings of the National Academy of Sciences 2005; 102: 17436–17441.

[37] Tuluc F, Lai JP, Kilpatrick LE, Evans DL, Douglas SD. Neurokinin 1 receptor isoforms and the control of innate immunity. Trends in Immunology 2009; 30: 271–276.

[38] Mammen M, Choi S-K, Whitesides GM. Polyvalent Interactions in Biological Systems: Implications for Design and Use of Multivalent Ligands and Inhibitors. Angewandte Chemie International Edition 1998: 2754–2794.

[39] Hardman R. A Toxicologic Review of Quantum Dots: Toxicity Depends on Physicochemical and Environmental Factors. Environ Health Perspect 2006; 114: 165–172.

[40] Soo Choi H, Liu W, Misra P, et al. Renal clearance of quantum dots. Nat Biotechnol 2007; 25: 1165–1170.

[41] Bolonna AA. Partial agonism and schizophrenia. The British Journal of Psychiatry 2005; 186: 7–10.

[42] Gether U, Kobilka BK. G Protein-coupled Receptors. J. Biol. Chem. 1998; 273: 17979–17982.

[43] Kobilka BK, Deupi X. Conformational complexity of G-protein-coupled receptors. Trends in Pharmacological Sciences 2007; 28: 397–406.

[44] Muñoz M. Involvement of substance P and the NK-1 receptor in pancreatic cancer. WJG 2014; 20: 2321.

[45] Seifert R, Wenzel-Seifert K, Gether U, Kobilka BK. Functional differences between full and partial agonists: evidence for ligand-specific receptor conformations. The Journal of pharmacology and experimental therapeutics 2001; 297: 1218–1226.

[46] Bock A, Chirinda B, Krebs F, et al. Dynamic ligand binding dictates partial agonism at a G protein–coupled receptor. Nat Chem Biol 2013; 10: 18–20.

[47] Almeida TA, Rojo J, Nieto PM, et al. Tachykinins and tachykinin receptors: structure and activity relationships. Current medicinal chemistry 2004; 11: 2045–2081.

[48] Quartara L. The tachykinin NK1 receptor. Part I: Ligands and mechanisms of cellular activation. Neuropeptides 1997; 31: 537–563.

[49] Lee CM, Campbell NJ, Williams BJ, Iversen LL. Multiple tachykinin binding sites in peripheral tissues and in brain. European Journal of Pharmacology 1986; 130: 209–217.

[50] Gentilucci L, Marco R de, Cerisoli L. Chemical modifications designed to improve peptide stability: incorporation of non-natural amino acids, pseudo-peptide bonds, and cyclization. Current pharmaceutical design 2010; 16: 3185–3203.

[51] Malavolta L, Cabral FR. Peptides: Important tools for the treatment of central nervous system disorders. Neuropeptides 2011; 45: 309–316.

[52] Suk JS, Xu Q, Kim N, Hanes J, Ensign LM. PEGylation as a strategy for improving nanoparticle-based drug and gene delivery. Advanced Drug Delivery Reviews 2016; 99: 28–51.

[53] Roberts MJ, Bentley MD, Harris JM. Chemistry for peptide and protein PEGylation. Adv. Drug Deliv. Rev. 2002; 54: 459–476.

[54] Veronese FM, Mero A. The impact of PEGylation on biological therapies. BioDrugs : clinical immunotherapeutics, biopharmaceuticals and gene therapy 2008; 22: 315–329.

[55] Fay F, Hansen L, Hectors, Stefanie J. C. G., et al. Investigating the Cellular Specificity in Tumors of a Surface-Converting Nanoparticle by Multimodal Imaging. Bioconjugate Chem. 2017; 28: 1413–1421.

[56] Walsh DA. Angiotensin converting enzyme in human synovium: increased stromal [125I]351A binding in rheumatoid arthritis. Annals of the Rheumatic Diseases 2000; 59: 125–131.

[57] Emanueli C, Grady EF, Madeddu P, et al. Acute ACE inhibition causes plasma extravasation in mice that is mediated by bradykinin and substance P. Hypertension (Dallas, Tex. : 1979) 1998; 31: 1299–1304.

[58] Dray A, Bevan S. Inflammation and hyperalgesia: highlighting the team effort. Trends in Pharmacological Sciences 1993; 14: 287–290.

- 18 -

- 19 -

Chapter 2

Goals of the thesis

The goal of this thesis was to investigate the neurokinin-1 receptor as a potential target site for multivalent receptor blockade. Taking previous findings on multivalent G-protein-coupled receptor (GPCR) targeting into account, e.g. the increase in selectivity, specificity and ligand affinity to the target site, this work focused on challenging aspects of PEGylation of synthetic hydrophobic peptide and non-peptide NK_1R antagonists and their coupling to PEGylated quantum dots (QDs). Irrespective of neurokinin-1 receptor targeting, the principle of enzymatic peptide ligand activation on the surface of nanoparticles was investigated, based on angiotensin I to angiotensin II conversion by ACE and AT_1 receptor targeting as a new tool for site-specific targeting.

As the neurokinin-1 receptor is involved in inflammation and pain, its role is also discussed in the context of autoimmune diseases, like RA, but also in cancer. An efficient antagonistic targeting could be highly beneficial in their therapy. Since the NK_1R is peripherally expressed on different cell types of the human body and its expression increases at the time when an immune response occurs, this receptor seems to offer great potential for selective and specific antagonistic surface receptor targeting with a minimizing effect of inflammation and pain. The interrelation of the neurokinin-1 receptor to inflammation and pain in general and how different ligands can interact with the neurokinin-1 receptor, as well as the cost-benefit of PEGylation of such ligands are described in **Chapter 1**.

Based on this scientific background, the expression status of the NK_1R was checked on different cell types, e.g. bovine chondrocytes as a potential target cell in RA, different cancer cell types, and transfected CHO cells as a positive control. Within these expression studies, the influence of the main neurokinin-1 receptor agonist, substance P was tested in respect to intracellular pathways. These studies are shown in **Chapter 3**.

The idea behind multivalent binding antagonists is to make potent ligands more selective against cells with overexpression of the respective target receptor and the receptor blockade itself more efficient because of a prolonged arrest of the multivalent binding ligand at the target site. Fluorescent nanoparticles are a common tool to investigate such multivalent interactions. Therefore, fluorescent PEGylated QDs were used for ligand coupling to the surface of nanoparticles and to study their interactions with neurokinin-1 receptor positive cells. The synthesis strategy and the nanoparticle characterization are shown in **Chapter 4**.

Besides PEGylated QDs, branched 8-arm PEGs were used for multivalent cell interaction studies. In contrast to QDs, PEGs are classified as non-toxic biomaterials and they do not interfere with luminescence-based calcium assays. Therefore, they offered an effective tool for determining their binding affinities as well as the ligand coupling efficiency. These binding studies are depicted in **Chapter 5**.

Besides peptide-based antagonists, a small molecular weight antagonist, named aprepitant was modified to make it amenable for further PEG coupling, either to branched PEGs or PEG-coated nanoparticles. The synthesis strategy is shown in **Chapter 6**.

Another new strategy for site-specific multivalent nanoparticle targeting is presented in **Chapter 7**, the final chapter. This strategy is based on an enzyme driven activation mechanism of ligands, which are immobilized on the surface of nanoparticles. For these studies, the ACE driven angiotensin I to angiotensin II conversion was used and the successful conversion was checked by AT_1 receptor binding studies.

Chapter 3

Identification of target cell candidates with neurokinin-1 receptor expression

Abstract

The neurokinin-1 receptor (NK_1R) is a quite promising target receptor for multivalently binding nanoparticles for either tumor or non-tumor targeting because of its strict overexpression in pathological states and because of its action at the interface of the immune and nervous system. Though its direct role in the generation and perception of pain responses is controversial, its influence in the initiation and promotion of the immune response is certain. The presence of high local immune cell-derived cytokine concentrations leads to the release of substance P from peripheral afferent nerve terminals. Substance P is the major ligand for the NK_1R and triggers the immune response by pro-angiogenesis mechanisms, which facilitate the recruitment of further immune cells. This so-called neurogenic inflammation represents an effective way to protect the body from noxious stimuli. The main disadvantage of neurogenic inflammation is that there is a risk for irrepressible immune responses, especially in the case of cancer and autoimmune diseases (e.g. RA). Therefore, proinflammatory cytokine dependent NK_1R expression on various human glioblastoma and breast cancer cells and chondrocytes, obtained from bovine cartilage was investigated. Here, IL-1 dependent NK_1R mRNA expression was found in all tested cells. However, the existence of the functional full-length receptor version was not verified in calcium assays. In bovine chondrocytes, substance P directly contributes to cartilage destruction by up-regulation of the matrix-metalloproteinase MMP-13. Therefore, an effective antagonistic treatment of the NK_1R may be a highly promising strategy to relieve typical inflammatory symptoms in early RA and prevent further destructive processes in later disease stages.

Introduction

The peripheral nervous system and the immune system cannot be considered as two separately acting machineries [1]. The crosslink between both is drawn by the same molecular recognition pathways, which offer them a way to communicate. This mechanism is called neurogenic inflammation, with the goal of forming an integrated and rapid protective defense of the body. Due to the high speed of the signal transduction pathway of sensory and autonomic nerve fibers, which are widely distributed in peripheral tissues and organs, the neurogenic modulation of immunity is quite effective [1]. However, in the case of pathological states, as in cancer or autoimmune diseases (e.g. RA), this interaction also contributes to the exacerbation and progression of the disease [2].

The NK₁R and its primary agonist, substance P are two of the key players in neurogenic inflammation, since they are both upregulated during inflammation [3]. It is suggested that elevated substance P levels in plasma and synovial fluid may be a hallmark of chronic inflammation [4]. Substance P conveys vasodilatation, indicated by an increase in blood vessel size and an increase in permeability as well as neovascularization. Recent evidence suggests that substance P mediated stimulation of angiogenesis occurs in inflamed peripheral tissues like the synovial membrane in RA or different types of tumors [5,6]. Through these newly formed highly permeable blood vessels, immune cells are able to infiltrate into the joint cavity or into tumor tissues to release in turn cytokines like IL-1α and IL-1β and other pro-inflammatory factors, like TNF-α [7]. In the case of RA, the synovial membrane becomes hypertrophic and the high doses of inflammatory factors provoke the release of neuropeptides like substance P from articular afferent unmyelinated C nerve fibers within the soft tissues of the joint [7–9]. An additional factor for substance P release is local mechanical overload, which causes increasing compressive forces and hypoxia and may further sensitize these nerves and contribute to pain [10]. Prolonged peripheral nerve sensitization leads to enhanced responses of the spinal cord and thalamic neurons [11] (Figure 1). The released substance P activates NK₁Rs, which are typically over-expressed on glial cells of the CNS and peripheral infiltrated immune cells in the synovium and synovial endothelial cells and even on articular chondrocytes [12–15]. In RA, a chronic stage is reached, when the inflammatory symptoms last more than three months. In this state, the immune cells are underrepresented and are replaced by tissue destruction, mainly caused by

ECM degrading matrix-metalloproteinases (MMPs), which are promoted by inflammatory transmitters and substance P [13].
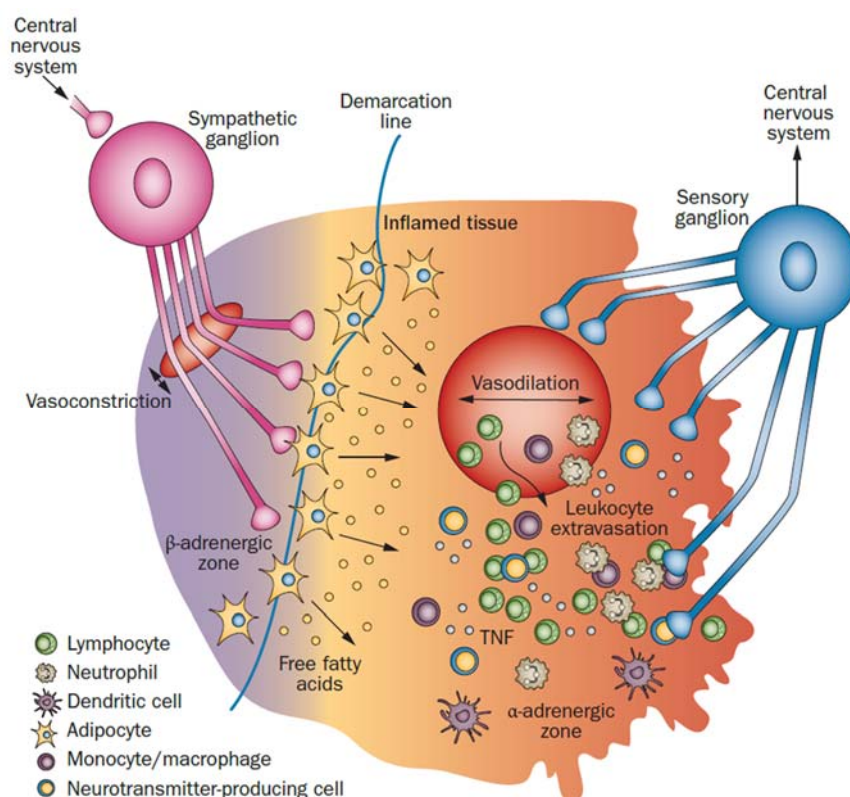

Figure 1: The dominating part in neuronal innervations of an inflamed tissue is taken by sensory nerve fibers. In response to cytokine stimulation, the ends of these nerve fibers release various neuropeptides, including substance P, which cause vasodilatation and the recruitment of immune cells into the inflamed tissue. Reprinted from Nat Rev Rheumatol 9, 2, 117–126 by G. Pongratz and R. H. Straub, 2013. Copyright by Nature Publishing Group. Reprinted by permission [16].

An effective antagonistic targeting of substance P by a neurokinin-1 receptor blockade seems to be a promising strategy to mitigate typical inflammatory and painful symptoms in either cancer or in early and late stages of RA. For this reason, the NK₁R expression on different tumor cell lines as well on bovine chondrocytes as potential target cells for multivalent nanoparticle-based antagonistic NK₁R treatment was investigated. In this context, it was additionally looked on NK₁R mRNA expression levels in response to stimulation with the proinflammatory factor IL-1β. Further, whether substance P has an influence on MMP-1 and MMP-13 expression on IL-1β stimulated bovine chondrocytes was investigated. The aspect

of ECM degradation in response to cytokines and neuropeptides is intriguing since it is a substantial requirement for nanoparticle diffusion into cartilage and subsequent NK_1R targeting on chondrocytes. Because NK_1R mRNA levels do not directly reflect the functional receptor density on the cell surface, calcium assays were performed with all cell lines to identify a target cell with high NK_1R density for multivalent drug testing.

Materials and methods

All chemicals were obtained from Sigma Aldrich (Taufkirchen, Germany) in analytical grade unless stated otherwise. Dulbecco's phosphate-buffered saline (DPBS) pH 7.4 consisting of 1.5 mM KH_2PO_4, 8 mM Na_2HPO_4, 2.7 mM KCl and 138 mM NaCl was purchased from Life Technologies/Thermo Scientific (Darmstadt, Germany). Ultrapure water was obtained from a Milli-Q water purification system (Millipore, Billerica, MA, USA).

Tumor cell lines, U87 MG gliloblastoma, MDA-MB-231 and MCF-7 breast cancer cell lines were purchased from ATCC [17,18]. U87 MG cells were grown in Eagle´s Minimum Essential Medium (EMEM) without pyruvat with 10% FCS, MDA-MB-231 in McCoy´s medium with 5% FCS and MCF-7 in EMEM with pyruvat and 10% FCS. Primary bovine chondrocytes were isolated by Johanna Lempp from the department of Pharmaceutical Technology (Universität Regensburg) from freshly obtained bovine knee joints and grown in cell culture medium (CCM), consisting of DMEM (Gibco/Thermo Scientific, Darmstadt, Germany), 10 mM HEPES, non-essential amino acid (Gibco/Thermo Scientific, Darmstadt, Germany), 46 µg/ml proline, 50 µg/ml ascorbic acid, 1% Penicillin/Streptomycin (Gibco/Thermo Scientific, Darmstadt, Germany), 10% FCS. DBA-1J mouse knee joints were kindly provided from Prof. Rainer Straub (Klinik und Poliklinik für Innere Medizin, Universität Regensburg). Dr. Ralf Schwandner (Amgen Research GmbH, BioPark Regensburg) kindly provide a stable transfected neurokinin-1 receptor expressing CHO cell line. Cells were grown in DMEM:F12 (1:1) medium with 1.2 g/l $NaHCO_3$, 15 mM HEPES, 1% Penicillin-Streptomycin, 10% FCS and 600 µg/ml hygromycin B (Carl Roth, Karlsruhe, Germany) supplementation.

The peqGOLD Total RNA Kit and the peqGOLD DNase I Digest Kit were used to extract mRNA and to remove potentially present DNA. For reverse transcription, two kits were used: The AffinityScript QPCR cDNA Synthesis Kit was bought from Agilent Technologies, Waldbronn Germany and the PeqGOLD cDNA Synthesis Kit H Minus was bought from Peqlab, Erlangen, Germany. For classical Polymerase chain reaction (PCR), the peqGOLD Taq-DNA-Polymerase Kit from Peqlab, Erlangen, Germany was used. As reaction buffer, the 10x reaction buffer S was always chosen, with a $MgCl_2$ content of 15 mM. For

quantitative real-time PCR, the SYBR Green qPCR Kit was obtained from Agilent Technologies, Waldbronn, Germany.

Human interleukin-1α (IL-1α) was purchased from PeproTech, Hamburg, Germany. Human interleukin-1β (IL-1β) was purchased either from MACS Miltenyi Biotec, Bergisch Gladbach, Germany or from PeproTech, Hamburg, Germany. Reconstitutions were made by dissolving 10 µg of provided interleukins in 100 µl sterile filtered Millipore water to obtain 0.1 mg/ml stock solutions. Working solutions of 0.01 mg/ml were prepared in 0.1% BSA in DPBS.

Neurokinin-1 receptor expression studies in 2D cancer cell culture upon 24 hours interleukin-1β stimulation by RT-PCR

U87 MG and MDA-MB-231 cells were seeded in a six-well cell culture plate in a cell density of $0.5*10^6$ cells per well and were grown overnight at 37°C and 5% CO_2 in a medium with 10% FCS. Stimulation over 24 hours was started 12 hours after cell adherence in a medium without FCS. On the second day after seeding, stimulation time points of 6 hours, 3 hours, 1 hour and the control without stimulation were prepared equivalently.

After IL-1β stimulation, the medium was removed and replaced by 1 ml phenol containing TRIzol reagent for cell lysis and incubated for 5 min at room temperature. In each well, the total cell lysate was removed with the help of a cell scraper and transferred to a 2 ml Eppendorf tube. For phase separation, 200 µl of chloroform were added and mixed by thorough up and down pipetting for 15 seconds. To induce complete phase separation, the mixture was centrifuged at 12000 rcf for 15 min at 4°C. The upper phase was transferred in a fresh Eppendorf tube and washed with 500 µl isopropanol by gentle shaking, and RNA was precipitated by incubation at room temperature for 10 min. The extracted RNA was sedimented by a further centrifugation at 14000 rcf for 30 min at 4°C. Then the supernatant was removed and the obtained RNA pellet was air dried. Then the pellet was washed in 1 ml 75% ethanol by gentle shaking and a centrifugation step at 9400 rcf for 5 min at 4°C. The RNA pellet was dried again after removal of the supernatant. The obtained RNA was dissolved in 15 µl RNase free water and heated to 55°C for at least 10 min. The obtained

samples were stored at -80°C until use. The RNA content was determined with a NanoDrop UV meter. For cDNA generation, 2 µg RNA were reverse-transcribed with an oligo(dT) primer and random primer mix, consisting of 170 ng and 30 ng respectively. It was considered that an existing short receptor version, lacking some C-terminal amino acids for G-protein binding, has no Poly-A tail for oligo(dT) primers. With the obvious excess of oligo(dT) primers, the mRNA of full-length receptor version should be preferably transcribed in the RT reaction. The resulting cDNAs were used as templates for amplification in PCRs.

Neurokinin-1 receptor expression studies in 2D bovine chondrocyte cell culture by 24 hours IL-1α and IL-1β stimulation by RT-PCR

To evaluate whether the NK₁R is expressed in general and whether there is a change in expression in the state of inflammation, primary bovine chondrocytes were stimulated in a 2D culture with two different interleukins, and mRNA was subsequently isolated for RT-PCR. Therefore, bovine chondrocytes of the first passage were cultured in T25 cell culture flasks (Corning, Wiesbaden, Germany) in CCM. Confluent cells were washed with warm DPBS and then stimulated with interleukins, either 10 ng/ml IL-1α or IL-β (PreproTech, Hamburg, Germany) in phenol red free CCM without FCS and 0.1% BSA and incubated for 24 h at 37°C and 5% CO_2 atmosphere. The peqGOLD Total RNA Kit and the peqGOLD DNase I Digest Kit were used to extract mRNA and to remove potentially present DNA. Both kits were used according to the manufacturer´s instructions. The RNA content was determined at a NanoDrop UV meter. Then 1 µg RNA was reverse-transcribed with the peqGOLD cDNA Synthesis Kit H Minus, using an oligo(dT) primer and random primer mix of 170 ng to 30 ng. The resulting cDNAs were used as templates for amplification in PCRs.

Polymerase chain reaction (PCR)

There are two versions of neurokinin-1 receptors - a full-length form and a truncated form generated by alternative splicing [19]. Compared to the full-length receptor version, the truncated receptor lacks 96 amino acids in the C-terminal part of the receptor sequence in

the cytosol and is therefore not able to bind and activate a G-protein and trigger intracellular calcium release upon extracellular agonist binding [20,21]. For the evaluation of cell lines, which express both types of neurokinin-1 receptors, appropriate primer pairs for PCR that span the cDNA for the full-length and the truncated receptor version were used. The PCR primers were ordered from Eurofins Genomics, Ebersberg, Germany and are listed in Table 1.

Table 1: Primer sequences

Target	Sequence (5´-> 3´)	T$_m$ in °C	GC content in %
Human NK$_1$R [22]	Forw.: AGGACAGTGACGAACTATTTTCTGG Rev.: CTGCTGGATAAACTTCTTCAGGTAG	61.3 61.3	44.0 44.0
Bovine NK$_1$R [23]	Forw.: TATTTACTCCATGACGGCTG Rev.: AGTCCCCAGGGATCTCACT	55.3 58.8	45.0 57.9
Human GAPDH	Forw.: CTGACTTCAACAGCGACACC Rev.: CCCTGTTGCTGTAGCCAAAT	59.4 57.3	55.0 50.0

For the detection of human neurokinin-1 receptor expression levels, a PCR was performed using the peqGOLD Taq-DNA-Polymerase Kit. For each reaction, a total volume of 25 µl with a primer content of 20 pmol (human NK$_1$R) and 10 pmol (bovine NK$_1$R) and 1 µl of cDNA template were used [22]. As reaction buffer, 10x reaction buffer S was chosen with a MgCl$_2$ content of 15 mM. All other components were applied according the manufacturer´s instructions.

The PCR program was based on those mentioned in the literature [22]:

1. Denaturation	94°C	9 min[1)]/2 min[2)/3)]	
2. Denaturation	94°C	30 sec[1)3)]/10 sec[2)]	
3. Annealing	50°C[1)]/55°C[2)/3)]	30 sec	45[1)]/40[2)]/35[3)] cycles
4. Elongation	72°C	30 sec[1)]/35 sec[2)]/15 sec[3)]	
5. Final elongation	72°C[1)/2)]/76°C[3)]	7 min[1)]/2 min[2)]/6 min[3)]	
6.	4°C	∞	

[1)] human NK$_1$R, [2)] bovine NK$_1$R, [3)] bovine MMP-1 and MMP-13 (see following section)

The amplified cDNA was finally observed in a gel electrophoresis with 2% agarose (Invitrogen/Thermo Scientific, Darmstadt, Germany) in 1x TAE buffer. The bands were detected with 0.4 µg/ml ethidium bromide, which was added to the pre-solid gel. For sample load, 20 µl of PCR reaction product were mixed with 4 µl 6x Loading Dye (Peqlab, Erlangen, Germany). For fragment size determination either the peqGOLD 50 bp (Peqlab, Erlangen, Germany) or 100 bp DNA ladder (Invitrogen/ ThermoFisher Scientific, Darmstadt, Germany) were used.

RT-PCR and qPCR for MMP-1 and MMP-13 mRNA expression analysis upon substance P stimulation in 2D bovine chondrocyte cell culture

Because of the lack of specific bovine neuokinin-1 receptor primers to study the influence of substance P on receptor expression in real-time qPCR, substance P mediated matrix-metalloproteinase (MMP-1 and MMP-13) expression was investigated, which would be an indirect proof for the existence of neurokinin-1 receptors on the surface of chondrocytes. Therefore, two different stimulation experiments were performed. In the first experiment, various substance P concentrations in a fixed timeframe of 24 hours were tested, starting from 1 nM and increasing up to 3 µM substance P. In the second experiment, a fixed concentration of 1 µM substance P was used, and the stimulation time was varied from 1 hour up to 48 hours. The RNA extraction and reverse transcription were performed as described in the former section. The resulting cDNAs were used as templates for amplification in polymerase chain reactions and for quantitative real-time PCR (qPCR) analysis, where expression levels were normalized to GAPDH housekeeping gene expression. Template cDNA was used in a volume of 10.5 µl and mixed to a final volume of 25 µl with components of the SYBR Green qPCR Kit (Agilent Technologies, Waldbronn, Germany), according to the manufacturer´s instructions, and mixed with 10 pmol of prepared bovine MMP-1, bovine MMP-13, or bovine GAPDH primer mix (primer sequences and characteristics are shown in Table 2). Real-time gene amplification was performed in a 96-well non-skirted plate with adhesive foil seal (4titude®Ltd., Berlin, Germany), using a spectrofluorometric thermal Mx3005P QPCR System (Agilent Technologies, Santa Clara, CA, USA). The cycling program started with an initial cycle at

95°C for 15 minutes, followed by 40 cycles, each starting at 95°C for 10 seconds and decreasing the temperature to 60°C and holding for 30 seconds, and ended with a final cycle at 95°C for 1 min, decreasing to 55°C and holding for 30 seconds, then increasing again to 95°C for 30 seconds. Data evaluation was performed with the system connected QPCR software MxPro (Agilent Technologies, Waldbronn, Germany).

Table 2: Primer sequences

Target	Sequence (5´-> 3´)	T_m in °C	GC content in %
Bovine MMP-1 [24]	Forw.: GCTTATGAGGTTGCCGACAG	59.4	55.0
	Rev.: ACGTTTTCCCAGTATCTTCCTC	58.4	45.5
Bovine MMP-13 [24]	Forw.: CGCGGAGAAACACTGATCTT	57.3	50.0
	Rev.: TCATAGGCGGCATCAATACG	57.3	50.0
Bovine GAPDH	Forw.: TTCTGGCAAAGTGGACATCG	57.3	50.0
	Rev.: CGTTCTCTGCCTTGACTGTG	59.4	55.0

Neurokinin-1 receptor immunostaining on cells in 2D culture

Because there is no guarantee for the presence of functional NK₁Rs in the cellular membrane by just verifying its expression at the RNA level, there was an attempt to detect the NK₁R on tumor cells with a specific human NK₁R antibody and a secondary fluorescent FITC antibody. The U87 MG, MDA-MB-231, and the receptor positive CHO-NK₁R cells were each seeded in a density of 10^5 cells/well in an 8-well μ-slide for microscopy purposes (Ibidi, Martinsried, Germany). After cell adherence overnight, the U87 MG and MDA-MB-231 cells were stimulated with 4 ng/ml IL-1β in Leibovitz medium for 3 hours and 1 hour to check for cytokine dependent receptor expression. Unstimulated cells served as a control. All cells were fixed with 4% paraformaldehyde in DPBS for 10 min at room temperature. The fixing solution was replaced by 10% goat serum in Leibovitz medium to block free valencies for at least 30 min at 37°C. Then the cells were incubated with 10 μg/ml of the primary NK₁R specific antibody (Novus Biologicals, Littleton, Colorado, USA) for 30 min

at 37°C. The primary antibody was removed and the cells were washed four times with 10% goat serum in DPBS. 10 μg/ml of the secondary FITC conjugated antibody (Abcam, Cambridge, UK) were administered to the cells and incubated for further 30 min at 37°C. The cells were washed again with 10% goat serum in DPBS. Finally, the cells were covered with Leibovitz medium. For FITC excitation, a 488 nm argon laser was used, and fluorescence emission was detected using a 505-530 band-pass filter. The pinhole was set at 252 μm. Gain adjustment was performed individually for each cell type by normalization against a control sample with only secondary FITC-antibody.

Fura-2 AM calcium assay as functional proof of NK₁R expression

Because the full-length NK₁R variant is a G_q-protein-coupled receptor, the measurement of intracellular calcium release in response to agonistic receptor stimulation is a smart, fast, and antibody-independent test for functional GPCR expression. Therefore, primary bovine chondrocytes, the glioblastoma cell line U87 MG and two breast cancer cell lines, MDA-MB-231 and MCF-7, were tested in a calcium assay for functional NK₁R expression. The CHO-NK₁R cells served as a positive control. The assay was performed exactly as described in Chapter 6.

Neurokinin-1 receptor immunostaining of bovine cartilage and DBA-1J mouse joint cryosection slices

In the final NK₁R expression experiment, chondrocytes with artificially induced arthritis in two different 3D models were used. The first was a bovine *in vitro* model, which was developed by Johanna Lempp, and the second was the well-established murine DBA-1J *in vivo* model with type II collagen-induced arthritis [25]. For the bovine *in vitro* model, cylindrical punches from the patella cartilage were incubated with the inflammation factors IL-1α and OSM in CCM media to obtain directed cartilage destruction [24]. In contrast to soft bovine cartilage tissue punches, the mouse joints had to be subjected to a preliminary decalcification step to soften the bones for tissue slice preparation. Therefore, the dissected knee joints of 16-week old DBA-1J mouse were fixed for 48 hours in 4% PFA solution and

washed two times with PBS buffer. Then the bones were softened by RDO rapid decalcifier (Apex Engineering Products Corporation, Aurora Illinois) over three days. The knee joints were then subjected to 20% sucrose and 5% fixing gel (Tissue-Tek® O.C.T. Compound medium) in DPBS overnight for cryoprotection. The bovine chondrocyte punches and mouse joints were separately embedded in fixing gel (Tissue-Tek® O.C.T. Compound medium) in Cryomold® trays (Sakura Finetek, Alphen aan den Rijn, The Netherlands) and frozen in liquid nitrogen cooled isopentane. Tissue slices of bovine cartilage of 10 μm thickness and 8 μm slices of DBA-1J mouse knee joints were produced at a Microm HM550 cryostat microtome (Thermo Scientific, Darmstadt, Germany) and transferred on SuperFrost® Plus microscope specimen slides and air dried. The tissues were rehydrated three times with DPBS and surrounded with a hydrophobic ImmEdge™ pen (Vector Laboratories, Inc., Burlingame, California). Each tissue section was blocked for 45 min with a blocking solution, consisting of 10% BSA, 10% goat serum in DPBS. For the bovine cartilage punches only, additional 10% FCS were used for blocking. The slices were washed three times with PBS for 5 min. The primary NK₁R specific antibody (Novus Biologicals, Littleton, Colorado, USA) was diluted to 10 μg/ml in 1% BSA in DPBS for bovine cartilage and in 1% BSA with 0.1% Tween 20 in DPBS for mouse knee joints and transferred onto the tissue sections and incubated at 4°C overnight. Controls without primary antibody were treated the same. The next day, the sections were made permeable by washing three times in 0.3% triton X-100 in DPBS for 5 min. Then the secondary Alexa Fluor 546 goat anti-rabbit IgG (H+L) was administered in a final concentration of 20 μg/ml, diluted in 1% BSA in DPBS onto bovine cartilage and 4 μg/ml in 1% BSA with 0.1% Tween 20 in DPBS onto mouse joints and incubated for at least 1.5 hours in a wet chamber at room temperature protected from light. All slices were washed again three times for 5 min in 0.3% triton X-100 in DPBS and one time in pure PBS. Then the slices were covered with one droplet of Mowiol-Mounting medium with 0.1% DABCO (1,4-Diazabicyclo[2.2.2]octane) and finally capped with a cover slip. Chondrocytes´ nuclei were stained with 0.2 μg/ml DAPI diluted in 500 μl Mowiol/DABCO. Microscopy fluorescence images were captured with an Axiovert 200 fluorescence microscope (Zeiss, Jena, Germany), connected to an AxioCamHR camera. The 63x objective was used and the samples were lightened by a mercury-vapor lamp for 300 ms using the Alexa Fluor 546 reflector and 1 ms using the DAPI reflector.

Results and discussion

RT-PCR for NK₁R expression analysis upon interleukin stimulation

That inflammatory factors have a direct influence on substance P and NK₁R expression in tumor cells is well documented in the literature. In this context, it has been shown that an inappropriate expression or regulation of tachykinin receptors on tumor cells, including the NK₁R, contribute to tumor growth and invasion by autocrine stimulation [7,17,22,26]. Therefore, mRNA expression analysis studies of the NK₁R upon IL-1β stimulation of U87 MG glioblastoma, MDA-MB-231 breast cancer cells, and bovine chondrocytes in 2D cell culture were performed. The results of these experiments suggested that the receptor expression was influenced in a time- and concentration-dependent manner of interleukin stimulation (Figure 2).
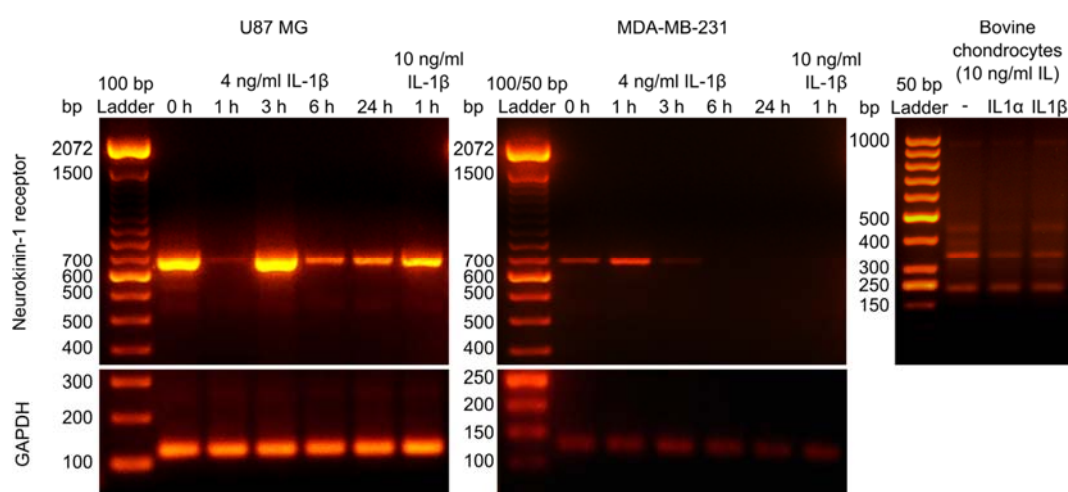
Figure 2: Stimulation of U87 MG glioblastoma cells (pass. 133) and MDA-MB-231 breast cancer cells (pass. 93) with 4 ng/ml human IL-1β and primary bovine chondrocytes with either 10 ng/ml human IL-1α or IL-1β in 2D culture. The human NK₁R was influenced by IL-1 in a time- and concentration-dependent manner. Long-term stimulation ≥3 hours resulted in NK₁R down-regulation. NK₁R bands were detected at 666 bp (human) and at 338 bp (bovine).

For U87 MG, it was found that 3 hours of 4 ng/ml IL-1β stimulation were ideal to reach a slight increase in NK₁R expression after a preliminary receptor mRNA down-regulation within the first hour of stimulation. This effect could be circumvented by increasing the

IL-1β concentration to 10 ng/ml. In MDA-MB-231 cells, the highest NK₁R expression was observed after 1 hour of stimulation with 4 ng/ml. In contrast to U87 MG cells, the increase of IL-1β to 10 ng/ml completely inhibited NK₁R expression in MDA-MB-231 cells. This observation of NK₁R down-regulation for long-term IL-1β stimulation was also made by Johnson & Johnson for human astrocytoma cell line UC11 [27]. For bovine chondrocytes, it was found that equivalent to the other IL-1β treated cell lines, an increase of the stimulation period up to 24 hours for either IL-1α or β lead to a decrease in NK₁R mRNA. It should be noted that, in contrast to the human NK₁R RT-PCRs, where specific bands were detected at 666 bp, the bovine NK₁R primers were not specific and multiple bands occurred beside the expected band at 338 bp (Figure 2).

RT-PCR and qPCR for MMP-1 and MMP-13 expression analysis upon substance P stimulation

To investigate whether there is a concentration-dependent effect of substance P on MMP-1 and MMP-13 expression in bovine chondrocytes, which were also stimulated with IL-1β, various substance P concentrations from 1 nM up to 3 µM in FCS free medium were tested within a stimulation period of 24 hours. In addition, a further look was taken at the effect of spantide I (SP I) in 10-fold excess as a competitor for substance P and NK₁R antagonist. In a preliminary classical RT-PCR, it was found that MMP-1 expression levels seem to be influenced by varying substance P concentrations (Figure 3).
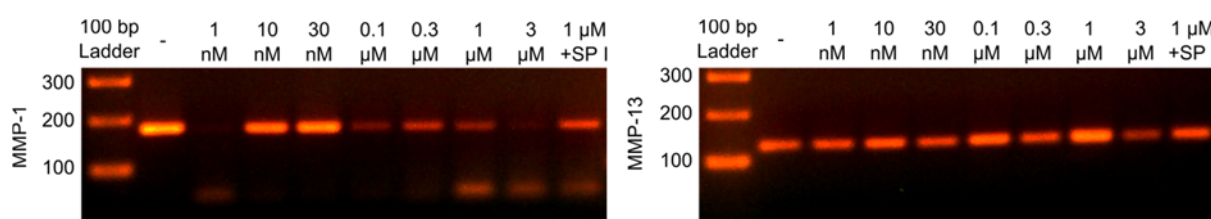

Figure 3: Stimulation of bovine chondrocytes in 2D cell culture with different substance P concentrations. MMP-1 was detected at 178 bp and MMP-13 at 128 bp. Band intensities are not related to GAPDH expression.

For a look in detail, a quantitative real-time PCR was performed and mRNA levels were normalized to GAPDH mRNA expression levels (Figure 4). The results indicated that

MMP-1 and MMP-13 mRNA expression significantly decrease with increasing substance P concentrations up to 300 nM, whereas MMP levels significantly increased by 1 µM substance P stimulation. For MMP-13 in particular, a significantly higher expression could be measured for 1 µM substance P stimulation compared to non-stimulated chondrocytes. In addition, it was found that if the NK$_1$R inhibitor spantide I was added in a concentration of 10 µM, the MMP expression could be suppressed, which indicate a direct influence of NK$_1$R mediated regulation of MMP expression. With a higher substance P concentration of 3 µM, the MMP expression could be down-regulated significantly.
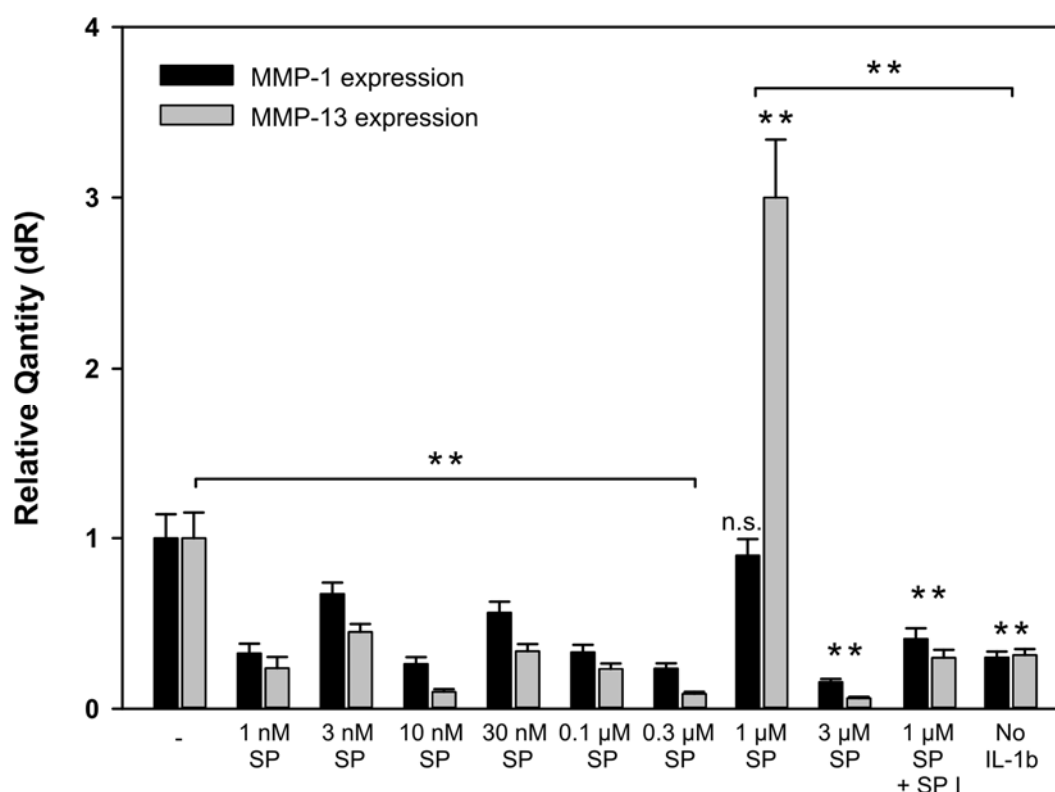
Figure 4: Quantitative real-time PCR of chondrocytes´ MMP-1 and MMP-13 mRNA expression upon stimulation with different substance P concentrations within 24 hours.

In further RT-PCR experiments, the influence of incubation time of substance P stimulation on MMP-1 and MMP-13 mRNA expression levels in bovine chondrocytes in 2D cell culture were investigated (Figure 5). Here, a constant substance P concentration of 1 µM in FCS free medium was used for stimulation within a time frame of 48 hours without substance P renewal.
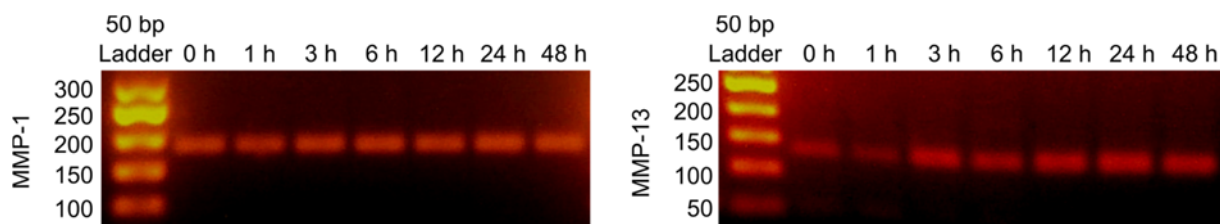
Figure 5: Stimulation of bovine chondrocytes in 2D cell culture with 1 µM substance P for 48 hours. MMP expression levels were examined.

In a quantitative real-time PCR, it was found that there are no significant changes for MMP-1 and MMP-13 expression levels during a stimulation period of 12 hours. Only after 24 hours substance P stimulation was a significantly higher MMP-13 expression detected, which decreased again to the basal expression level after 48 hours (Figure 6).
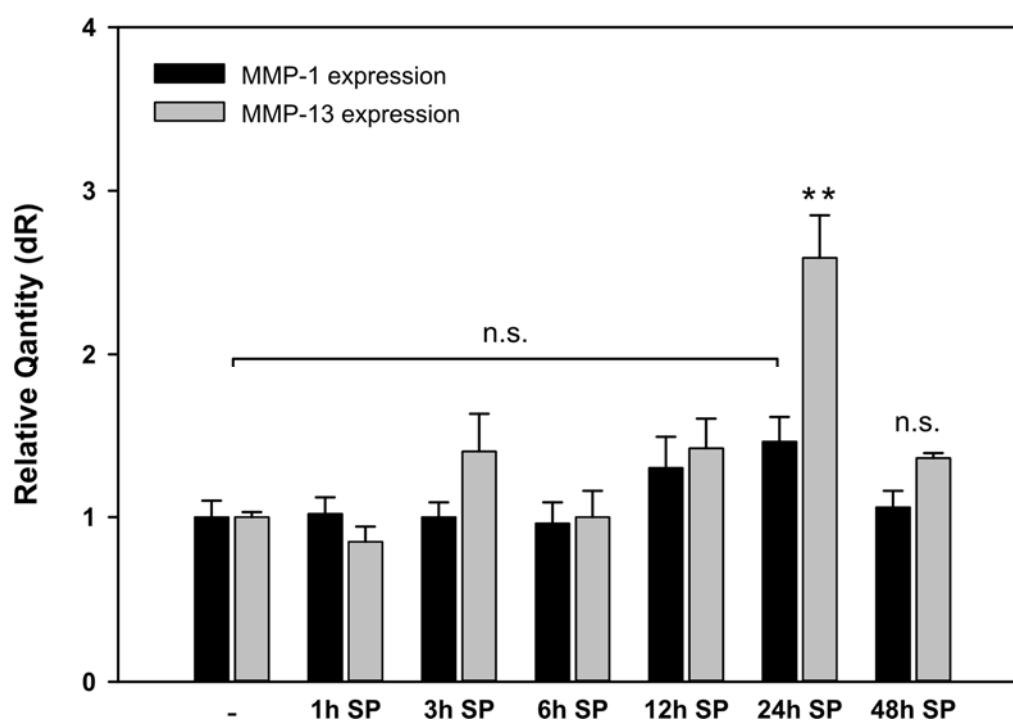

Figure 6: Quantitative real-time PCR of chondrocytes´ MMP-1 and MMP-13 mRNA expression upon substance P stimulation over 48 hours. After 24 hours, there is a significant change in expression of MMP-13, but not for MMP-1. After 48 hours, the MMP-13 expression decreases again to the basis mRNA level.

Neurokinin-1 receptor immunostaining

NK$_1$R immunostaining experiments were carried out for CHO-NK$_1$R cells as a positive control and for the tumor cell lines U87 MG and MDA-MB-231 with and without preliminary 4 ng/ml IL-1β stimulation over 3 hours and 1 hour, respectively (Figure 7). It was found that there is specific FITC fluorescence detectable for both tumor cell lines, but less compared to the positive CHO-NK$_1$R control (Figure 7A, B, D). In addition, no significant changes in fluorescence intensity could be observed for IL-1β stimulated cells, which indicated no difference in functional receptor expression (Figure 7C, E). U87 MG cells particularly seem to suffer from IL-1β stimulation, which resulted in an increasing number of cell debris and are detectable as bright shining green spots (Figure 7C). The used primary antibody does not discriminate between the full-length and the intracellular C-terminal truncated NK$_1$R version because it is able to bind to an extracellular N-terminal binding domain of the NK$_1$R. Therefore, even with the presence of any NK$_1$R version, a positive staining is yielded.
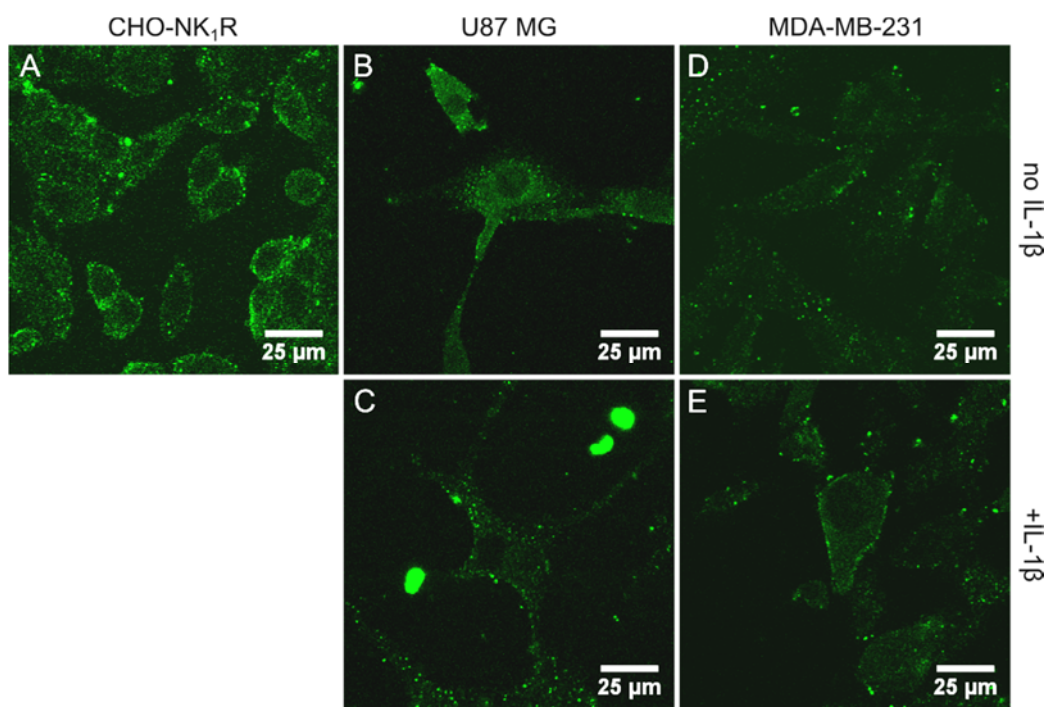

Figure 7: NK$_1$R immunostaining of different cells. Compared to CHO-NK$_1$R cells (A), there is less receptor staining for U87 MG and MDA-MB-231 tumor cells (B, D). U87 MG cells suffered from 3 hours IL-1β stimulation (C), since many cell debris in the form of bright shining green spots were visible. For both tumor cell lines, there is no significantly different receptor staining between unstimulated (B, D) and IL-1β stimulated (C, E) cells.

Fura-2 AM calcium assay

In a functional calcium assay, only about 2% of the maximum reached calcium signal (obtained by the positive CHO-NK$_1$R cell line) was measured for bovine chondrocytes and for the tumor cell lines U87 MG and MDA-MB-231 upon stimulation with 1 μM substance P. The literature mentions that the binding affinity of substance P to the extracellular N-terminal region is 10-fold reduced for the truncated NK$_1$ receptor version and elicits a strongly diminished or even absent calcium response because of the shortened C-terminus and therefore missing G$_q$-protein binding site [28,29]. The results of this experiment suggested that, although NK$_1$R expression was detected for bovine chondrocytes, U87 MG, and MDA-MB-231 cells at the mRNA level, with and without IL-1 stimulation, the full-length receptor density is either too low or tends to be zero. Therefore, these cell lines are not useful for affinity studies with multivalently binding nanoparticles by calcium assays. For this reason, CHO-NK$_1$R cells were used for further binding studies (Figure 8).
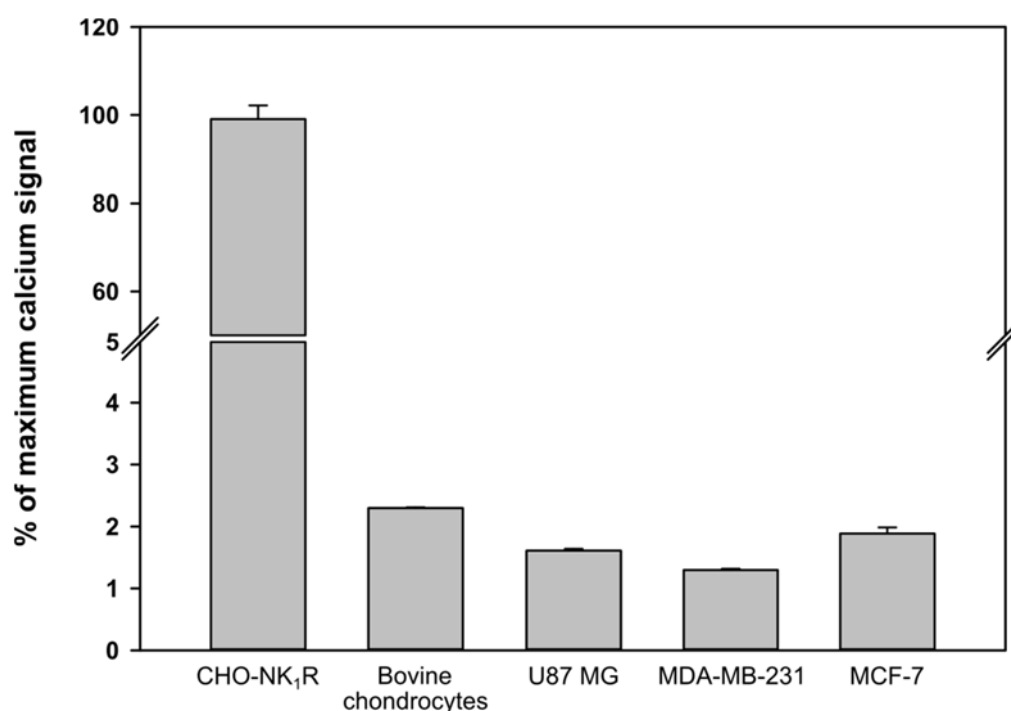

Figure 8: All tested cells did not show a significant response to 1 μM substance P, compared to the positive CHO-NK₁R control cells. The signal intensity is only about 2% of the maximum measured calcium signal. These data suggested that the NK₁R is not present on the cell surface in an adequate receptor density to perform binding studies with multivalently binding nanoparticles.

Neurokinin-1 receptor immunostaining of bovine cartilage and DBA-1J mouse joint cryosection slices

In bovine cartilage tissue slices, a slight specific NK_1R immunostaining on chondrocytes could be identified, although the antibody was not yet tested for bovine specificity (Figure 9). As functional neurokinin-1 receptors could not be detected on isolated bovine chondrocytes in 2D cell culture in a calcium assay, this experiment raised the hope of finding NK_1Rs on chondrocytes within their natural extracellular matrix (ECM) environment. Another aspect is that chondrocytes in this model did not suffer from 2D cell culture related enzymatic treatments such as collagenase or trypsin, which could be one cause for GPCR loss. Nevertheless, in RA, cartilage becomes progressively destroyed by matrix-metalloproteinase (MMP) triggered ECM degradation. This is due to the accumulation of inflammatory factors in the synovium, which are able to diffuse into cartilage to incite chondrocytes to produce MMPs, which in turn destroy the ECM and make it progressively leakier. In such a pathological state, chondrocytes will become increasingly accessible for nanoparticle-based treatment [24]. According to our current knowledge, antagonistic NK_1R targeting could reduce or even stop chondrocyte derived MMP expression and could consequently prevent further cartilage destruction.
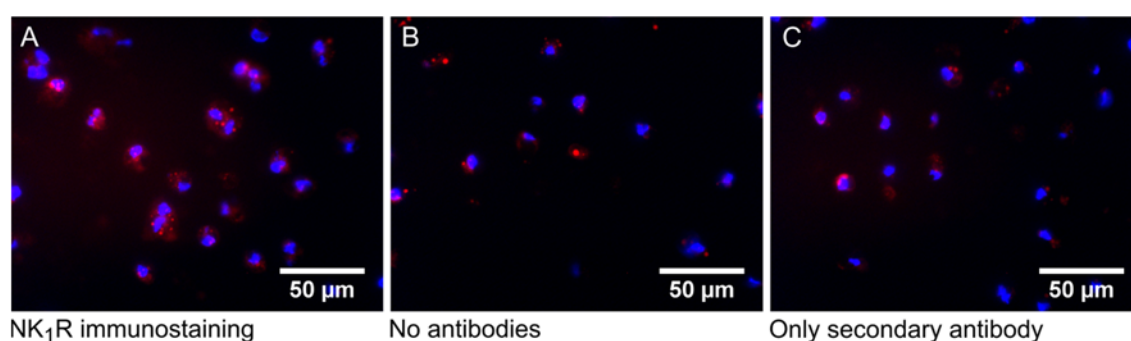

Figure 9: NK₁R immunostaining of chondrocytes in artificially destructed bovine cartilage tissue slices. Cell nuclei were DAPI-stained for orientation.

For DBA-1J mouse joints, no specific NK$_1$R staining could be detected. The reasons for this could be manifold. The loss of GPCRs during the decalcifying procedure should not be overlooked, but also, the immunostaining conditions, in respect to antibody concentrations and incubation time, etc. could have been somehow inappropriate (Figure 10).
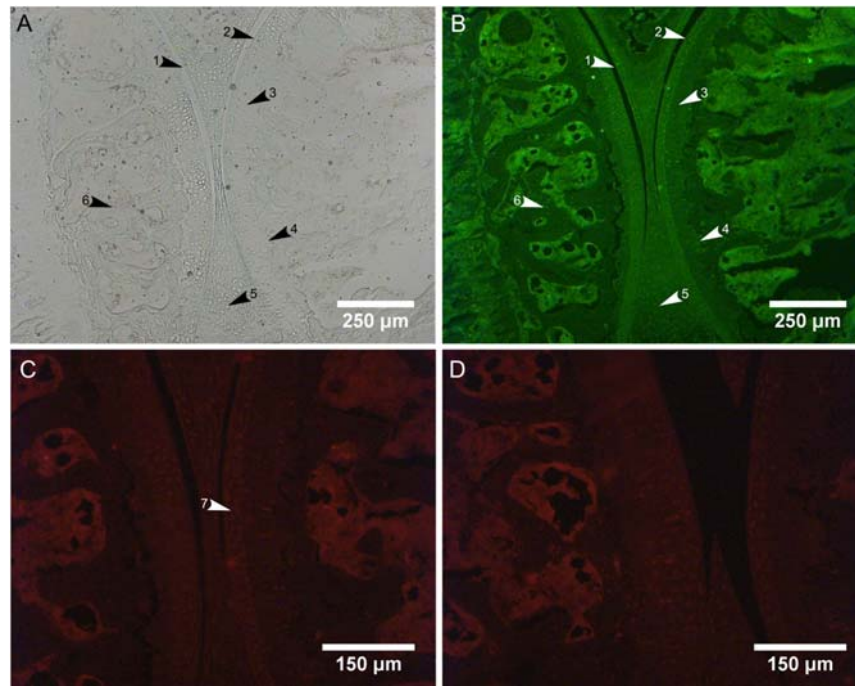

Figure 10: Kryosections of DBA-1J mouse joints: A) Bright field with equivalent B) Background fluorescence picture. C) Immunostaining of NK$_1$R with red secondary Alexa Fluor 546 antibody against specific primary NK$_1$R antibody. D) Control with only secondary antibody. There is no receptor staining visible for articular chondrocytes. Arrows: 1) joint space, 2) articular surface, 3) deep zone, 4) tidemark, 5) meniscus, 6) bone, 7) no specific red NK$_1$R staining of articular chondrocytes in the articular surface and deep zone.

Conclusion

Based on the results of this chapter, it is concluded that the inflammatory factor IL-1β has a direct influence on NK$_1$R expression levels in U87 MG glioblastoma and MDA-MB-231 breast cancer cell lines and primary bovine chondrocytes in 2D cell culture. For U87 MG and MDA-MB-231 cells, it was found that the NK$_1$R mRNA is upregulated within the first 3 hours IL-1β stimulation, but down-regulated for long-term IL-1β stimulation. Here, less NK$_1$R expression at the mRNA level was observed for MDA-MB-231 cells than for U87 MG cells. In further experiments, a closer look was taken at the expression of functional

NK_1Rs in the cellular membrane by NK_1R immunostaining and substance P induced calcium influx measurements. For both cancer cell lines, the data indicated only low receptor density. In calcium experiments, which offered the opportunity to discriminate between a full-length (with G-protein binding site) and a truncated receptor version (without G-protein binding site), only about 2% of maximum reached calcium signal (obtained by the positive CHO-NK_1R cell line) were measured for both cancer cell lines, U87 MG and MDA-MB-231. These results were quite disappointing because these non-transfected cells could not be used for further receptor binding studies of antagonist modified multivalent binding nanoparticles in fluorescence-based calcium assays. Nevertheless, NK_1R mRNA was found in bovine chondrocytes, and the results of NK_1R immunostaining in bovine cartilage tissue sections were quite promising. In addition, it could be demonstrated in 2D cell culture that IL-1β and substance P contribute together to the regulation of the chondrocytes´ surrounding ECM behavior by the selective regulation of MMP´s gene expression. In this context, it could be shown that MMP-13 in particular is regulated in a time- and concentration-dependent manner by substance P and can be antagonized by the specific NK_1R antagonist spantide I, which lets assume that this intracellular signaling pathway is triggered via NK_1Rs. This aspect is intriguing since the literature also mentions that MMP-13 has an impact on the progression of arthritis [30]. Finally, it is concluded that the short version of the NK_1R may be more prominent on the surface of all tested cell types and offer the opportunity for NK_1R targeting, specifically due to the impact on MMP regulation. Due to the lack of the C-terminal G_q-protein binding site of this truncated NK_1R splice variant, no intracellular calcium signals were detectable. For this reason, the NK_1R transfected CHO cells were used for further studies to predict the affinity of generated multivalent ligands.

References

 [1] Chiu IM, von Hehn, Christian A, Woolf CJ. Neurogenic inflammation and the peripheral nervous system in host defense and immunopathology. Nat Neurosci 2012; 15: 1063–1067.

[2] Muñoz M, Rosso M, Coveñas R. A New Frontier in the Treatment of Cancer: NK-1 Receptor Antagonists. CMC 2010; 17: 504–516.

[3] Muñoz M, Coveñas R. Involvement of substance P and the NK-1 receptor in human pathology. Amino Acids 2014; 46: 1727–1750.

[4] Wayne Marshall K, Chiu B, Inman RD. Substance p and arthritis: analysis of plasma and synovial fluid levels. Arthritis & Rheumatism 1990; 33: 87–90.

[5] Lewis KM, Turner RJ, Vink R. Blocking Neurogenic Inflammation for the Treatment of Acute Disorders of the Central Nervous System. International Journal of Inflammation 2013; 2013: 1–16.

[6] Seegers HC. Enhancement of Angiogenesis by Endogenous Substance P Release and Neurokinin-1 Receptors During Neurogenic Inflammation. Journal of Pharmacology and Experimental Therapeutics 2003; 306: 8–12.

[7] Lotz M, Carson D, Vaughan J. Substance P activation of rheumatoid synoviocytes: neural pathway in pathogenesis of arthritis. Science 1987; 235: 893–895.

[8] Kidd BL, Mapp PI, Blake DR, Gibson SJ, Polak JM. Neurogenic influences in arthritis. Annals of the Rheumatic Diseases 1990; 49: 649–652.

[9] Kido MA, Kiyoshima T, Kondo T, et al. Distribution of substance P and calcitonin gene-related peptide-like immunoreactive nerve fibers in the rat temporomandibular joint. Journal of dental research 1993; 72: 592–598.

[10] Wojtys EM, Beaman DN, Glover RA, Janda D. Innervation of the human knee joint by substance-P fibers. Arthroscopy: The Journal of Arthroscopic & Related Surgery 1990; 6: 254–263.

[11] Schaible H, Jarrott B, Hope PJ, Duggan AW. Release of immunoreactive substance P in the spinal cord during development of acute arthritis in the knee joint of the cat: a study with antibody microprobes. Brain Research 1990; 529: 214–223.

[12] Fan TD, Hu D, Guard S, Gresham GA, Watling KJ. Stimulation of angiogenesis by substance P and interleukin-1 in the rat and its inhibition by NK1 or interleukin-1 receptor antagonists. British Journal of Pharmacology 1993; 110: 43–49.

[13] Im H, Li X, Muddasani P, et al. Basic fibroblast growth factor accelerates matrix degradation via a neuro-endocrine pathway in human adult articular chondrocytes. J. Cell. Physiol. 2008; 215: 452–463.

[14] Peterson M, Svärdsudd K, Appel L, et al. PET-Scan Shows Peripherally Increased Neurokinin 1 Receptor Availability in Chronic Tennis Elbow: Visualizing Neurogenic Inflammation? PLoS ONE 2013; 8: e75859.

[15] Walsh DA, Mapp PI, Wharton J, et al. Localisation and characterisation of substance P binding to human synovial tissue in rheumatoid arthritis. Annals of the Rheumatic Diseases 1992; 51: 313–317.

[16] Pongratz G, Straub RH. Role of peripheral nerve fibres in acute and chronic inflammation in arthritis. Nat Rev Rheumatol 2013; 9: 117–126.

[17] Bigioni M, Benzo A, Irrissuto C, Maggi CA, Goso C. Role of NK-1 and NK-2 tachykinin receptor antagonism on the growth of human breast carcinoma cell line MDA-MB-231. Anticancer Drugs 2005; 16: 1083–1089.

[18] Zhou Y, Zhao L, Xiong T, et al. Roles of full-length and truncated neurokinin-1 receptors on tumor progression and distant metastasis in human breast cancer. Breast Cancer Res Treat 2013; 140: 49–61.

[19] Khan MM, Douglas SD, Benton TD. Substance P–Neurokinin-1 receptor interaction upregulates monocyte tissue factor. Journal of Neuroimmunology 2012; 242: 1–8.

[20] Lai JP. Full-length and truncated neurokinin-1 receptor expression and function during monocyte/macrophage differentiation. Proceedings of the National Academy of Sciences 2006; 103: 7771–7776.

[21] Lai J, Lai S, Tuluc F, et al. Differences in the length of the carboxyl terminus mediate functional properties of neurokinin-1 receptor. Proceedings of the National Academy of Sciences 2008; 105: 12605–12610.

[22] Guo C. Interleukin-1ß upregulates functional expression of neurokinin-1 receptor (NK-1R) via NF-kB in astrocytes. GLIA 2004; 48: 259–266.

[23] Reibiger I, Aust G, Tscheudschilsuren G, Beyer R, Gebhardt C, Spanel-Borowski K. The expression of substance P and its neurokinin-1 receptor mRNA in the bovine corpus luteum of early developmental stage. Neuroscience Letters 2001; 299: 49–52.

[24] Lempp J, editor. In-vitro model for cartilage in rheumatoid arthritis and its application for nanoparticle diffusion characterization 2017.

[25] Brand DD, Latham KA, Rosloniec EF. Collagen-induced arthritis. Nat Protoc 2007; 2: 1269–1275.

[26] Rao G, Patel PS, Idler SP, et al. Facilitating role of preprotachykinin-I gene in the integration of breast cancer cells within the stromal compartment of the bone marrow: a model of early cancer progression. Cancer research 2004; 64: 2874–2881.

[27] Johnson CL, Johnson CG. Tumor necrosis factor and interleukin-1 down-regulate receptors for substance P in human astrocytoma cells. Brain Research 1991; 564: 79–85.

[28] Douglas SD. Neurokinin-1 receptor: functional significance in the immune system in reference to selected infections and inflammation. Annals of the New York Academy of Sciences 2011; 1217: 83–95.

[29] Mashaghi A, Marmalidou A, Tehrani M, Grace PM, Pothoulakis C, Dana R. Neuropeptide substance P and the immune response. Cell. Mol. Life Sci. 2016; 73: 4249–4264.

[30] Wang M, Sampson ER, Jin H, et al. MMP13 is a critical target gene during the progression of osteoarthritis. Arthritis Res Ther 2013; 15: R5.

- 49 -

Chapter 4

Multivalently binding quantum dots for neurokinin-1 receptor targeting

Abstract

Multivalent receptor binding nanoparticles represent one option to make cellular membrane receptor targeting more selective, more specific, and even more efficient. In some pathological states, certain GPCR types with relevant influence on cell behavior seem to be overrepresented on the cell surface. These kinds of GPCR offer a great potential to serve as target sites for cell treatment in the form of efficient receptor blockade by antagonists, which are immobilized on the outer shell of nanoparticles. The neurokinin-1 receptor (NK_1R) is one of these GPCRs, which is expressed ubiquitously by cells in the body in the physiological state, but its expression increases rapidly onto immune competent cells in various autoimmune diseases (e.g. RA) or cancer. In particular, spantide I functionalized QDs, which are shielded by a PEG corona, would be a powerful nanoparticle-based theranostic tool to investigate the prevalence of the receptor at target sites with raising immune response and to study their anti-inflammatory and analgesic potential. Therefore, spantide I, which is an NK_1R antagonistic peptide, was coupled to amino-PEG coated QDs. In this chapter, the favored ligand coupling strategy to QDs and their characterization are depicted. Finally, the particles were tested for specific interactions with CHO-NK_1R positive cells.

Introduction

Active GPCR targeting by nanoparticles decorated with bioactive ligands is a major topic in the nanomedicine field [1–4]. In cancer therapy, for example, a primary research goal for ligand coated nanoparticles is an accumulation in a controlled and selective manner to cells and tissues carrying a specific target above a threshold surface concentration [5,6]. This is in contrast to passive transportation of nanoparticles and their accumulation at the site of a tumor by leaky vasculature and poor lymphatic drainage based on EPR effect (enhanced permeability and retention). Besides effective receptor blockade by a multivalent binding mode with high avidity of antagonist coated nanoparticles, research has also focused on directed drug delivery into cells via endocytotic pathways [7]. In particular, the therapeutic index of multivalently binding nanoparticles, which are able to bind several target GPCRs simultaneously, will increase, while lowering systemic side effects, because off-target cells are left with lower surface GPCR coverage unaffected [7]. Not to be overlooked is the fact that repeating chemical patterns on the nanoparticle´s surface cause an increased risk of immune response. The challenge here is to find an ideal ligand-to-PEG ratio on the surface of the nanoparticle to reach multivalent binding effects on the one hand and long half-lives for the nanoparticles due to PEG derived stealth properties to minimize unspecific uptake on the other hand [8,9]. Since nanoparticles cannot easily cross the BBB [10], nanoparticle-based antagonistic targeting of the NK₁R is limited to peripheral target cells, e.g. of the peripheral immune system and peripheral pain transmitting nerve endings, which reside, for example, in the synovial membrane within the joint. It is expected that efficient multivalent antagonistic NK₁R targeting would therefore offer great potential to reduce local inflammatory and pain symptoms in autoimmune diseases like RA, without unwanted side effects in the CNS. The nanoparticles of choice for the experiments in the present chapter were semiconductor QDs, due to their excellent optical properties and their great potential in biomedical fields [11]. In this work, spantide I, a peptide NK₁R antagonist, was coupled to amino-PEG shielded QDs and tested for specific cell binding in *in vitro* tests with NK₁R positive CHO cells. For QD coupling, a sulfhydryl group was introduced in the amino acid sequence of the peptide [12]. The chemistry used for spantide I coupling to amino-PEG shielded QDs and subsequent nanoparticle characterization are presented in this chapter. In this context, amino-PEG QDs from different companies were used for spantide I coupling

to investigate whether the source of nanoparticles has an impact on nanoparticle charge properties, on coupling efficiency, and finally on specific or unspecific binding to target cells.

Materials and Methods

All chemicals were purchased from Sigma Aldrich (Taufkirchen, Germany) in analytical grade or higher if not stated otherwise. Dulbecco´s phosphate-buffered saline (DPBS) pH 7.4 was composed of 1.5 mM KH$_2$HPO$_4$, 2.7 mM KCl, 138 mM NaCl. Nanoparticle binding buffer for FACS analysis was composed of 20 mM Tris, 150 mM NaCl, 2 mM CaCl$_2$, 1 mM MgCl$_2$, 1 mM MnCl$_2$ and 10% FCS, pH 7.4. Ultrapure water was obtained from a Milli-Q water purification system (Millipore, Billerica, MA, USA).

Dr. Ralf Schwandner (Amgen Research GmbH, BioPark Regensburg) kindly provide a stable transfected neurokinin-1 receptor expressing CHO cell line. Cells were grown in DMEM:F12 (1:1) medium with 1.2 g/l NaHCO$_3$, 15 mM HEPES, 1% Penicillin-Streptomycin, 10% FCS and 600 µg/ml hygromycin B (Carl Roth, Karlsruhe, Germany) supplementation.

Peptide ligands, spantide I (D-Arg[1], D-Trp[7,9], Leu[11])-Substance P, a neurokinin-1 receptor antagonist, and angiotensin I (1-9) trifluoroacetate salt, an agonistic precursor peptide for angiotensin II receptor targeting (AT$_1$R), were ordered from Bachem (Bubendorf, Switzerland).

Yellow to red emitting amino-PEG-QDs were ordered from different companies. Qdots® 655 ITK™ amino (PEG) CdSe/ZnS core shell QDs in 50 mM borate, pH 8.3, FWHM <30 nm, quantum yield >80% were ordered from Life Technologies/Thermo Scientific (Darmstadt, Germany). Orange amino (PEG) CdSe/ZnS core shell QDs (QSA-620) in water, FWHM <25 nm, quantum yield >50% and orange carboxy CdSe/ZnS QDs (QSH-620) were ordered from Strem Chemicals Inc. (Kehl, Germany) (Figure 1). Yellow amino (PEG) CdSe/ZnS core shell QDs (QSA-580) in water, FWHM <25 nm, quantum yield >50% and red amino (PEG) CdSSe/ZnS core shell QDs (QSA-665) in water, FWHM <35 nm, quantum yield >50% were ordered from Ocean NanoTech (San Diego, USA).

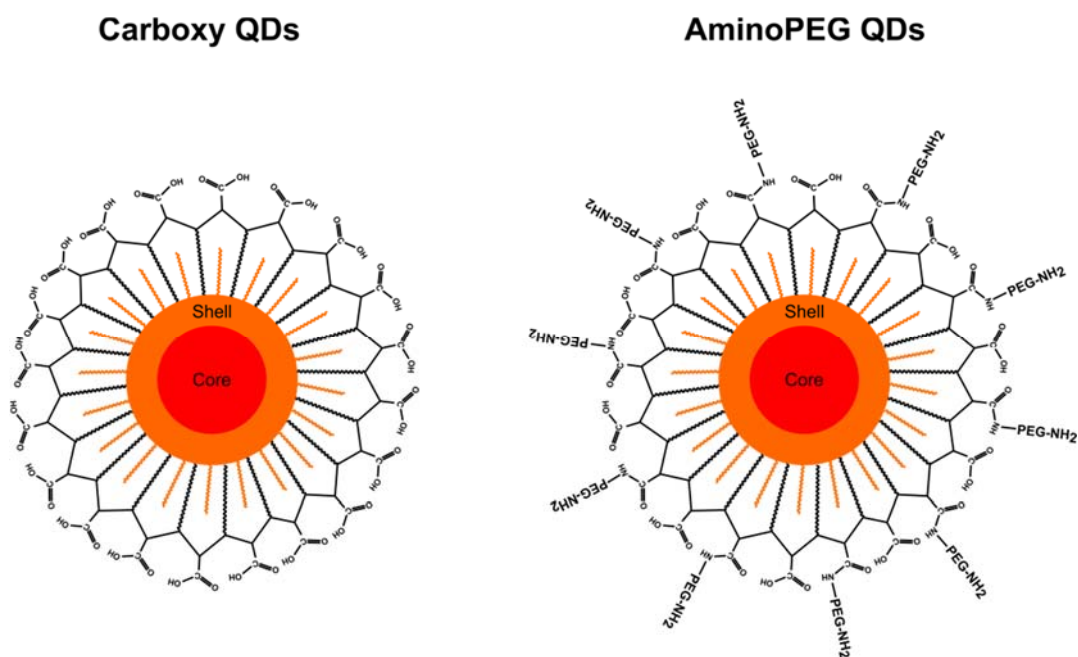**Carboxy QDs**   **AminoPEG QDs**

Figure 1: Yellow to red emitting QDs consist of a Cd(S)Se core and a ZnS shell. The organic layers are formed by a monolayer of oleic acid/octadecylamine (shown in orange) and a monolayer of amphiphilic polymer (shown in black). The thickness of the organic layer of carboxy QDs (Left: QSH-QDs) is 4 nm and for amino-PEG QDs (Right: QSA-QDs) is about 6 nm, according to the manufacturer. The hydrodynamic size is 8–10 nm larger for carboxy QDs and 12–14 nm larger for amino-PEG coated QDs than their respective inorganic core sizes (Figures are adapted from Strem Chemicals Inc. product catalog and [13]).

Nanoparticle modification for peptide coupling

For ligand to amino-PEG-QD coupling, the heterobifunctional linker chemistry with sulfo-SMCC (Sulfosuccinimidyl-4-(*N*-maleimidomethyl) cyclohexane-1-carboxylate) was used to make the particles reactive for covalent thiol group coupling [14]. The sulfo-NHS ester group of the sulfo-SMCC-linker reagent is an amine reactive group for QD activation against sulfhydryl-containing ligands. Such ligands can be coupled in form of a Michael addition reaction to the maleimide group (Figure 2).
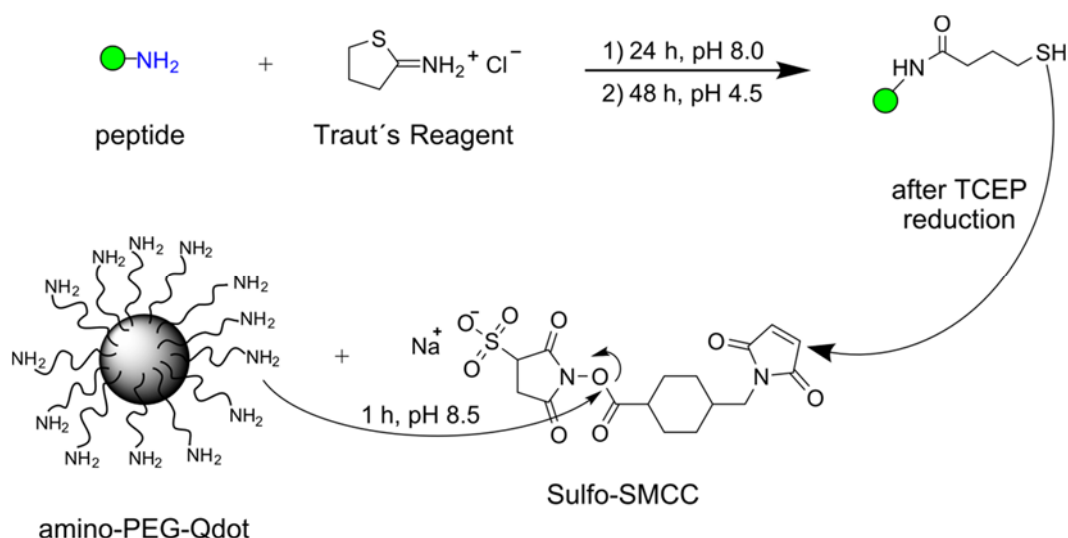
Figure 2: Pattern of peptide and QD functionalization for thiol-free peptide ligands. Thiolated peptides were coupled in a Michael addition to maleimide functionalized PEGylated QDs.

All reaction steps were carried out in LoBind Eppendorf tubes to minimize peptide and particle adsorption to the vial material. For a single coupling reaction, 160 pmol QDs were mixed with sulfo-SMCC linker reagent in 1000-fold excess. The reaction took place in a total volume of 200 μl in 50 mM borate buffer pH 8.5 for 1 hour at room temperature under gentle shaking. To separate unreacted sulfo-SMCC from activated QDs, a size exclusion chromatography with a disposable Sephadex G-25, PD-10 column (GE Healthcare, Munich, Germany) was performed. PBS buffer was used as mobile phase. Quantum dot fluorescence containing fractions were collected.

Peptide thiolation for nanoparticle coupling

Because there are no thiol groups in all neurokinin-1 receptor antagonists, e.g. spantide I and also angiotensin receptor agonists, e.g. angiotensin I and II, sulfhydryl groups were introduced using 2-iminothiolane (Traut´s reagent), which is reactive with α- or ε-amine groups (Figure 2). The Traut´s reagent can be used within a pH-range of 7–10 and preserves the positive charge of peptide ligands to keep them soluble. For one thiolation reaction, about 2 mg peptide was weighted in a LoBind Protein Eppendorf tube and solubilized in 0.1 M borate buffer, 1 mM EDTA, pH 8.0 to a highly concentrated stock solution of 4 mM. The Traut´s reagent was diluted in the same borate buffer and subsequently added to the peptide

in 2.5-fold excess. The reaction was performed in a glass vial with a magnetic stirrer at room temperature for 24 h at pH 8.0. To avoid the formation of N-substituted iminothiolane, the product was acidified to pH 4.5 by adding a small volume of acetic acid. Afterwards the excess of not reacted 2-iminothiolane was removed by a 48 h dialysis. For this purpose, a 1 ml Float-A-Lyzer® G2 dialysis unit with a molecular-weight cutoff (MWCO) of 100-500 Da was used in 300 ml dialysis buffer. Two different acidic sodium acetate dialysis buffers were used. The first one consisted of 50 mM sodium acetate and 1 mM EDTA, pH 4.5 and the second one consisted of a 10-fold reduced sodium acetate concentration of 5 mM. Each buffer was changed twice during 48 hours dialysis.

Determination of peptide thiolation efficiency by RP-HPLC

To separate sulfhydryl-containing peptides from non-thiolated peptides, a gradient RP-HPLC was performed. A C18(2) column with 100 Å particle diameter and pore size of 5 μm, 250x4.6 mm was used (Phenomenex, Luna®, Aschaffenburg, Germany). The mobile phase was a mixture of water + 0.1% TFA (A) and acetonitrile + 0.1% TFA (B). The gradient was run from 40% B to 60% B within 15 min and returned to 40% B within 7 min for thiolated spantide I and from 10% B to 70% B within 15 min and back to 10% B within 7 min for thiolated angiotensin I. Prior to the sample injection, the system was run for 3 min with the initial mobile phase mixture. The oven temperature was set to 35°C and flow to 1 ml/min. The peptides (spantide I and angiotensin I) were detected at 280 nm and 275 nm, respectively, because. 2-iminothiolan was detected via UV-Vis at 248 nm.

Quantification of sulfhydryl groups via Ellman´s assay

After dialysis and proof of Traut´s reagent complete removal by RP-HPLC, the amount of sulfhydryl groups was determined using an Ellman´s assay. The Ellman´s reagent (DTNB = 5.5'-dithio-bis-[2-nitrobenzoic acid]) reacts quantitatively with free sulfhydryl groups in their reduced form. For sulfhydryl quantification, the resulting yellow product was detected at 412 nm. An L-Cysteine hydrochloride standard curve served for quantification.

Peptide ligand to nanoparticle coupling

Prior to use of the peptide for QD coupling, 60 nmol of the thiolated peptide were reacted with 35-fold molar excess of the disulfide reducing agent tris (2-carboxyethyl) phosphine (TCEP) for 30 min under gentle shaking. In parallel, 6 to 12 nmol of reduced peptide were immediately added to Sulfo-SMCC activated QDs. The pH was checked and found to be at 7.0-7.5 and the mixture was reacted for 1 h at room temperature. Unreacted maleimide groups were inactivated by adding 5 µl of 1:1000 diluted 2-mercaptoethanol to the reaction and reacted for a further 30 min. The following purification procedure consisted of alternating ultrafiltration and size exclusion chromatography steps. An Amicon ultrafiltration unit with an MWCO of 100 kDa (Millipore, Billerica, MA, USA) was used to remove unreacted peptide and 2-mercaptoethanol by centrifugation for 10 min at 1500xg, using a swinging rotor, followed by a size exclusion purification using a Sephadex G-25, PD-10 column (GE Healthcare, Munich, Germany) and a further equivalent ultrafiltration step. The resulting concentrated sample was quantified by fluorescence measurement in 96-well plate format, calibrated against unreacted QD dilutions, using a FluoStar Omega fluorescence microplate reader (BMG Labtech, Ortenberg, Germany). Depending on the QDs used, various excitation and emission wavelengths were used.

Agarose gel electrophoresis

The peptide ligand modification of amino-PEG coated QDs was followed by agarose gel electrophoresis, which is a common strategy to characterize the electrophoretic mobility of nanoparticles due to their PEG shell size and charge characteristics. Therefore, a 0.5% agarose gel was prepared in basic TAE buffer. In each gel pocket, 1 pmol of QD sample was loaded before and after ligand functionalization. The electrophoresis was run at 80 Volt in TAE buffer for 2 hours. In the case of smaller and more mobile carboxy-QDs (QSH-620) without PEG coating, the gel was run for only 10 min. The localization of QDs in the gel was observed by UV illumination.

TEM images of quantum dots before and after coupling

2 x 1 µl of 60 mM QD solution in water were fixed on TEM grids. Although QDs show high self-contrast, they were stained with 2 x 1 µl 1% phosphotungstic acid, pH 7.

Zeta potential

Zeta potential measurements were performed with dynamic light scattering using a Zetazizer instrument (Malvern, Herrenberg, Germany). The QDs were diluted in water and filled in a clear disposable zeta potential cuvette.

Flow cytometry analysis for nanoparticle binding and uptake

Red (QSA-665) or yellow (QSA-580) QD samples (Ocean NanoTech, San Diego, CA, USA) in 20 nM concentration, either spantide I-modified with and without antagonist excess for nanoparticle displacement (10 µM spantide I or 10 µM aprepitant) or non-modified QDs as a check for unspecific binding were diluted in binding buffer. CHO-NK₁R positive cells were seeded in a 24-well plate in a cell density of 10^6 and grown for 48 hours. The cells were washed with warm DPBS and then incubated with pre-warmed nanoparticle solutions for 1 hour at 37°C, with 5% CO_2 for nanoparticle binding and uptake. The solutions were aspirated and the cells were washed with warm DPBS, harvested by trypsinization for 5 min at 37°C. After adding the double volume of 10% FCS in Leibovitz, the cell suspensions were spun down at 200 g for 5 min at 4°C. Cell pellets were washed with ice cold DPBS and centrifuged again at 200 g for 5 min at 4°C. For FACS analysis, the cells were resuspended in cold PBS and stored on ice until measurement at a FACSCalibur flow cytometer (Becton Dickinson, Franklin Lakes, NJ, USA). Red QSA-665 and yellow QSA-580 QDs were excited at 488 nm and emission was detected in the FL3 channel with a 670 nm longpass filter for red and FL2 channel with a 585 nm/42 nm band-pass filter for yellow QDs. Flow cytometry data were analyzed by Flowing Software version 2.5 (Turku Centre for Biotechnology, Turku, Finland). The geometrical mean of fluorescence values was determined for 10^5 counts from fluorescence histograms and the background was corrected by control cells without QDs. One-way analysis of variance (ANOVA) statistical analysis

was carried out with SigmaPlot 12.5 with pairwise multiple comparison procedures (Holm-Sidak method) with $P<0.05$.

Fluorescence microscopy for nanoparticle binding and uptake

The unmodified and spantide I-modified QDs were tested for cellular binding and uptake by fluorescence microscopy and to determine whether a competing free antagonist reduces cell binding. CHO-NK1R positive transfected cells were seeded into 8-well microscopy μ-slides (Ibidi, Martinsried, Germany) at a cell density of 10^5 cells per well and grown for 48 hours at 37°C and 5% CO_2. After washing the cells with warm DPBS, pre-warmed 10 nM QD samples in Leibovitz´s medium supplemented with 0.1% BSA were added onto the cells and incubated for 1 hour at 37°C and 5% CO_2. The cells were washed with DPBS and finally covered with Leibovitz´s medium for microscopy with a Plan-Apochromat 63x/1.4 Oil objective of a Zeiss Axiovert 200 microscope with heating unit and an LSM 510 laser-scanning device (Zeiss, Jena, Germany). Quantum dots were excited with a 488 nm argon laser and emission was detected using a band-pass filter 560-615 nm.

Results and discussion

Determination of thiolation efficiency of spantide I and angiotensin I by gradient RP-HPLC

After one hour of thiolation of spantide I, only 19.5% of total peptide contained a thiol group (Figure 3). Therefore, the thiolation reaction was prolonged to 24 hours. After removal of unreacted 2-iminothiolan by dialysis, the yield of thiolated peptide increased to 59%. The removal of unbound 2-iminothiolan is an essential step, since it is known that Traut´s reagent interacts with Ellman´s detergent and distorts thiol quantification by Ellman´s assay.
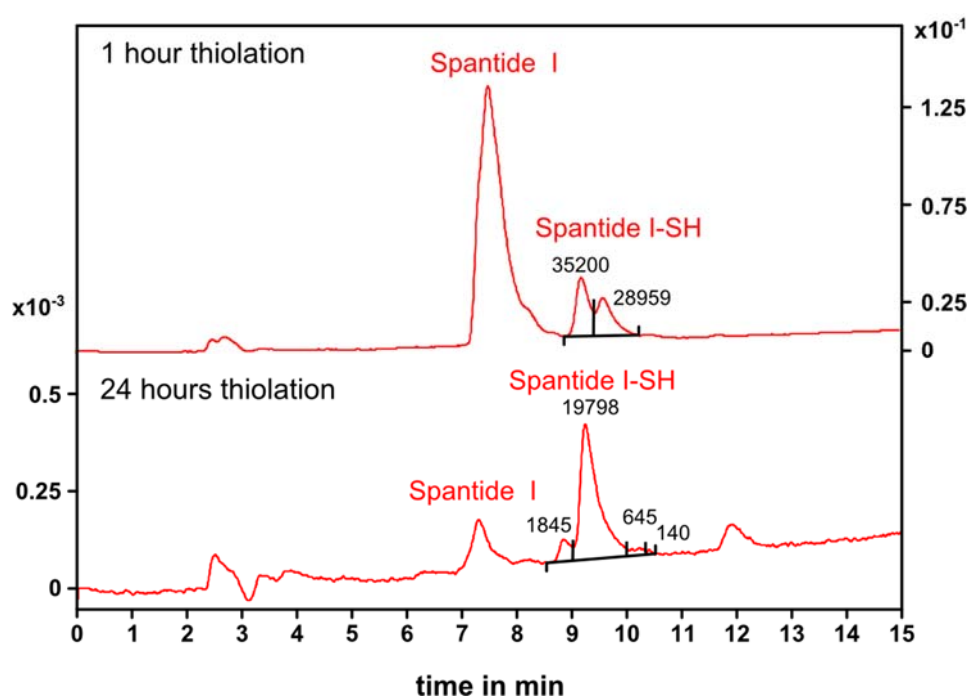
Figure 3: Comparison of gradient RP-HPLC of spantide I after 1 hour and 24 hours thiolation. The gradient run took 15 min from 40% acetonitrile to 60% with 0.1% TFA. Spantide I was detected by tryptophan absorbance at 280 nm. Peak integration for total peptide and only thiolated peptide give information about thiolation efficiency and offers the opportunity to compare with data obtained from Ellman´s assay. After 24 hours thiolation the proportion of thiolated to non-thiolated spantide I shifted to the thiol-product side.

The quantification of peptide was accomplished by integration of free spantide I in different concentrations to get a standard curve out of the area calculated under the curves. Reacted spantide I was run with the same gradient integrated in the same manner to calculate total peptide amount, thiolated, and non-thiolated spantide I. The chromatogram of the thiolated spantide I sample was integrated after 24 hours from minute 8.5 to 10.5 to calculate thiolated peptide amount and relate it to total peptide amount by integration from minute 6.5 to 10.5 (Figure 3). It was found that 59% of total peptide contains thiol groups.

For angiotensin I, 93% peptide related thiol groups were observed (Figure 4). Peak shoulders for spantide I indicated different peptide species with more than one thiol group, which was also confirmed by HPLC-MS analysis. In contrast, the thiolation of angiotensin I was very efficient and only mono-thiolated products were detected.
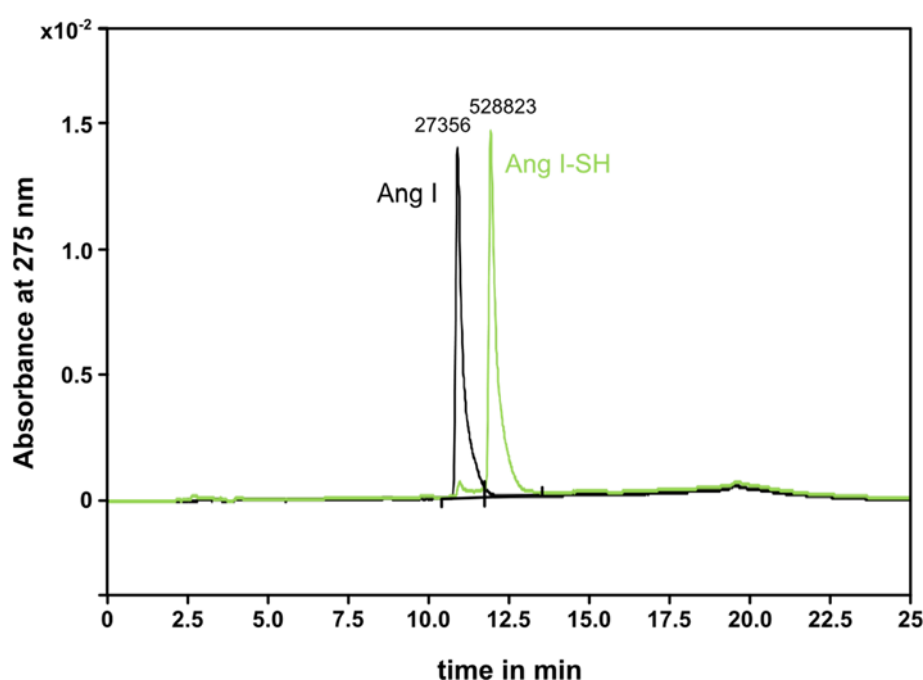
Figure 4: Gradient RP-HPLC of angiotensin I after 24 hours thiolation and acidic dialysis. The gradient run took 25 min from 10% acetonitrile to 70% with 0.1% TFA. Thiolation efficiency is 93% for angiotensin I. Only one mono-thiolated product is formed.

The gradient RP-HPLC offered a quality check for the successful removal of unreacted Traut´s reagent and unwanted cyclic N-substituted 2-iminothiolane at an absorbance of 248 nm (Figure 5). Compared to the thiolated product without acidic dialysis, there is no

unbound and N-substituted 2-iminothiolane present after 48 hours acidic dialysis. Therefore an acidic dialysis is highly recommended to reach a pure thiolated product on the one hand and to hydrolyze N-substituded 2-iminothiolane products to prevent the loss of sulfhydryl groups due to ring formation at basic pH values on the other hand [15].
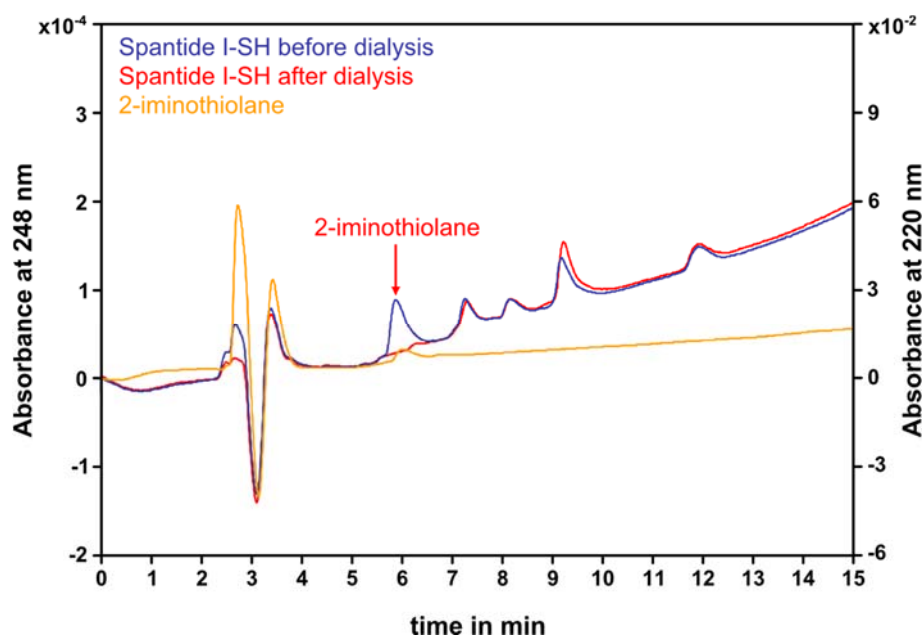

Figure 5: Dialysis is an efficient method for removing unreacted Traut´s reagent and avoiding the formation of N-substituted 2-iminothiolane. Thiolated spantide I, before and after dialysis was detected at 248 nm and free 2-iminothiolane was detected at 220 nm.

Thiol group quantification by Ellman´s assay

The differential spectra of Ellman´s reagent reacted thiolated spantide I and angiotensin I showed that, after acidic dialysis, the absorbance maximum at 248 nm is drastically decreased and the tryptophan absorbance peak at 280 nm becomes more prominent for spantide I (Figure 6). In contrast, the absorbance peak at 412 nm is lowered, which is also a hint for the successful removal of unreacted 2-iminothiolane by the dialysis process. The quantified thiolated peptides were used for the coupling reaction with Sulfo-SMCC activated amino-PEG coated QDs.
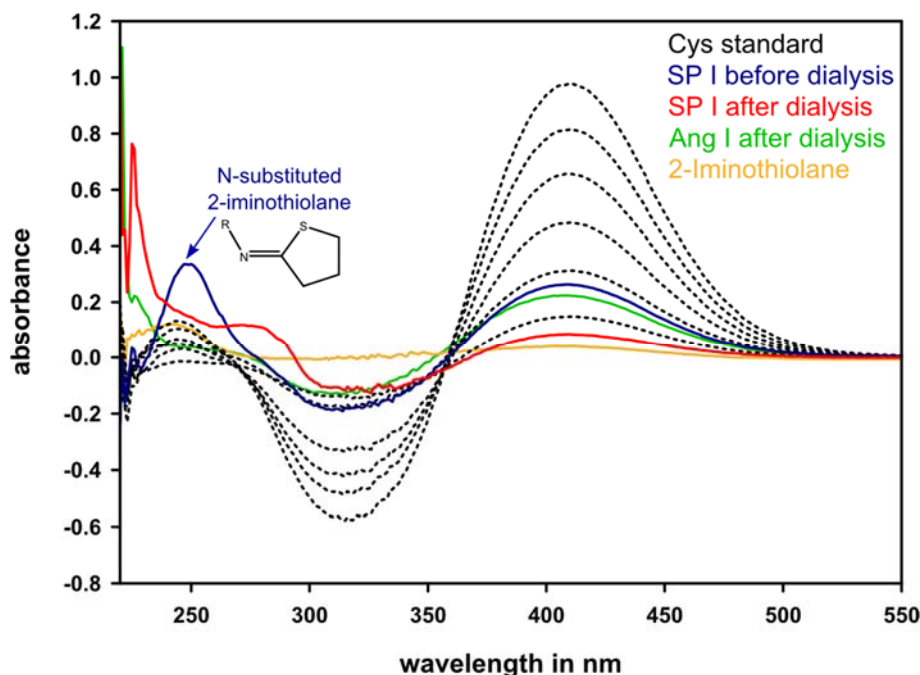
Figure 6: Differential spectra of spantide I and angiotensin I samples reacted with Ellman´s reagent. Thiols were quantified at 412 nm by using an L-Cystein hydrochloride standard curve (0.25 to 1.5 mM). Unreacted 2-iminothiolane can be successfully removed by acidic dialysis.

Nanoparticle characterization by gel electrophoresis

Small negatively loaded and not PEGylated Carboxy-QDs run, because of their negative surface charge, within a short time frame of 10 min to the positive pole; they were detected as a narrow band (Figure 7). Amino-PEG modified QDs were able to run in both directions of the gel, depending on their PEG shell properties [16]. This would be expected, since low molecular weight amino-PEG chains cannot completely cover underlying negatively charged carboxy groups on the QD core and run, therefore, like pure Carboxy-QDs to the positive pole, but with less speed. With an increasing PEG chain length, these negatively charged carboxy groups become counterbalanced by the charge properties of amine groups at the ends of PEG chains and the QDs move to the negative pole. If peptide ligands are coupled to amine groups of QDs, the charge and size properties change, and the particles consequently move differently in the gel, compared to unmodified QDs. The literature mentions that the movement in the gel is pH independent [17]. Amino-PEG QDs of different distributors (Life Technology, Strem Chemicals Inc., and Ocean NanoTech) show different
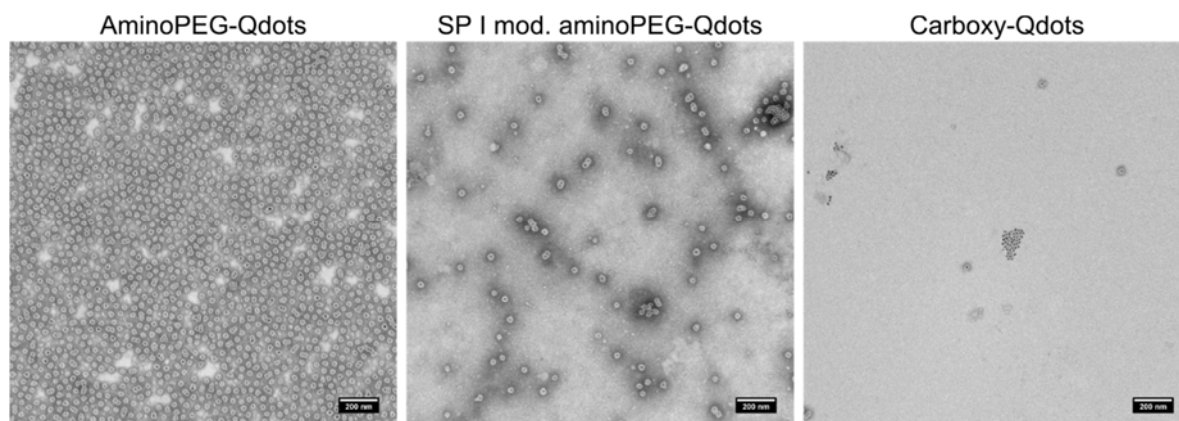
characteristics. Life Technology QDs have a lower PEG density, compared to Strem Chemicals Inc. and Ocean NanoTech QDs. The latter have similar characteristics.

Figure 7: Agarose gel electrophoresis (0.5% agarose). Amino-PEG QDs of different distributors showed different mobility properties within 2 hours at 80 V. Independent from coupled peptide (spantide I or angiotensin I) coupling, the moving directions were changed for QSA-620 QDs and red QSA-665 QDs, but not for 655 ITK™ QDs and yellow QSA-580 QDs. Smaller sized carboxy-functionalized QDs moved to the anode within 10 min.

TEM images of quantum dots before and after coupling

Based on TEM imaging, it was found, that only moderate aggregation occurs for amino-PEG QDs after ligand coupling (Figure 8). A corona is visible for the PEGylated QDs, which could be due to the quite dense PEG shell, surrounding the dark QD core. The QDs show the expected core size of 10 nm. Carboxy QDs without PEG shell had a higher tendency to aggregate and were therefore not equally distributed, compared to amino-PEG-QDs. Also, for spantide I-modified QDs, islands of aggregated particles occurred (Figure 8). Since it is known that the ideal size for interaction with cells is 40–50 nm, QDs fit perfectly due to their hydrodynamic size in this size range [18].

| AminoPEG-Qdots | SP I mod. aminoPEG-Qdots | Carboxy-Qdots |

Figure 8: TEM images of amino-PEG QDs (Strem Chemicals Inc.), before and after modification with spantide I and naked carboxy QDs.

Zeta potential

All used unconjugated QD species had negative zeta potentials (Figure 9): Quantum dots from Strem Chemicals: Carboxy QDs: -46.5 mV ± 7.8 (according to manufacturer: -30 mV to -50 mV), amino-PEG-QDs: -5.6 mV ± 4.5 (according to manufacturer: -20 mV to +10 mV). Quantum dots from Ocean NanoTech: Red QSA-665 amino-PEG-QDs: -5.9 mV ± 11.8 and yellow QSA-580 amino-PEG-QDs: -18.0 mV ± 5.9. After peptide ligand modification, the zeta potentials changed. Angiotensin I-modified QDs showed a more negative zeta potential of -26.8 mV ± 12.7 compared to unmodified amino-PEG-QDs, whereas spantide I-modified QDs tended to have less negative zeta potentials or even a positive potential, depending on the QDs used. For Strem Chemicals QDs, a zeta potential of 2.1 mV ± 7.0 was measured, and for red and yellow Ocean NanoTech QDs, potentials of 4.1 mV ± 7.6 and 5.4 mV ± 6.3 were observed, respectively. These findings were reasonable, as there is a gain of free carboxy groups for angiotensin I-modified QDs because of the unprotected C-termini of the peptide ligands. This is not the case for spantide I, because of its amidation of the C-terminal amino acids and the higher content of positively charged amino acids like lysine and arginine.
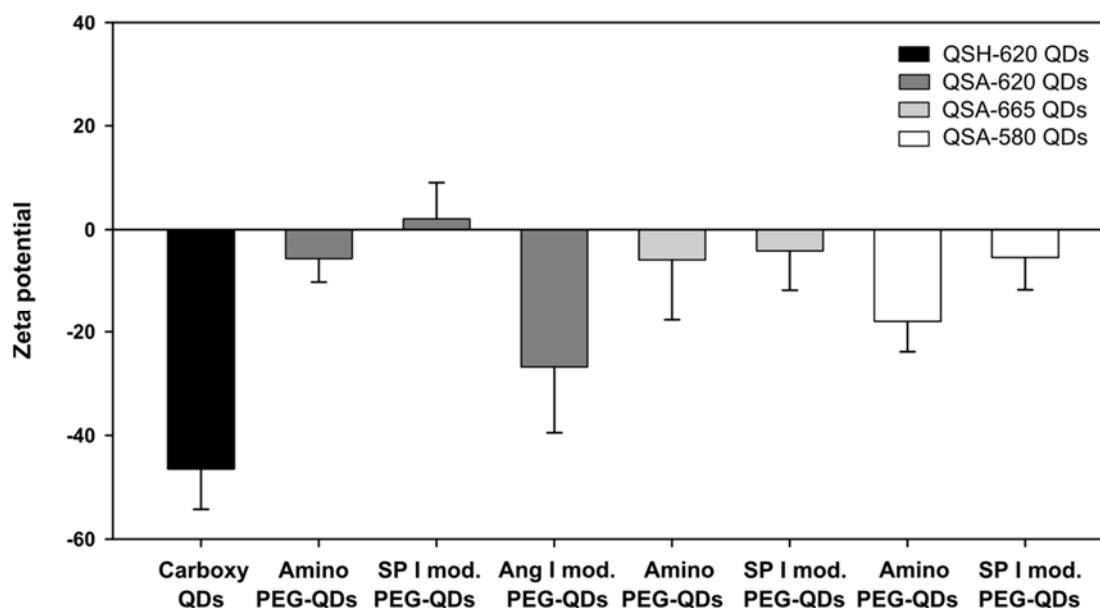
Figure 9: Zeta potentials of unmodified amino-PEG-QDs are slightly negative and become more negative after angiotensin I coupling, whereas spantide I-modified QDs tended to have less negative zeta potentials or even a positive potential, depending on the QDs used. Non-PEGylated carboxy QDs are shown as a control.

FACS analysis

For quantitative analysis of nanoparticle binding and uptake, different spantide I-modified QDs were tested by flow cytometry with CHO-NK$_1$R cells (Figure 10). It was found that the red QDs, which have shown different mobility in agarose gel electrophoresis after ligand coupling have a significant specific receptor binding in contrast to yellow QDs, where the mobility in agarose gel electrophoresis was unchanged and indicated non-efficient spantide I coupling (Figure 7C). A high unspecific nanoparticle binding was observed for unmodified amino-PEG QDs. A phenomenon that was observed for all amino-PEG QDs obtained from different distributors. A simple explanation could be a charge dependent effect that is also mentioned by other working groups, in particular beside negatively charged particles for positively charged particles, compared to neutral particles [2].
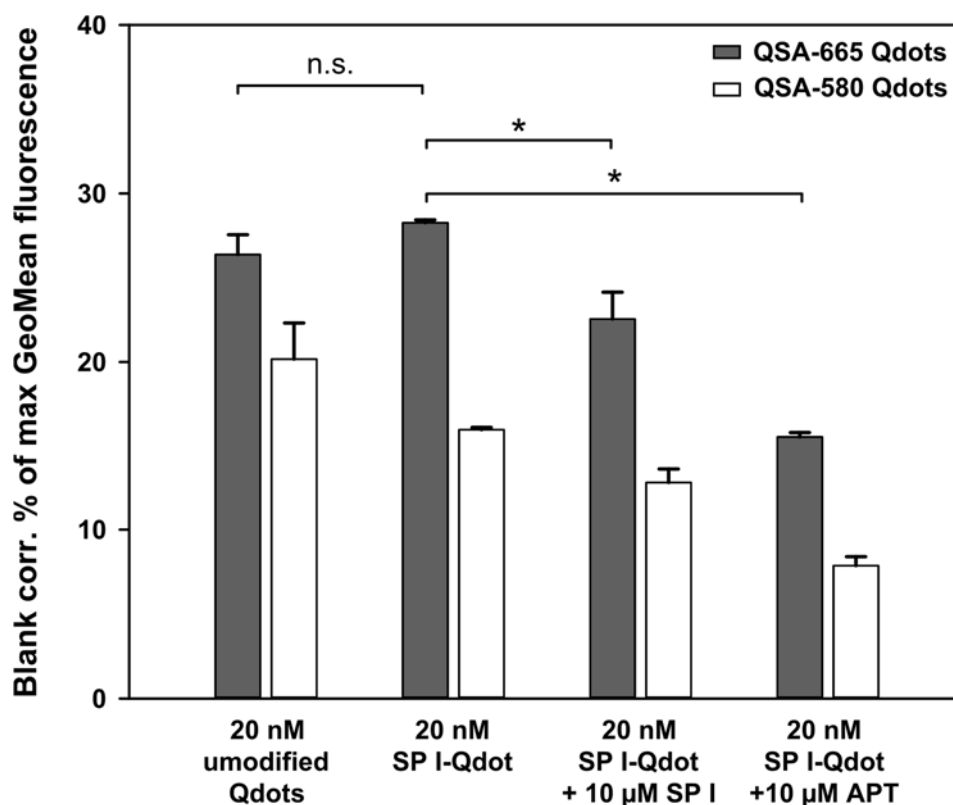
Figure 10: FACS analysis showed that spantide I-modified QDs can be displaced by the free NK₁R antagonists spantide I and aprepitant, which indicated specific binding of red spantide I coated QSA-655 QDs. Yellow spantide I coated QSA-580 QDs showed the same tendency, but here the test for significance was negative, which could be explained by inefficient ligand labeling. The unspecific binding of unmodified QDs to CHO-NK₁R cells is similar to NK₁R specific binding of spantide I-modified QDs.

Ligand specific uptake of peptide coupled quantum dots

It is well known from literature data that unspecific QD uptake depends on particle size, charge, and shape, even if the particles are shielded by a PEG corona [19]. The data, obtained by fluorescence microscopy, showed that most particle fluorescence was obtained by unmodified amino-PEG QDs (Figure 11). This result confirmed the hypothesis for unspecific nanoparticle uptake, driven by free exposed amine groups on the nanoparticle surface [20]. One hurdle of such nanoparticle uptake studies is that it is quite difficult to discriminate between unspecific pinocytosis and receptor mediated internalization [19,21]. One method for detecting GPCR mediated nanoparticle binding and uptake is to perform a displacement experiment by the addition of a competitive free antagonist to the receptor

positive cells. In the present experiment, only a limited reduction of neurokinin-1 receptor mediated binding and uptake could be obtained by the addition of free spantide I to spantide I-modified QDs in the displacement study.
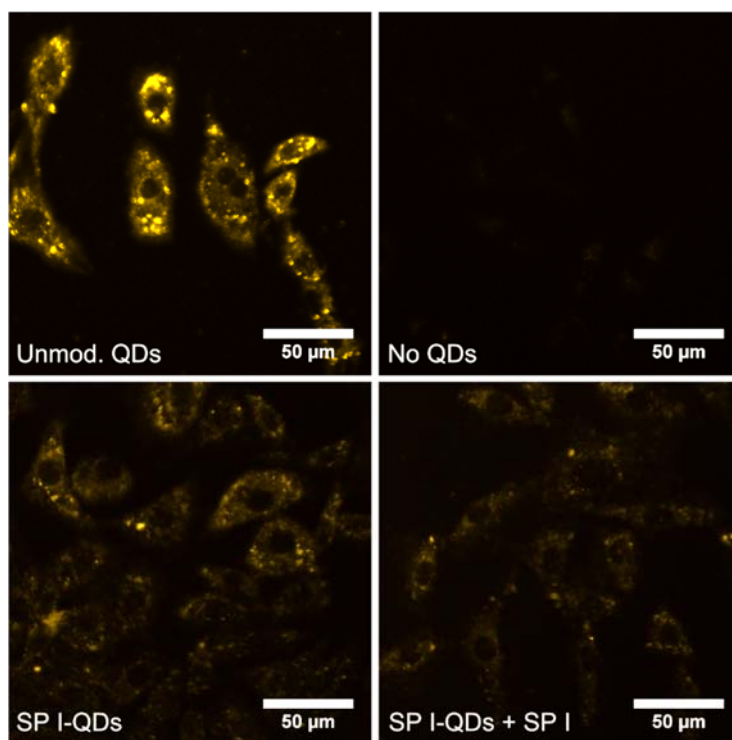
Figure 11: Fluorescence microscopy images of QD uptake in neurokinin-1 receptor positive CHO cells. A high unspecific uptake was observed for unmodified amino-PEG-QDs (Strem Chemicals Inc.). NK₁R-mediated binding could not be confirmed for certain by reduced nanoparticle binding if free ligand was added as a competitor to cells.

Conclusion

The introduction of thiol groups into cystein-free peptide ligands is a common strategy for water-soluble ligands to couple them to maleimide functionalized nanoparticles, like QDs. It was found that thiolation reaction is quite efficient for the very hydrophilic angiotensin I, whereas it is highly reduced for spantide I, although there are two different modification sites for 2-iminothiolane. In other experiments (data not shown), zero thiolation was produced in the trial to introduce sulfhydryl groups in shorter and more hydrophobic spantide variants. In nanoparticle uptake experiments with receptor positive CHO-NK₁R cells, high unspecific nanoparticle binding was examined for amino-PEG modified QDs. This unspecific binding was even stronger than the binding obtained for spantide I functionalized nanoparticles. In this context two aspects are discussed in the literature: Nanoparticle charge and PEG density seem to play a critical role for unspecific cell binding capacity. Here in particular, free amino-PEG groups showed high unspecific binding to cells. Unspecific nanoparticle binding strongly hampers the proof of concept of receptor mediated multivalent nanoparticle binding and uptake by GPCR. However, it could be shown in FACS displacement experiments with high concentrations of free competing antagonists that nanoparticle binding was inhibited, which indicates receptor mediated nanoparticle binding. The low thiolation efficiency for the peptide could be the main reason for a resulting low nanoparticle coupling propensity. In addition, double thiolated peptides could also be the reason for low ligand densities on the surface of nanoparticles. This also minimizes the chance for multivalent interactions. Since the C-terminal receptor interacting part of the peptide mainly consists of hydrophobic amino acids, there is also the chance for ligand inversion inside the PEG shell, a phenomenon that is also discussed for highly hydrophobic small non-peptide receptor antagonists [22].

Supplementary information

Excitation and emission spectra of the QDs, which were used in the FACS binding studies show, that there are no spectral shifts after ligand modification, which could have influenced the fluorescence properties (Figure 12 and Figure 13).
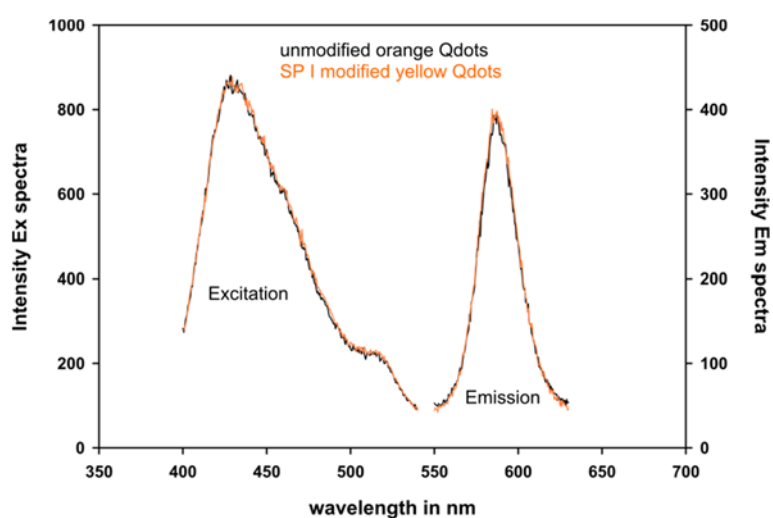

Figure 12: Excitation and emission spectra of yellow QSA-580 QDs before and after spantide I coupling. There are no spectral differences.
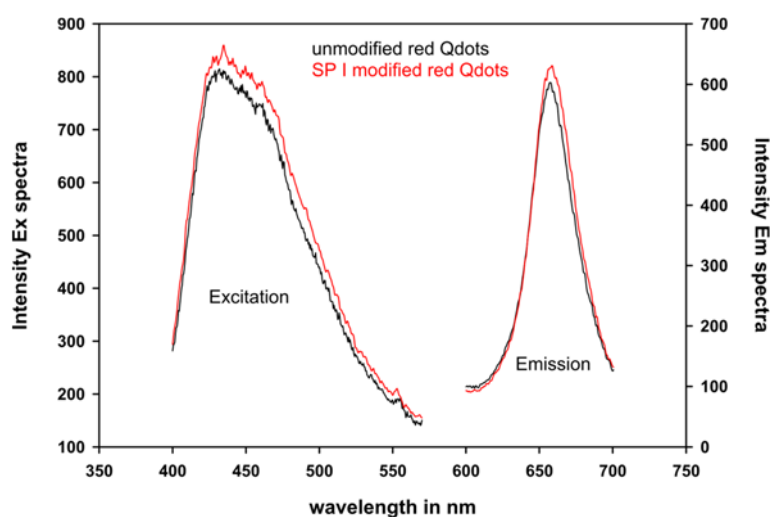

Figure 13: Excitation and emission spectra of red QSA-665 QDs before and after spantide I coupling. There are no spectral differences.

References

[1] Modery-Pawlowski CL, Sen Gupta A. Heteromultivalent ligand-decoration for actively targeted nanomedicine. Biomaterials 2014; 35: 2568–2579.

[2] Mout R, Moyano DF, Rana S, Rotello VM. Surface functionalization of nanoparticles for nanomedicine. Chem. Soc. Rev. 2012; 41: 2539.

[3] Delehanty JB, Boeneman K, Bradburne CE, Robertson K, Bongard JE, Medintz IL. Peptides for specific intracellular delivery and targeting of nanoparticles: implications for developing nanoparticle-mediated drug delivery. Therapeutic Delivery 2010; 1: 411–433.

[4] Hild W. G protein-coupled receptors function as logic gates for nanoparticle binding and cell uptake. Proceedings of the National Academy of Sciences of the United States of America (PNAS) 2010; 107: 10667–10672.

[5] Pearce TR, Shroff K, Kokkoli E. Peptide Targeted Lipid Nanoparticles for Anticancer Drug Delivery. Adv. Mater. 2012; 24: 3803–3822.

[6] Martinez-Veracoechea FJ, Frenkel D. Designing super selectivity in multivalent nano-particle binding. Proceedings of the National Academy of Sciences 2011; 108: 10963–10968.

[7] Tesauro D, Accardo A, Aloj L, Morelli G, Aurilio M. Receptor binding peptides for target-selective delivery of nanoparticles encapsulated drugs. IJN 2014: 1537.

[8] Irvine DJ. Drug delivery: One nanoparticle, one kill. Nat Mater 2011; 10: 342–343.

[9] Schöttler S, Landfester K, Mailänder V. Controlling the Stealth Effect of Nanocarriers through Understanding the Protein Corona. Angew. Chem. Int. Ed. 2016; 55: 8806–8815.

[10] Saraiva C, Praça C, Ferreira R, Santos T, Ferreira L, Bernardino L. Nanoparticle-mediated brain drug delivery: Overcoming blood–brain barrier to treat neurodegenerative diseases. Journal of Controlled Release 2016; 235: 34–47.

[11] Wang J, Han S, Ke D, Wang R. Semiconductor Quantum Dots Surface Modification for Potential Cancer Diagnostic and Therapeutic Applications. Journal of Nanomaterials 2012; 2012: 1–8.

[12] Hennig R, Pollinger K, Tessmar J, Goepferich A. Multivalent targeting of AT 1 receptors with angiotensin II-functionalized nanoparticles. Journal of Drug Targeting 2015; 23: 681–689.

[13] Yang L, Mao H, Wang YA, et al. Single chain epidermal growth factor receptor antibody conjugated nanoparticles for in vivo tumor targeting and imaging. Small 2009; 5: 235–243.

[14] Hermanson GT. Bioconjugate techniques.

[15] Singh R, Kats L, Blättler WA, Lambert JM. Formation of N-Substituted 2-Iminothiolanes When Amino Groups in Proteins and Peptides Are Modified by 2-Iminothiolane. Analytical Biochemistry 1996; 236: 114–125.

[16] Daou TJ, Li L, Reiss P, Josserand V, Texier I. Effect of Poly(ethylene glycol) Length on the in Vivo Behavior of Coated Quantum Dots. Langmuir 2009; 25: 3040–3044.

[17] Wang W, Ji X, Kapur A, Zhang C, Mattoussi H. A Multifunctional Polymer Combining the Imidazole and Zwitterion Motifs as a Biocompatible Compact Coating for Quantum Dots. J. Am. Chem. Soc. 2015; 137: 14158–14172.

[18] Jiang W, Kim, Betty Y. S., Rutka JT, Chan, Warren C. W. Nanoparticle-mediated cellular response is size-dependent. Nature Nanotech 2008; 3: 145–150.

[19] Kelf TA, Sreenivasan, V K A, Sun J, Kim EJ, Goldys EM, Zvyagin AV. Non-specific cellular uptake of surface-functionalized quantum dots. Nanotechnology 2010; 21: 285105.

[20] Liu W, Howarth M, Greytak AB, et al. Compact Biocompatible Quantum Dots Functionalized for Cellular Imaging. J. Am. Chem. Soc. 2008; 130: 1274–1284.

[21] Behzadi S, Serpooshan V, Tao W, et al. Cellular uptake of nanoparticles: journey inside the cell. Chem. Soc. Rev. 2017; 46: 4218–4244.

[22] Pearson RM, Sen S, Hsu H-j, et al. Tuning the Selectivity of Dendron Micelles Through Variations of the Poly(ethylene glycol) Corona. ACS Nano 2016; 10: 6905–6914.

Chapter 5

The challenge of site-specific ligand PEGylation in the synthesis of multivalently binding drugs

Abstract

Multivalent binding drugs can be designed using different scaffolds for individual modification with multiple equal or different ligand types, which are then able to bind multiple over-expressed GPCRs at the same time with high avidity. Examples for such scaffolds are branched PEGs, for example 8armPEGs or PEG-coated nanoparticles. The requirements for PEG scaffolds are that they have appropriate functional groups for ligand coupling on the one hand, and on the other hand that their chain lengths are ideal to reach multiple receptors in the cell membrane. The first requirement involves several challenges, which include that the PEG reaction site should be not localized in the receptor interacting region of the ligand and the PEGylation should be site-specific to hold the ligand´s binding affinity loss at a minimum. In this context, it was demonstrated, based on spantide I, a neurokinin-1 receptor peptide antagonist, that PEGylation can radically change the ligands´ binding properties to its receptor. It was found that, due to two possible reaction sites, double PEGylations occur if the PEG is used in excess. Besides changing the peptide to PEG ratio to the side of peptide excess, it is also possible to use protective groups to prevent double PEGylation. Interestingly, it was discovered that some peptide antagonists also show different agonistic potentials upon PEGylation in aequorin based luminescence calcium assays. Furthermore, it was found that the N-terminal region beside the C-terminal region seems to be somehow essential for receptor recognition and binding since truncation of the peptide also led to a loss in affinity.

Introduction

The conjugation of peptides and proteins to PEG is established as a common strategy to alter the pharmacokinetic profiles of drugs, and thereby improve their therapeutic potential [1]. There are several advantages of PEG conjugation: The circulation of drugs is prolonged because of the protection against enzymatic digestion, the filtration by the kidneys is slowed down and fewer neutralizing antibodies are generated [2–4]. One challenge of drug PEGylation is to overcome random multiple PEGylation to prevent a total efficacy loss of the drug due to steric interference with the drug-target binding interaction [5,6]. Multiple PEGylation takes place if more than one functional group for PEG coupling is present in the chemical structure of the drug molecule [7]. In the case of linear PEG chains, this would result in a substantial affinity loss, greater than for mono-PEGylated products. For branched PEG polymers, there is the additional aspect of intra- and intermolecular cross-linking. This fact should also be considered when drugs are coupled to the PEG chains of nanoparticles, like PEG-coated QDs. Multiple reaction sites for the PEG chains to one drug molecule result in a decreased drug modification rate of the particle on the one hand, which means a decreased number of ligands per particle; on the other hand, particle aggregation as a result of cross-linking can occur. These observations were made for different peptide ligands, such as the neurokinin-1 receptor. For example, besides its N-terminal α-amine group, spantide I also has an ε- amine group of a lysine side chain, which is likely to couple to NHS-ester functionalized PEGs. Single PEGylated products are gained either by use of an excess of free peptide ligand or by introducing a protective group for the N-terminal amine group, by acetylation, for example. If the N-terminal lysine containing part of the peptide ligand is not mandatory for receptor binding, it is also possible to use truncated peptide molecules. Both strategies have some disadvantages. For the first strategy, there is the need for a very efficient purification strategy to remove the excess of unreacted peptide ligands, which could cause interference in affinity measurements and disturb uptake experiments because free molecules compete with particle bound molecules. For the second strategy, missing positively charged residues cause the loss of solubility, which make chemistry in aqueous solution impossible. In summary, this chapter addresses chemical challenges concerning changes in the peptide´s amino acid composition, the covalent coupling of a PEG chain, and the influence of these chemical modifications on the biological activity the drug.

Materials and methods

All chemicals were purchased from Sigma Aldrich (Taufkirchen, Germany) in analytical grade or higher if not stated otherwise. Dulbecco´s phosphate-buffered saline pH 7.4 consisting of 1.5 mM KH_2PO_4, 8 mM Na_2HPO_4, 2.7 mM KCl, and 138 mM NaCl was purchased from Life Technologies/Thermo Scientific (Darmstadt, Germany). Full-length peptides, substance P-methyl ester and spantide I, were ordered from Bachem (Bubendorf, Switzerland). Short peptide versions (GlyShortSP I, LysShortSP I, and AcLysShortSP I) were synthesized by Synpeptide Co., Ltd. (Shanghai, China), see Table 1.

Table 1: Neurokinin-1 receptor agonists and antagonists

Peptide	Sequence
substance P-methyl ester	H-Arg-Pro-Lys-Pro-Gln-Gln-Phe-Phe-Gly-Leu-Met-OMe
spantide I	H-D-Arg-Pro-Lys-Pro-Gln-Gln-D-Trp-Phe-D-Trp-Leu-Leu-NH$_2$
GlyShortSP I	Gly-Pro-Gln-Gln-D-Trp-Phe-D-Trp-Leu-Leu-NH$_2$
LysShortSP I	Lys-Pro-Gln-Gln-D-Trp-Phe-D-Trp-Leu-Leu-NH$_2$
AcLysShortSP I	Ac-Lys-Pro-Gln-Gln-D-Trp-Phe-D-Trp-Leu-Leu-NH$_2$

Peptide truncation

There exist several N-terminal truncated short-version peptides of the neurokinin-1 receptor agonists and antagonists, so-called C-terminal fragments [8]. In particular, the short agonist versions of substance P (hexa(6-11)-, hepta(5-11)- and octa(4-11)-substance P) show equipotent or even more potent binding characteristics than the full version peptide [9,10]. This strengthens the assumption that the N-terminal peptide region is not essential for

neurokinin-1 receptor recognition and activation. Based on this fact, spantide I was modified in various ways to prevent double PEGylated products due to two possible PEGylation sites at the N-terminal α-amino group and ε-amino group of the lysine residue at position 3. One strategy was to eliminate the lysine residue through shortening the peptide sequence up to proline and replacing lysine with glycine for only the α-amino group. A further strategy was to keep the lysine group and protect the N-terminal amino acid with an acetyl group (Figure 1). All used peptides are listed in Table 1.
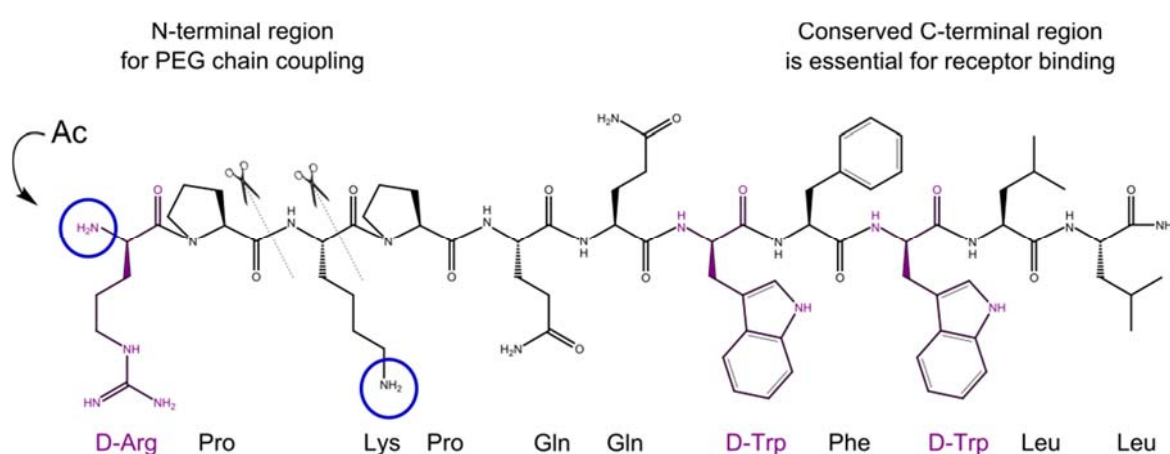
Figure 1: N-terminal peptide modification to prevent double PEGylated products. Spantide I was either truncated (positions are indicated by the scissors) or acetylated at the N-terminal amino group.

Peptide PEGylation: Coupling of peptides to linear and branched PEGs

It is known that the highly conserved and for receptor binding essential region of most peptide ligands for the neurokinin-1 receptor is located in the C-terminus of the peptide amino acid sequence. Therefore, a PEGylation strategy for amine-directed PEGylation was chosen. Using NHS-ester activated PEG-derivatives is a preferred chemistry for obtaining the modification of primary amines. Various commercially available functionalized PEGs are available on the market, such as various sized linear PEGs and branched multi-armPEGs, which could act beside different nanoparticles as scaffolds to obtain star-shaped

multivalently receptor binding antagonists after ligand coupling to the end of each PEG-arm [11–13] (Figure 2). These 8armPEGs consist of a hexaglycerol core structure synthesized by ethoxylation of hexaglycerol (JenKem Technology, Plano, Texas, USA). Succinimydyl succinate functionalization for 8armPEG20k was performed by Susanne Kirchhof, according to [14] and for mPEG5k by Luise Tomasetti from the Department for Pharmaceutical Technology (Universität Regensburg). For later synthesis, mPEG5k-NHS ester was bought from Rapp Polymere (Tuebingen, Germany).
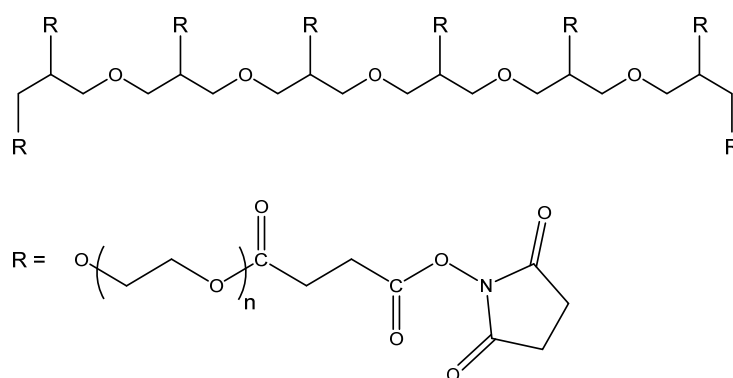
Figure 2: 8armPEG succinimidyl succinate with a hexaglycerol core structure. Arm chain length and final molecular weight are determined by the number of ethylene glycol units.

For PEGylation with linear mPEG5k, various PEGylation conditions were tried to observe the influence on peptide PEGyglation in respect to multiple-PEGylated products by changing molar ratios and site directed α- or ε-amine group PEGylation by changing pH-conditions from neutral to basic, respectively. For branched 8armPEGylation, the peptide concentration was generally used in excess (1:16) to prevent double PEGylation and cross-linking and to yield high peptide to PEG ratios (Figure 3). For these samples, a sufficient purification procedure was obligatory to completely remove unreacted peptide ligands. The standard molar ratio for linear PEGylation was 1:2 for peptide to PEG to ensure total PEGylation of peptide ligands and to enforce, in some cases, double PEGylation, e.g. for spantide I and unprotected Lys-terminal Short-spantide I. The PEGylation reactions were performed in 50 mM filtered borate buffer, pH 8.5. In one trial, this borate buffer was further adjusted with 1 M HCl to pH 7.0. Both components, peptide and PEG, were solubilized in a

high concentrated solution in the correspondent borate buffer and mixed 1:1 to the final concentrations of 4 mM linear PEG to 2 mM peptide. And in case of 8armPEG20k, 0.21 mM branched 8armPEG20k to 3.36 mM spantide I. The reactions were stirred overnight at room temperature in a thin glass vial. The reaction products were purified by size exclusion chromatography with a Sephadex-G25 column, PD-10 (GE Healthcare, Freiburg, Germany). The collected fractions were analyzed by a combination of tryptophan absorbance and emission measurements; also, PEG staining with iodine crystals in a TLC chamber was performed in parallel by pipetting 2 µl of each fraction on a TLC plate. The early eluting fractions, containing both peptide and PEG, were pooled and further purified by several ultrafiltration steps. Because of the high hydration capacity of PEG (two H_2O molecules per PEG unit), an MWCO of 10 kDa could be used for linear mPEG5k-peptide conjugates because their hydrodynamic radii increase up to 5- to 10-fold [2]. The same MWCO was used for branched 8armPEG20k-peptide conjugates to remove the much smaller unbound peptide molecules easily and efficiently.

8armPEG20k-SC

16 x spantide I
(primary amine)

RT, ~20h
pH 8.5
borate buffer

8 armPEGk-spantide I
(stable amide bond)

N-Hydroxy-
succinimide
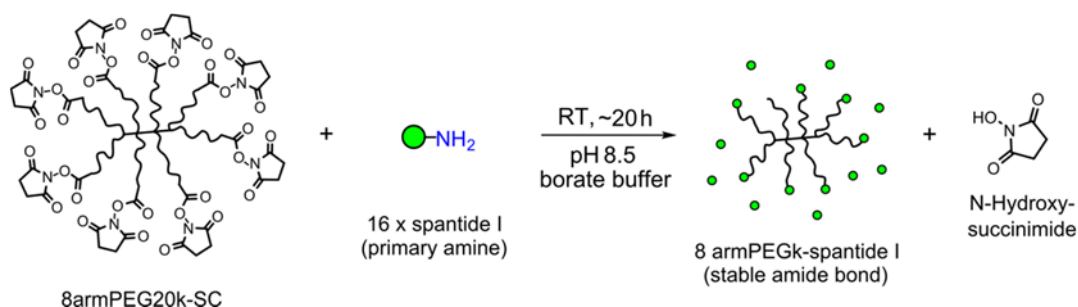
Figure 3: Peptide amine groups were coupled to NHS-ester functionalized PEGs. PEGylation reactions were performed at room temperature under gentle stirring over approximately 20 hours. For Lysine directed PEGylation, a basic borate buffer with pH 8.5 was used.

Determination of peptide to PEG ratio for 8armPEG-peptide conjugates

To determine how many ligands are bound per branched 8armPEG molecule after in-depth purification, the peptide and PEG were quantified in two separate calibration curve based assays in a 96-well format. The peptide was quantified via tryptophan emission and PEG via Child´s assay [15]. The molar ratio was calculated out of the results of both assays. For PEG-

quantification, 25 µl of a 0.1 N iodine solution (Carl Roth, Karlsruhe, Germany) were added to 50 µl of a 5% barium chloride solution in 1 M HCl, preloaded into a well of an absorbance well plate, were intensely mixed with 125 µl of PEG-sample (either PEG-standard or PEG-peptide conjugate), and were reacted for 20 min at room temperature. The absorbance was then detected at 535 nm (Figure 4).
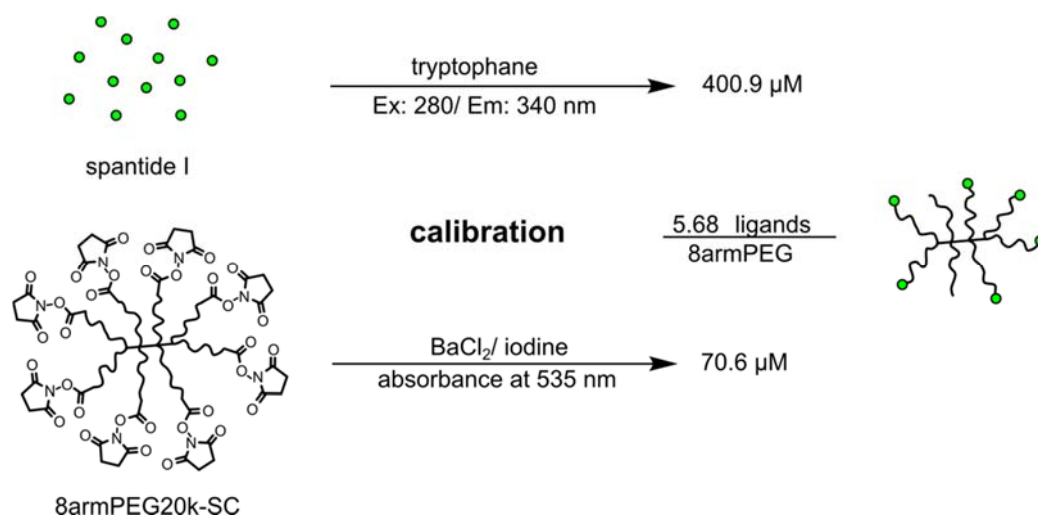

Figure 4: Peptide to PEG ratios were determined in two separate quantification steps. The ratios represent the ligand coupling quality.

PEG-peptide-conjugate analytics by RP-HPLC/HPLC-MS

To confirm the success of PEGylation for linear methoxyPEG-peptide-conjugates, an HPLC-MS analysis was performed to separate modified from unmodified and single from double PEGylated products by HPLC and assign the average masses to each obtained peak. Because of an increasing polydispersity with higher molecular weights, the HPLC-MS analysis was not possible for branched 8armPEG-peptide-conjugates. Thus, a reverse phase high performance liquid chromatography (RP-HPLC) method was developed especially for branched 8armPEG-peptide-conjugates to confirm the successful peptide to PEG coupling on the one hand, and to have a proof for efficient elimination of unreacted peptide by SEC and multiple ultrafiltration steps on the other hand. A Shimadzu Class VP HPLC system, composed of a LC-10ATvp pump, an SIL-10ADvp auto injector, a CTO-10 ASvp column

oven, an RF-10AXL flurorescence detector, and an SCL-10Avp system controller was used (all components: Shimadzu Europe GmbH, Duisburg, Germany). A C18 column with 300 Å, 5 μm (Vydac, 218 TP) was used as stationary phase for gradient elution within an optimized 35 min program from 40% to 60% acetonitrile with constant 0.1% TFA within 25 min. The peptide was detected by excitation at 280 nm, measuring the emission at 340 nm. For the highly hydrophobic peptide GlyShortSP I, an isocratic method could be established, using 40% acetonitrile and 60% water with constant 0.1% TFA. Both peptide and PEGylated peptide are eluting within 25 min (Figure 7).

PEG-peptide-conjugate analytics by Tricine-SDS-PAGE

PEGylation success for linear and even branched 8armPEG-peptide conjugates can be visualized also by a Tricine-SDS-PAGE, which is an SDS-PAGE with high resolution for especially small peptides. The method used was adapted from Hermann Schägger [16]. The gel consists of three superposed gels, with increasing acrylamide/bisacrylamide composition from the top to the bottom, starting with a 4% stacking gel, followed by a 10% spacer gel and a 16% separation gel. For each gel preparation, the appropriate volumes of 30% acrylamide solution (Rotiphorese® Gel A, Carl Roth) and 2% bisacrylamide solution (Rothiphorese® Gel B, Carl Roth) were mixed to obtain the desired polymer percentages. To start the radical polymerization, TEMED and 10% APS solutions were added. For the stacking and spacer gels, a 3x gel buffer was used for polymer dilution that consisted of 3 M tris, 1 M HCl, and 0.3% SDS, pH 8.45. An amount of 1 μg peptide or PEG was respectively loaded in separate gel pockets after mixing with a non-reducing loading buffer consisting of 3% SDS (w/v), 30% glycerol (w/v), 0.05% Coomassie and 150 mM Tris, adjusted to pH 7 with 1M HCl. For the gel electrophoresis, two buffers were used at the same time, separated by the inner and outer chamber of the gel chamber. The inner chamber was filled with a cathode buffer, consisting of 1 M Tris, 1 M tricine, 1% SDS, pH 8.25, which is the sample touching buffer while sample loading into the gel pockets. The anode buffer was made of 1 M tris and 0.225 M HCl to reach a pH of 8.9. This buffer was filled in the outer gel electrophoresis chamber. The initial voltage was set to 30 V to allow the samples to penetrate into the stacking gel. After 40 min, the voltage was increased to 200 V and run for 1 h 15 min. After electrophoresis, the gel was rested for 20 hours in a fixing solution, consisting of 50% methanol, 10% acetic acid, and 100 mM ammonium acetate, where the gel shrunk in size.

The Coomassie staining was performed in 0.025% Coomassie G-250 with 10% acetic acid for double the fixation time. Then the gel was bleached for 1 hour in 10% acetic acid and transferred to water. For subsequent iodine staining, the Coomassie stain was removed with 50% methanol in 50 mM ammonium hydrogen carbonate and washed several times in water. The iodine staining was obtained by 10 min incubation in 5% barium chloride solution and 15 min in iodine solution and 5–10 min in water.

Circular dichroism for peptide "secondary structure" determination

To exclude changes in the peptide conformation upon PEGylation, which could influence the peptide´s ability to bind into the receptor binding pocket, circular dichroism measurements were performed before and after PEGylation in water solution. The measurement took place under 6 l/min nitrogen flow and below 600 V high tension voltage of the lamp in the far UV region from $\lambda = 250 - 190$ nm, using a 2 mm quartz cuvette with a Jasco J-810 CD spectropolarimeter (Spectroscopic Co. Ltd, Tokyo, Japan). The obtained spectra were smoothed with a Savitzky-Golay algorithm, and the mean molar ellipticity was calculated.

$$\theta = \frac{CD * 100 * MW}{c * d * x}$$

Θ = mean residue ellipticity in deg*cm^2*dmol^{-1}

CD = measured value in mdeg

MW = molecular weight in kDa

c = concentration in mg/ml

d = layer thickness of cuvette in cm

x = number of amino acids per protein/peptide

Binding studies via Aequorin calcium assay

Neurokinin-1 receptor ligand binding studies were performed with a stable transfected neurokinin-1 receptor expressing CHO cell line, which Dr. Ralf Schwandner (Amgen Research GmbH, BioPark Regensburg) kindly provided. Besides the neurokinin-1 receptor gene, these cells also carry on the same vector a gene for apoaequorin expression, which is

a useful tool for intracellular calcium detection and an antibiotic resistance gene against hygromycin B for positive clone selection. The vector used is a bicistronic internal ribosome entry site (IRES) vector (Clontech, California, USA), which allows the simultaneous expression of the neurokinin-1 receptor and the antibiotic resistance separately, but from the same RNA transcript, so there is almost no risk of a loss of receptor expression if cells are permanently kept in DMEM:F12 (1:1) medium with 1.2 g/l NaHCO$_3$, 15 mM HEPES, 1% Penicillin-Streptomycin, 10% FCS and 600 µg/ml hygromycin B (Carl Roth, Karlsruhe, Germany) supplementation. The principle of calcium detection via an aequorin-derived luminescence, which is triggered by receptor mediated changes in intracellular calcium levels after addition of a coelenterazine derivative, was once established by EuroScreen [17,18].

High cell density frozen aliquots from $1*10^7$ to $2*10^7$ cells per ml were stored in FCS with 10% DMSO in liquid nitrogen until use, a method to preserve cell viability up to 90%. One aliquot was thawed at the day of the calcium assay and directly resuspended in fresh CCM. DMSO was removed by centrifugation at 200xg. For intracellular calcium dependent apoaequorin activation, the cell penetrating luminescent substance coelenterazine (PJK GmbH, Kleinbittersdorf, Germany) was used for cell loading. Therefore, a cell pellet with 20 million cells was resuspended in 4 ml 5 µg/ml coelenterazine containing, 8 mM L-glutamine and 1% PenStrep supplemented with Leibovitz´s medium and incubated for 2 hours in the dark by gentle shaking in a small Petri dish at 75 rpm at room temperature. Then the cell suspension was diluted to $1*10^6$/ml by adding 16 ml of 8 mM L-glutamine and 1% PenStrep containing Leibovitz´s medium and transferred to a standard sized Petri dish for shaking for a further 2 hours in the dark at 100 rpm. After coelenterazine loading, the cells were ready for calcium measurements at the MicroLumat Plus luminescence microplate reader (Berthold Technologies, Bad Wildbad, Germany). A volume of 50 µl of free antagonists, PEGylated antagonists, as well as antagonist activated nanoparticles dilutions were filled in separate wells of a white 96-well plate (Greiner Bio-One, Frickenhausen, Germany). The two pumps of the luminescence plate reader injection system were equilibrated respectively with the prepared CHO-NK$_1$R cell suspension and a 200 pM substance P-OMe competitive agonist solution. With a delay of 1.6 seconds, 50 µl cell suspensions were injected into the well 50 µl preloaded antagonist solution and incubated

for 1 min. In the case of partial agonistic potential of the provided antagonist, an initial luminescence emission is provoked in this period. After 1 min of cell and antagonist incubation within the well, 100 µl of 200 pM competitive antagonist, which corresponds to the approximate EC_{80} value of 100 pM for substance P-OMe in the final well concentration, was injected with the second pump to measure the literal antagonistic luminescence emission for different neurokinin-1 receptor antagonists (Figure 5). Since this secondary signal becomes increasingly suppressed with increasing concentration and potency of applied antagonist, this signal is the basis for the subsequent ligand-specific dose-response curve formation to determine IC_{50} values (Figure 6). Therefore, the areas under the signal curves were calculated in triplicate for each antagonist concentration by integration and were plotted against the natural logarithm of used concentrations. All dose-response curves were normalized against the maximum calculated area in the calcium assay. The obtained dose-response points were fitted in SigmaPlot with an equation for sigmoidal dose-response with variable slope, to determine the ligand specific EC_{50}/IC_{50} values, which give information about the binding affinity.
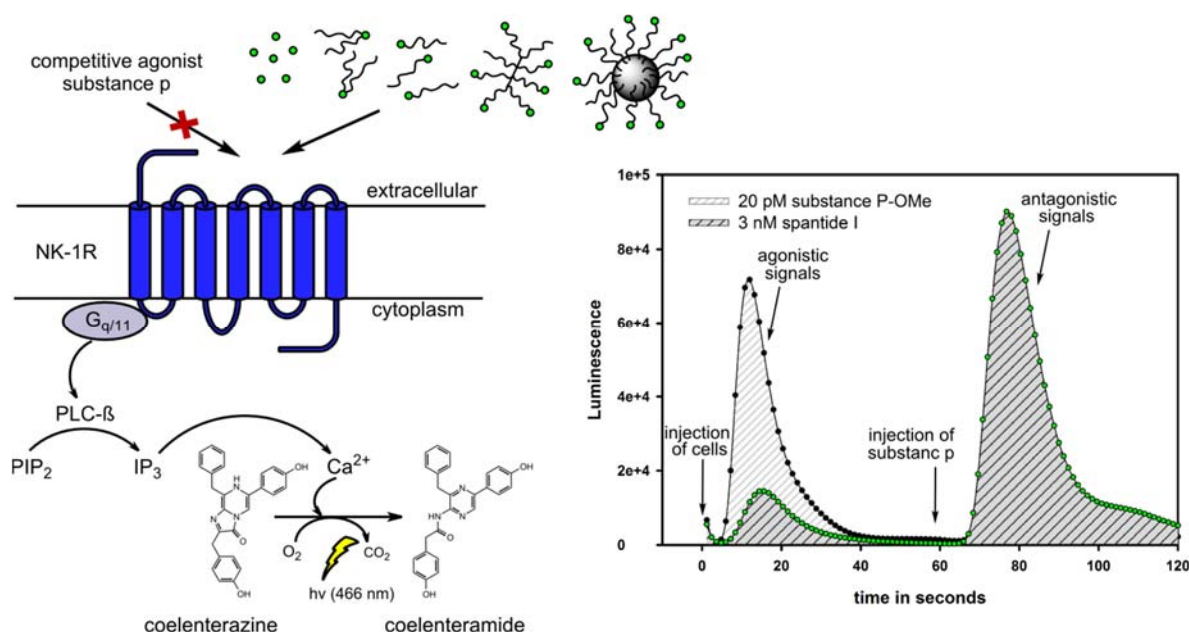
Figure 5: Principle of aequorin assay: The transfected NK_1R cell line expresses a 21 kDa photoprotein, derived from the jellyfish Aequorea Victoria, which is named as apoaequorin and forms a bioluminescent aequorin complex when linked to the chromophore cofactor coelenterazine and Ca^{2+}. The calcium binding induces an oxidation reaction, followed in an emission of light and the production of apoaequorin, coelenteramide, and CO_2 [1].
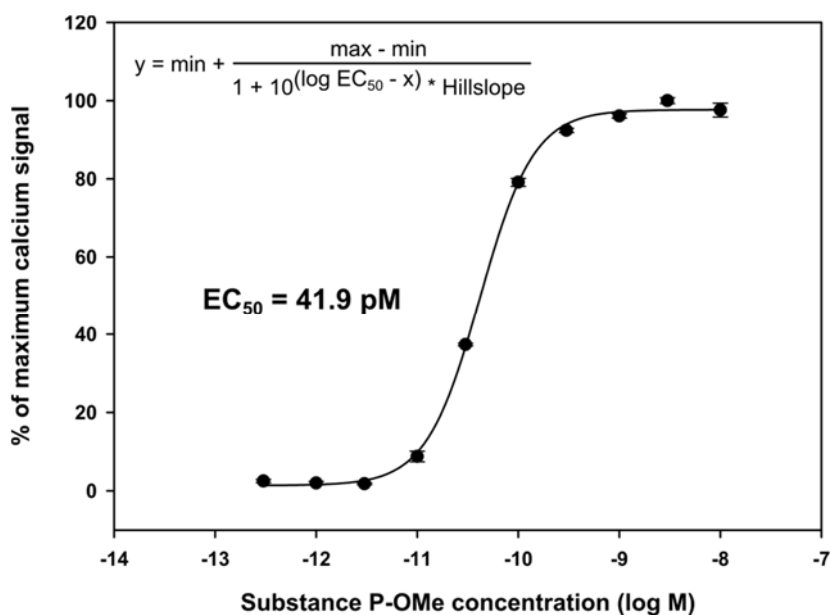
Figure 6: The EC$_{50}$ and IC$_{50}$ values were determined by sigmoidal dose-response curve fit function with variable slope. For the highly potent neurokinin-1 receptor agonist substance P-methyl ester (SP-OMe), an EC$_{50}$ value of 41.9 pM and an EC$_{80}$ of 103 pM were determined. For measurements in antagonist mode a competitive concentration of 100 pM SP-OMe was used.

Results and discussion

RP-HPLC for validation of purification procedure and successful PEGylation

For the linear PEG-peptide samples, an equivalent concentration of 20 µM of peptide was chosen to compare the areas under the chromatograms and to determine whether unPEGylated peptide was still present. A higher peptide concentration of 40 µM was chosen for the coupled spantide I, since it represents one of the highest used concentrations in the calcium binding studies and is compared to 10 µM free spantide I in the chromatogram (Figure 7). This coupling reaction is much more susceptible to failure in following purification procedures because of the high excess of used peptide ligand. However, compared to the free spantide I, there is no peptide elution at time point 7.4, which indicates successful purification of unbound peptide ligands that would disturb the results in ligand binding assays. For the 8armPEG20k-peptides, the chromatograms showed very heterogeneous and broad elution peaks between 12.5 and 25 min, which indicate different molecular sized structures because of heterogenous ligand occupancy per PEG. Also, linear mPEG5k-spantide I had a quite irregular peak structure with three not clearly separated peaks, which was a first hint for non-site-specific PEGylated products: Only Lys-PEGylated, only N-terminal-PEGylated, and double PEGylated. In addition, it could be confirmed that the purification procedure was successful by comparing unpurified and purified sample chromatograms at the elution time point of free unbound peptide (Figure 8).
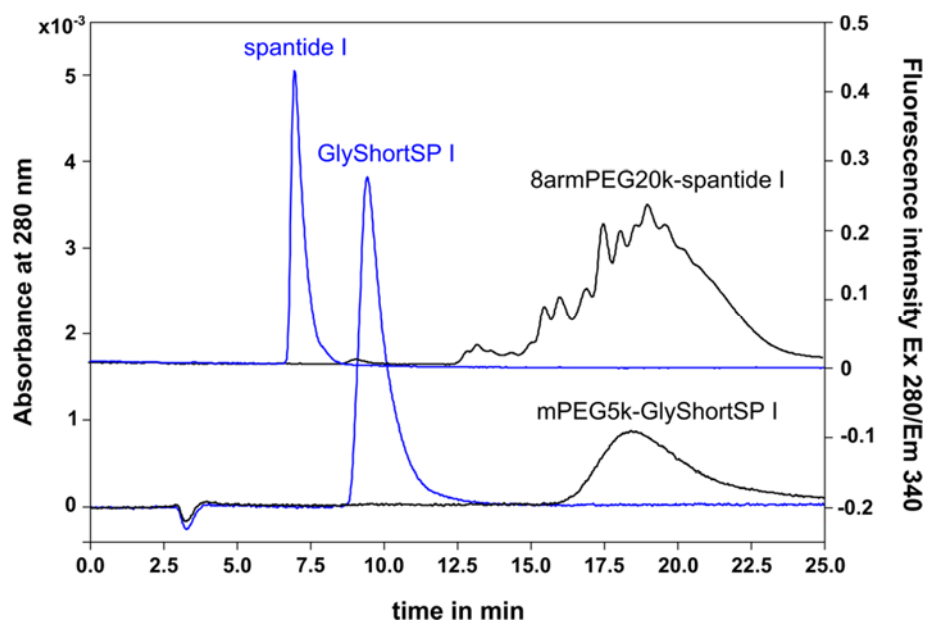
Figure 7: RP-HPLC chromatograms of a linear mPEG5k- and 8armPEG20k-peptide conjugate. For both products, there is no free unbound peptide detectable.
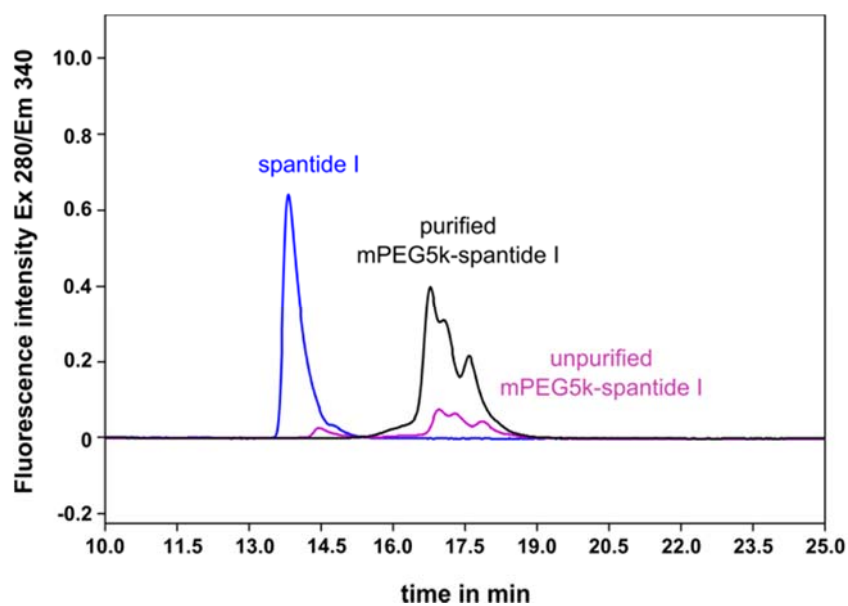

Figure 8: RP-HPLC chromatogram for mPEG5k-spantide I before and after thorough purification by size exclusion gel chromatography and several ultrafiltration steps.

Peptide to PEG ratios

The determination of peptide to PEG ratios for multivalent branched 8armPEGs showed that peptide solubility and the number of PEG binding sites have an influence on PEGylation efficiency. The mPEGylation of the most hydrophobic peptide GlyShortSP I was only possible when DMSO in a concentration of 15.7% was used for peptide reconstitution and the PEG was used in 2-fold molar excess. For 8armPEGylation, where the peptide is used in 16-fold molar excess, a DMSO concentration of 60% (v/v) was required to avoid peptide precipitation. In this case, the purification procedure is quite problematic, as the Sephadex G-25 resin and the Amicon ultrafiltration units are, according to the manufacturers, not resistant against organic solvents in higher concentrations. In addition, for the quantum coupling procedure introducing a sulfhydryl group into the peptide sequence, it was not possible to perform this reaction in DMSO. Thus, for further studies, GlyShortSP I was excluded. There is an increase in water solubility if a hydrophilic lysine is integrated in the peptide sequence; however, its solubility is not comparable to the full-length spantide I, which has an additional arginine as hydrophilic amino acid in its sequence. Therefore, 25% DMSO (v/v) was used in the PEGylation reaction. The determined peptide to 8armPEG20k ratios are the following: 7.89 spantide I per PEG, 7.25 LysShortSP I per PEG and 5.68 AcLysShortSP I per PEG. These ratios indicate that there is little double PEGylation, which would shift the ratio toward the PEG side, for non-acetylated peptide species. The site-specific mono-PEGylation strongly depends on the buffer conditions, especially the pH-value and the molar ratio of the educts used. In a PEGylation experiment with LysShortSP I and mPEG5k in basic 50 mM borate buffer, pH 8.5, where the educt ratios were varied from 1:2 to 2:1 for peptide to PEG, it could be observed, that double PEGylation only occurs in the case of PEG excess. Therefore, the PEG-cross-linking cases, caused by peptides with multiple PEGylation sites, shown in Figure are not relevant for spantide I- and LysShortSPI-8armPEG20k coupled products.
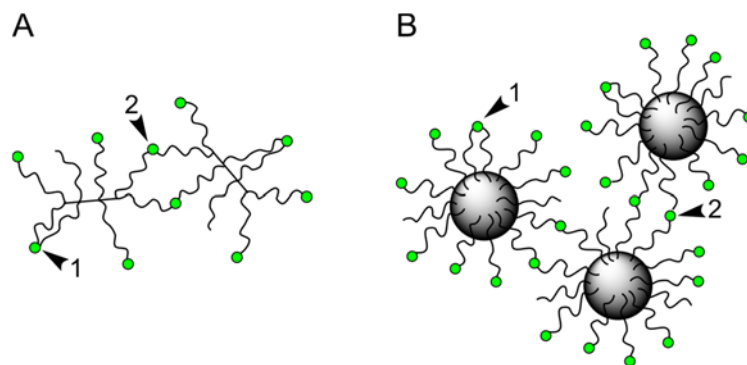
Figure 9: Possible cross-linking events for peptide ligands with two PEG binding sites. For A) Branched Polyethylene glycols and B) PEG-coated nanoparticles. The arrows indicate: 1) Intramolecular cross-linking and 2) Intermolecular cross-linking.

HPLC-MS for proof of concept of double PEGylation

In an HPLC-MS study, only the mass for mono-PEGylated LysShortSP I could be observed if the peptide was used in 2-fold excess to the used mPEG5k. A second possibility to reach controlled mono-PEGylation despite two or more possible PEG coupling sites within the peptide is to introduce an appropriate protective group for the N-terminal amine group, such as an acetyl group. Figure 10 shows that there is only one peak in the ESI TIC scan for the acetylated LysShortSPI, which indicates only one PEG per peptide, slightly shifted to the left, where unprotected peptide is used, but in high excess.
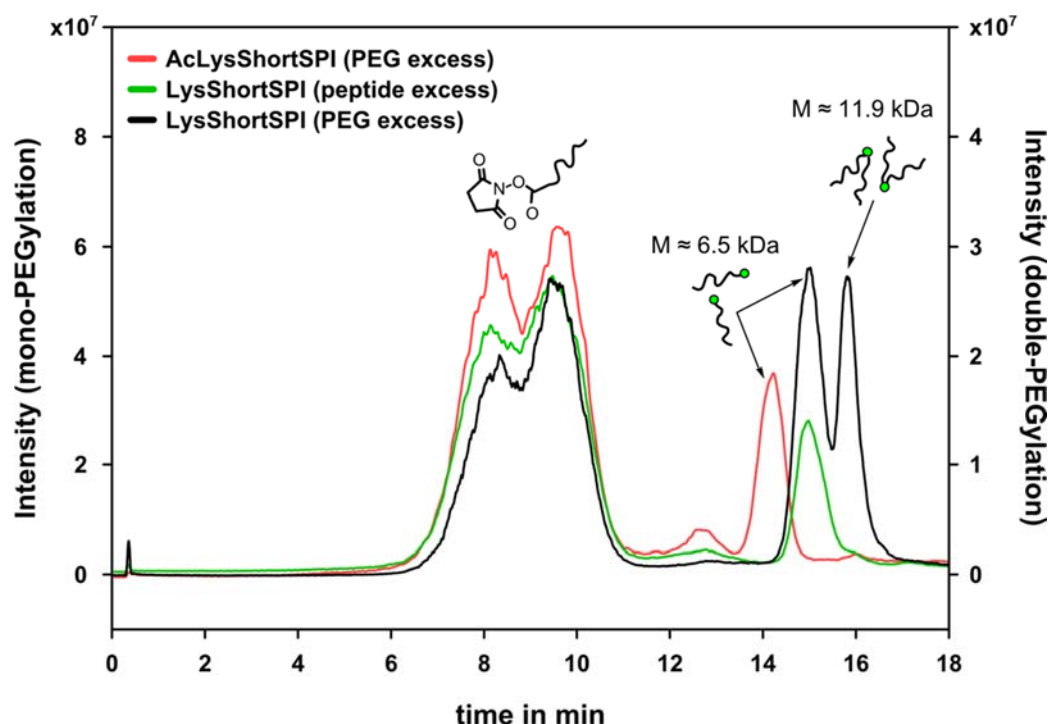
Figure 10: HPLC-MS analysis shows, that even for LysShort-spantide I, double PEGylations take place if PEG is used in excess. Mono-PEGylation occurs only for N-terminal acetylated Lys-ShortSP I or if the peptide is used in excess.

Tricine-SDS-PAGE as a qualitative proof for peptide PEGylation

The success of PEGylation could be determined in a qualitative manner by a Tricine-SDS-PAGE, for peptides coupled with linear mPEG5k. Compared to these, the branched 8armPEG20k-peptide-conjugates are not as mobile in the gel and became trapped between the spacer and the separation gel. The Tricine-SDS-PAGE gels are shown in Figure 11. Full-length peptides as well as PEGylated peptides can be observed with a Coomassie staining. Surprisingly, the unPEGylated LysShortSP I was not visible. After gel bleaching and iodine staining, only the PEGylated products were visible. PEG alone does not move in the gel. This method is recommended if only a qualitative proposition is desired for PEGylation success because the resolution is highly concentration dependent, especially to the peptide, and not comparable to that of an absorbance or fluorescence-based HPLC detection method.
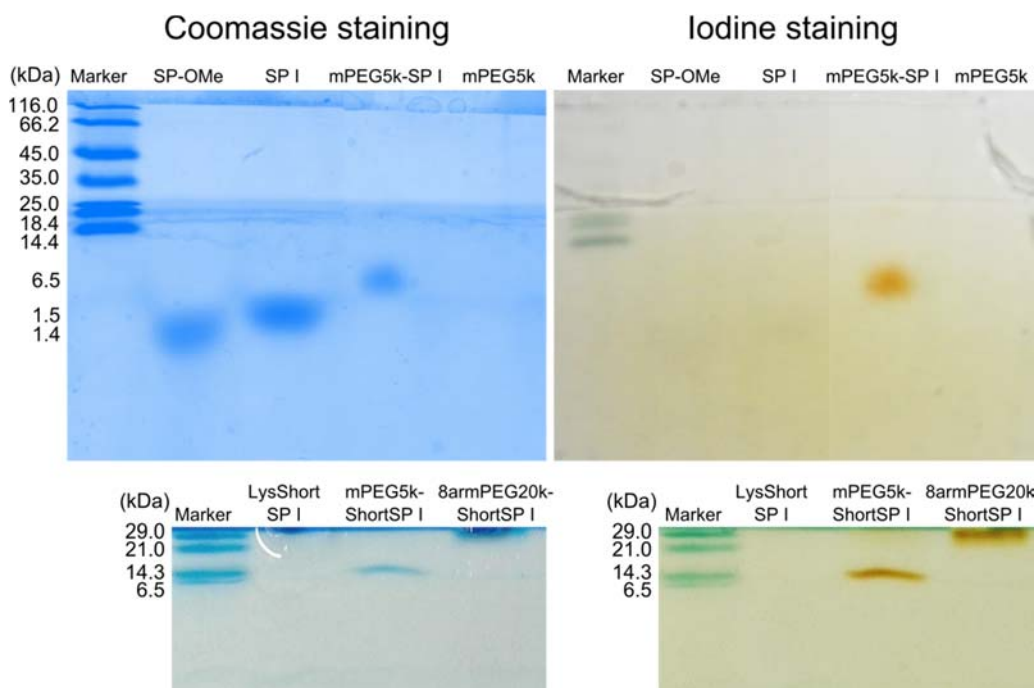
Figure 11: Tricine-SDS-PAGE gels. On the left: Peptide specific Coomassie staining, and on the right: PEG specific iodine staining.

Circular dichroism measurements

As a check for possible changes in the peptide structure upon PEGylation, CD-spectra were recorded. It was found that there is no change in the CD-spectrum of the peptide after PEGylation. This indicates that there no modification in the peptide conformation due to the addition of one or two PEG chains (Figure 12). Since the peptide is relatively short, a real secondary structure cannot be determined, compared to proteins. Both spectra show negative maxima at 200 and 222 nm, which is coincides with the data in the literature for spantide I in water solution [19].
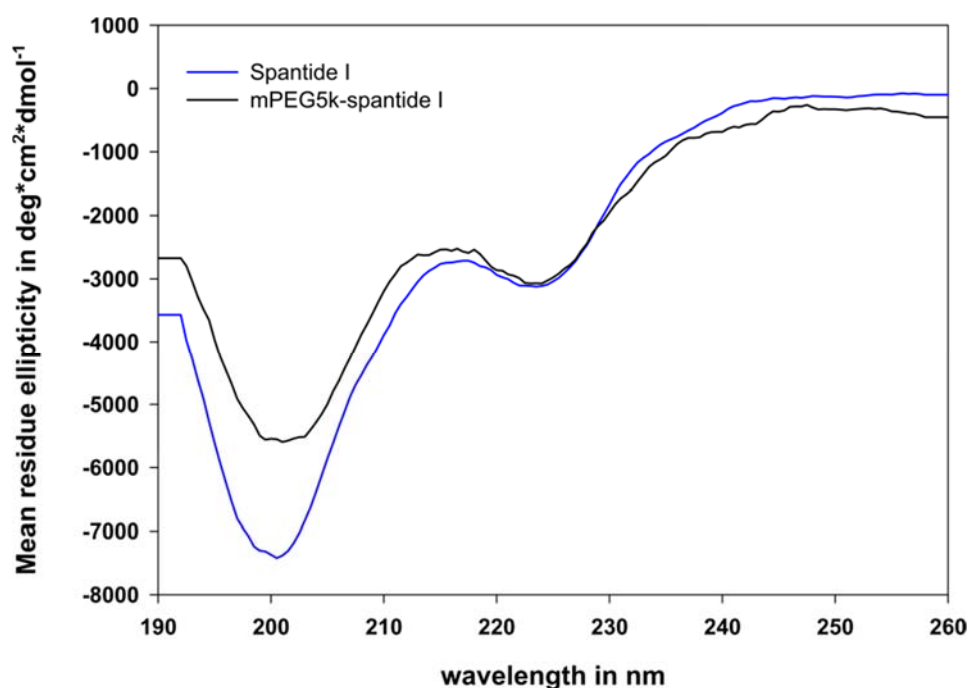
Figure 12: Circular dichroism spectra before and after PEGylation. There are no significant changes in peptide conformation.

Calcium assay binding studies

The influence of peptide truncation and PEGylation on the peptides´ affinity to neurokinin-1 receptors were evaluated in the described aequorin calcium assay. The full-length antagonist spantide I has a variable potency, ranging from IC_{50} = 10.9 nM and IC_{50} = 254.9 nM, depending on the reconstitution buffer and whether an initial agonistic signal is measured. Independent from this fact, there is a decrease in affinity up to the micromolar range for truncated peptides, and even more for mPEGylated peptides (Figure 13/ 14). This result is not surprising since it is known that receptor binding takes place with the C-terminal end of the peptide and long N-terminal bound PEG chains cause high entropy costs and are able to sterically hinder the ligand from gaining access to the receptor binding pocket. In this study it was found that this effect is even stronger if two PEG chains are bound to one peptide, because of the presence of two PEGylation sites. If there is only one PEGylation-site present, as with AcLysShortSP I, the decrease in affinity is only 2.3-fold upon mPEG5k coupling, compared to a 6-fold affinity loss for unprotected LysShortSP I and even >107.5-fold for the full-length spantide I (Figure 13/14 and Table 2). Compared to the linear mPEGylated

AcLysShort spantide I, the affinity for the 8armPEGylated AcLysShort spantide I is much worse, which could be due to fewer ligands bound per PEG (only 5.68, compared to the others with >7 ligands/PEG), which result in a non-multivalent receptor binding. One further indication for this hypothesis is the steep slope for 8armPEG20k-AcLysShortSPI compared to other 8armPEG-peptide conjugates, which indicates that there is no cooperativity present (Figure 15). As a result, the decrease in affinity is much greater, compared to the linear PEG-peptide-conjugate, because the effect of steric hinderance is exorbitantly greater. In contrast, multivalency could be observed for 8armPEG20k-spantide I and 8armPEG20k-LysShortSP I in the form of a regain in affinity, compared to the mPEGylated version. For 8armPEG20k-spantide I, an IC_{50} value of 53.4 nM was determined, which is a 4.9-fold affinity loss to the unmodified peptide (reconstituted in 0.1% acetic acid/PBS) and even a 4.8-fold gain in affinity, if compared to the unmodified spantide I (reconstituted in 1% DMSO), and a 513-fold improvement in affinity, compared to the mPEG5k-spantide I. A similar effect could be observed for the less potent LysShortSP I, where the initial affinity of unmodified peptide could also be improved 4.5-fold by multivalent receptor binding (Table 2).

Table 2: IC_{50} values of mono- and multivalent antagonists:

Monovalent antagonists (see Figure 13 and 14)			Multivalent antagonists (see Figure 15)	
Ligand type	**Free ligand**	**mPEG5k-coupled ligand**	**8armPEG20k-coupled ligand**	**QD-coupled ligand**
Spantide I	10.9 nM[*1] 254.9 nM[*2]	27.4 μM	53.4 nM	6.1 nM
LysShort SP I	5.7 μM	34.0 μM	1.28 μM	n.a.
AcLysShort SP I	2.3 μM	5.4 μM	67.6 μM	n.a

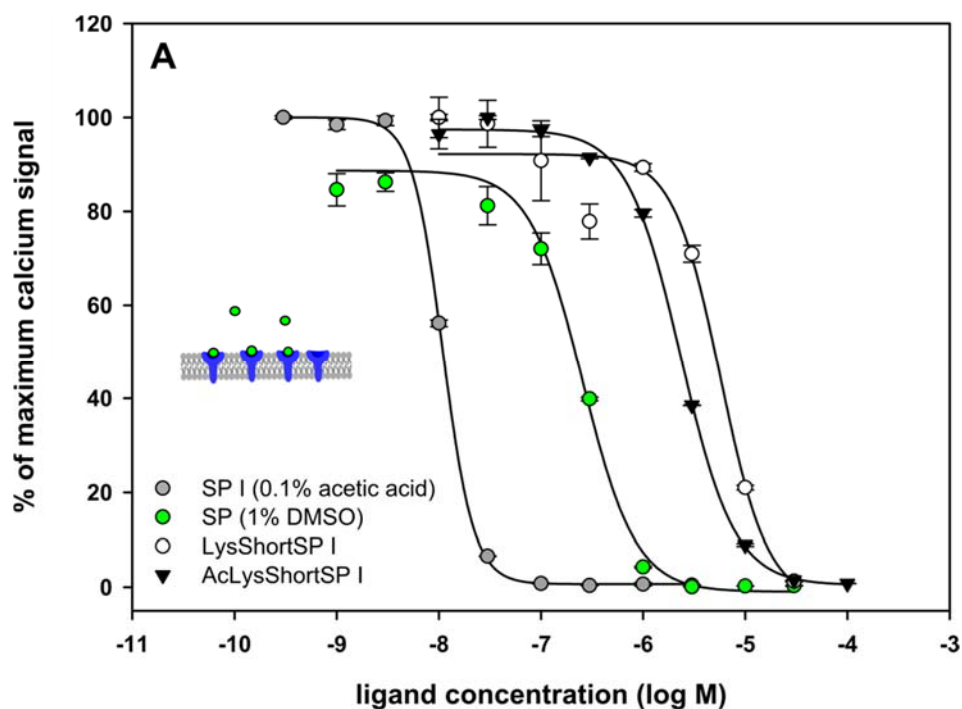[*1] **reconstituted in 0.1% acetic acid,** [*2] **reconstituted in 1% DMSO**

Figure 13: Aequorin assay with CHO-NK$_1$R cells: Dose-response curves of spantide I antagonists, including full-length spantide I, reconstituted in different 500 µM stock solution buffers with 0.1% acetic acid and 1% DMSO in PBS, respectively, and truncated versions (LysShortSP I and AcLysShortSP I). Mean values ± SE, n = 3. Corresponding IC$_{50}$ values are listed in Table 2.
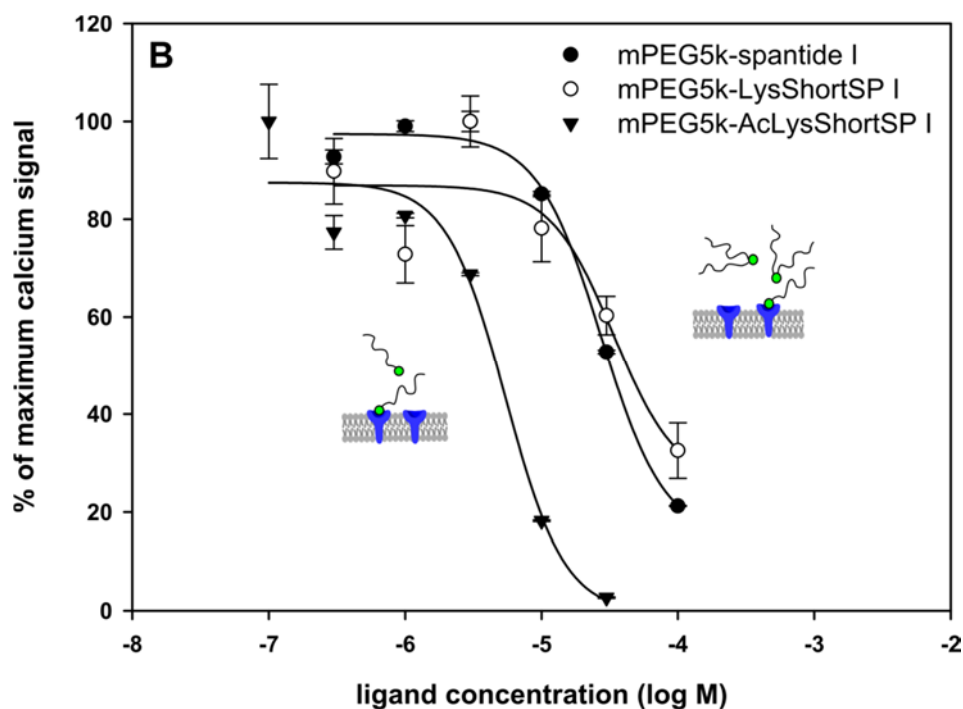
Figure 14: Influence of linear mPEG5k-chain on the spantide I, and truncated peptide ligands´ affinities. Mean values ± SE, n = 3. Corresponding IC$_{50}$ values are listed in Table 2.
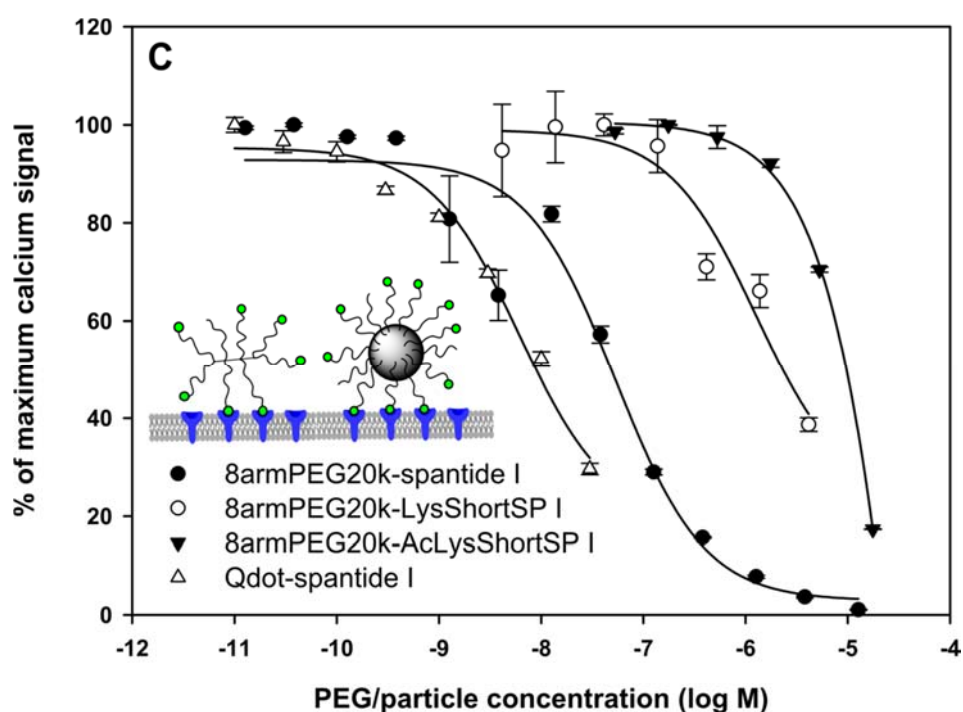
Figure 15: Dose-response curves for multivalent binding antagonists, including branched 8armPEG20k-peptide-conjugates and PEG-coated QDs. Mean values ± SE, n = 3. Corresponding IC$_{50}$ values are listed in Table 2.

In conclusion, it could be shown that the attachment of one or two PEG molecules to a peptide causes high entropy costs and results in increasing IC$_{50}$ values, proportional to the number of PEGs chains. Multivalent binding effects may counterbalance these pharmacodynamic adverse effects of coupled PEG by slower off-rates, cooperative effects due to receptor cross-linking, and a gain in enthalpy [20]. Multivalency by branched 8armPEG-scaffolds requires seven to eight ligands per 8armPEG20k molecule; otherwise, the pharmacodynamic adverse effects of bulky PEG predominate. In addition, there is a lack of binding enhancement and therefore no cooperative effect [21]. Not much is known about ideal receptor density, the minimum and maximum distances between receptors and the optimum of PEG chain length, which are tightly interplaying parameters for multivalent drug-receptor binding. One research group investigated the various receptor distances for rhodopsin in silico. They found that a linker length of 20–50 Å between two ligands is needed for simultaneous receptor binding. The minimum width of two densely packed rhodopsin receptors is about 70 Å, and for loosely packed receptors, it is a distance of 100 Å or more [20]. Each PEG monomer has a length of 3.5 Å [22]. For mPEG5k, several PEG monomers of n = 116 were observed by mass spectrometry. For branched 8armPEG20k, it is unfortunately not possible to obtain the exact number of repetitive PEG units, but one arm should represent a bit more than PEG2k, which correlates with the PEG layer of QDs. In a brush conformation, one PEG arm should therefore have a nominal length of approximately 165 Å.

Agonistic potential of antagonists

For some peptides and peptide-PEG conjugates, an agonistic potential was observed, which could be influenced by PEGylation. These observations raised new questions about various binding modes for PEGylated and unPEGylated peptides to the neurokinin-1 receptor binding pocket. An agonistic potential was measured in the aequorin calcium assay for the full-length spantide I, depending on how the peptide was reconstituted (Figure 16, A/B). Such preliminary agonistic calcium signals for antagonists are problematic because they reduce the number of intracellular available apoaequorin-coelenterazine complexes for the secondary antagonistic calcium signals for IC$_{50}$ value determination. Resulting IC$_{50}$ values should be considered in such cases with caution. In contrast, no agonistic calcium signals were measured after PEGylation (Figure 16, A/B).
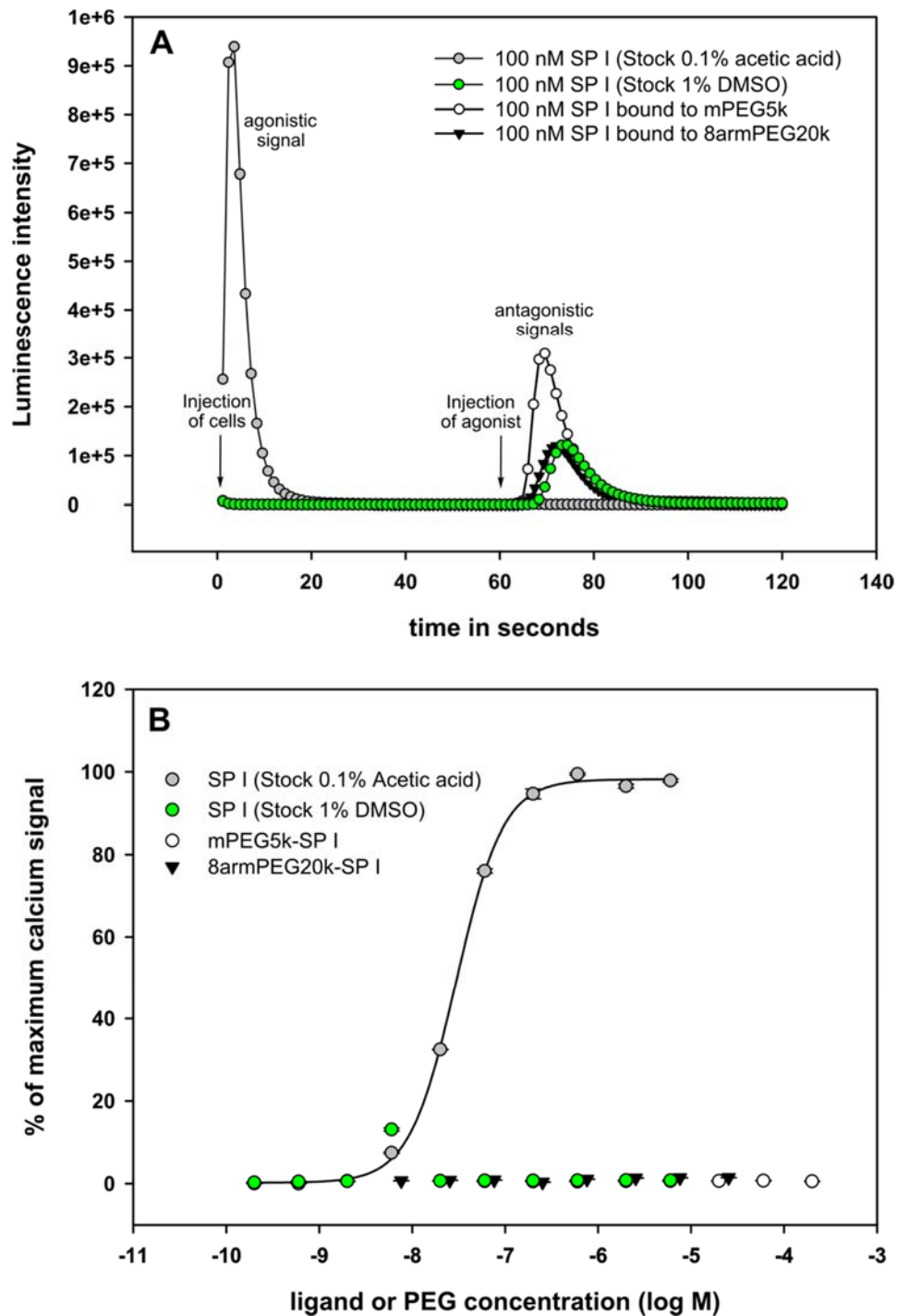
Figure 16: Agonistic potential of unPEGylated spantide I for diluted peptide in 0.1% acetic acid. A) Calcium signals, B) Dose-response curves: The agonistic potential of spantide I of the same lot can be prevented by changing the solvent into an acetic acid free solution. Other lots did not show agonistic effects. There is complete suppression of agonism upon PEGylation. Mean values ± SE, n = 3.

Interestingly, the opposite effect could be observed for AcLysShort-spantide I, independent from acidic reconstitution. Here, the unPEGylated peptide didn´t show any agonistic potential, but the mPEGylated and 8armPEGylated-AcLysShortSP I induced high agonistic calcium signals (Figure 17, A/B).
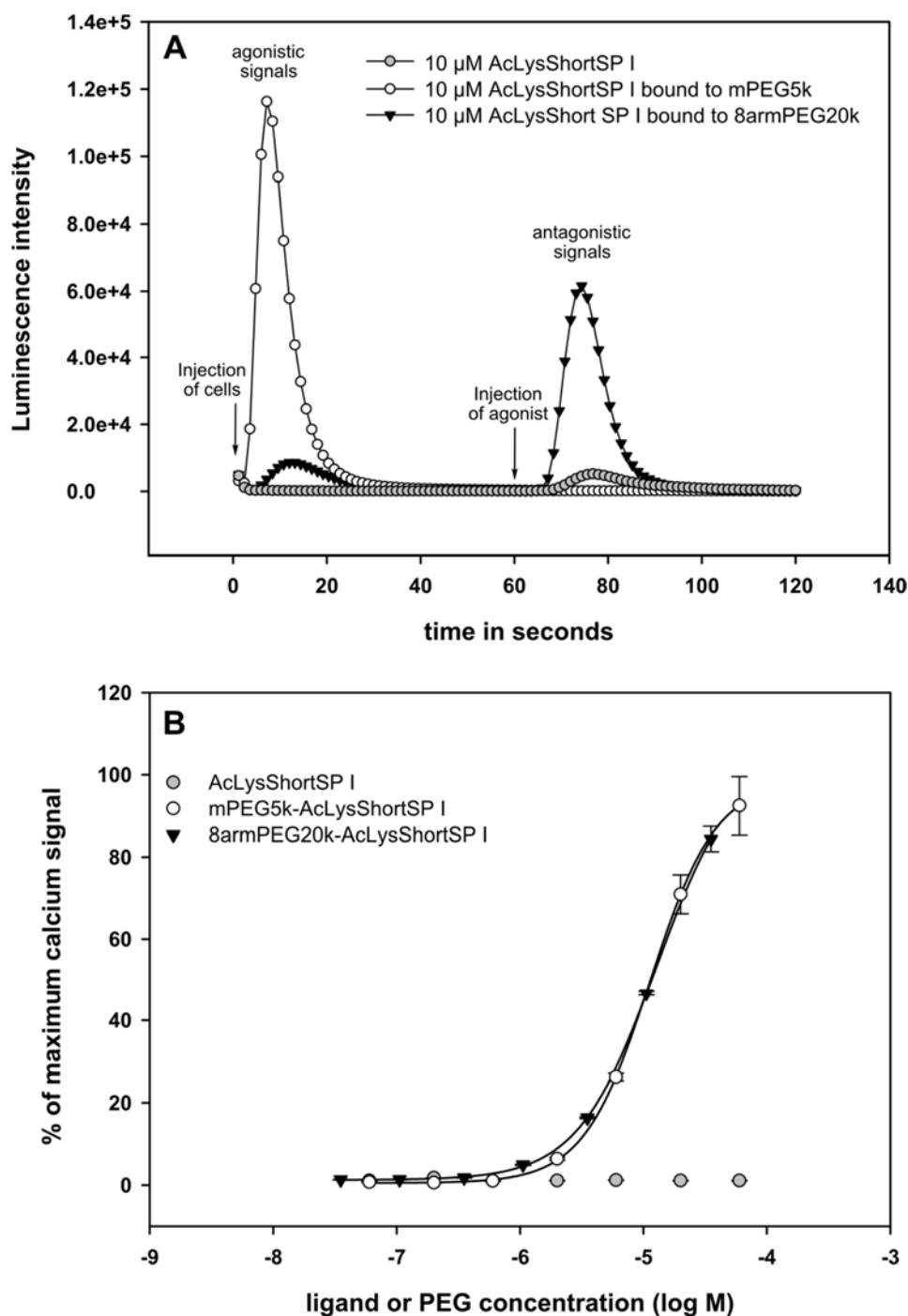
Figure 17: Induction of agonistic potential upon PEGylation for AcLysShortSPI. No agonism was observed for unPEGylated peptide. All peptides were diluted in PBS without acetic acid.

The literature mentions that some neuropeptides exhibit a residual agonistic effect for other non-neurokinin receptor species due to the substance P-like N-terminal tripeptide motive (Arg-Pro-Lys) [23]. D-amino acids are known to reduce these agonistic effects. Since the N-terminal sequence of spantide I is D-Arg-Pro-Lys, an agonistic potential of this drug was not expected, least of all for N-terminal PEGylated truncated peptides. One reason for the agonistic potential of full-length spantide I could be that proline as a so-called helix breaker amino acid, which sometimes causes problems in peptide synthesis, is responsible for coexisting shorter peptides without D-Arginine. First, this hypothesis was confirmed by the fact that other spantide I lots show reduced or no agonistic potential. But in HPLC-MS analysis, the true peptide masses for all used spantide I lots were identified. Another factor for high initial calcium signals can be acidic extracellular pH values, due to buffer components like acetic acid, which was used for peptide reconstitution. To investigate this, the peptide of the same lot was reconstituted in two different 500 μM stock solutions: in 1% DMSO/PBS and 0.1% acetic acid/PBS. Compared to the peptide in 0.1% acetic acid, a partial agonistic signal of 13.1% of maximum calcium signal for 6 nM spantide I was only measured if the peptide was reconstituted in a 1% DMSO/PBS solution. Nevertheless, it remains unclear why just mono-PEGylation induces an agonistic effect for AcLysShortSP I, independent from acetic acid reconstitution. One option may be that the PEG chain promotes another agonist-like peptide-receptor binding mode, also directed by the C-terminus of the peptide. Due to the small size and the highly hydrophobic nature of AcLysShortSP I, this peptide is possibly able to bind deeper in the receptor binding pocket to simply block the receptor. Upon PEGylation, there is an increase in solubility, and due to the bulky PEG chain, only the extracellular loops and therefore an agonistic receptor conformation is accessible. To obtain proof of this concept, the X-ray structure of the human neurokinin-1 receptor is necessary, which would make possible further investigation of the binding modes of PEGylated peptides *in silico*, to fully understand how PEGylation influences the peptide´s ability to interact with the receptor binding pocket.

Conclusion

There is a high concentration requirement of PEGylated spantide I species for clinical efficacy because N-terminal PEGylation decreases binding to membrane receptors but has the advantage of reduced clearance and immunogenicity. Double PEGylation of spantide I further increases the affinity loss to neurokinin-1 receptors because higher PEG to peptide ratio sterically reduces receptor binding at the cell surface, although binding is sufficient at very high ligand concentrations. Furthermore, simple N-terminal truncation of the peptide sequence leads to a great affinity loss. This indicates that the N-terminus sequence itself seems to be involved in receptor recognition and binding. Therefore, N-terminal truncation of the peptide sequence of spantide I is not an option to simplify the mono-PEGylation by elimination of amino acids, which are responsible for double PEGylation. The agonist activity of some peptide antagonists, which seem to be also mediated through the neurokinin-1 receptor make it difficult to determine true IC_{50} values in the aequorin based calcium assay due to consumption of bioluminescent aequorin complex. Nevertheless, it could be shown that there is a gain in affinity for 8armPEG-20k-spantide I due to multivalent receptor binding.

Supporting information

In HPLC-MS analysis, the mass and the number of repetitive PEG units of the succinimidyl succinate functionalized mPEG5k was determined. Its mass is 5267.29 Da with 116 PEG units with an error of $\Delta 0.5$ mDa = 0.4 ppm. Different PEGylated spantide I have different retention times in HPLC and therefore different mass peaks can be extracted (Figure 18 and Figure 19).
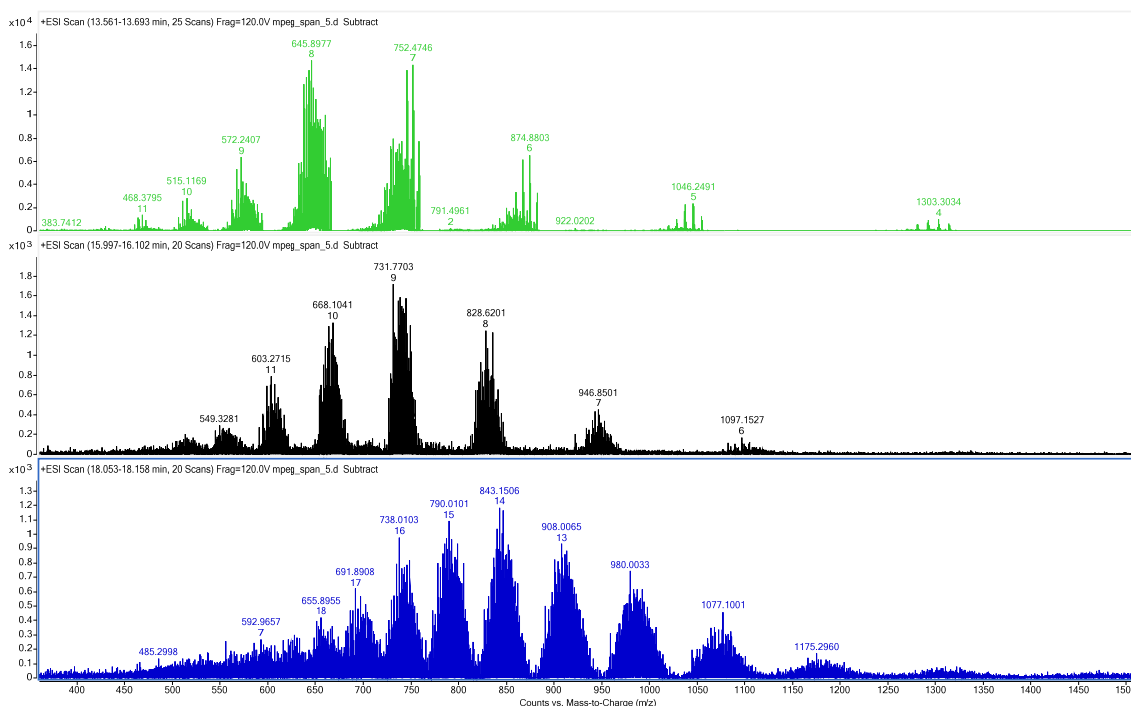

Figure 18: Mass spectra of different obtained peaks for mPEGylation products of spantide I: The calculated masses for unreacted mPEG5k, 5267.29 Da (green), mono-PEGylated spantide I, 6585.93 Da (black) and double-PEGylatded spantide I, 11804.10 Da (blue), were observed.
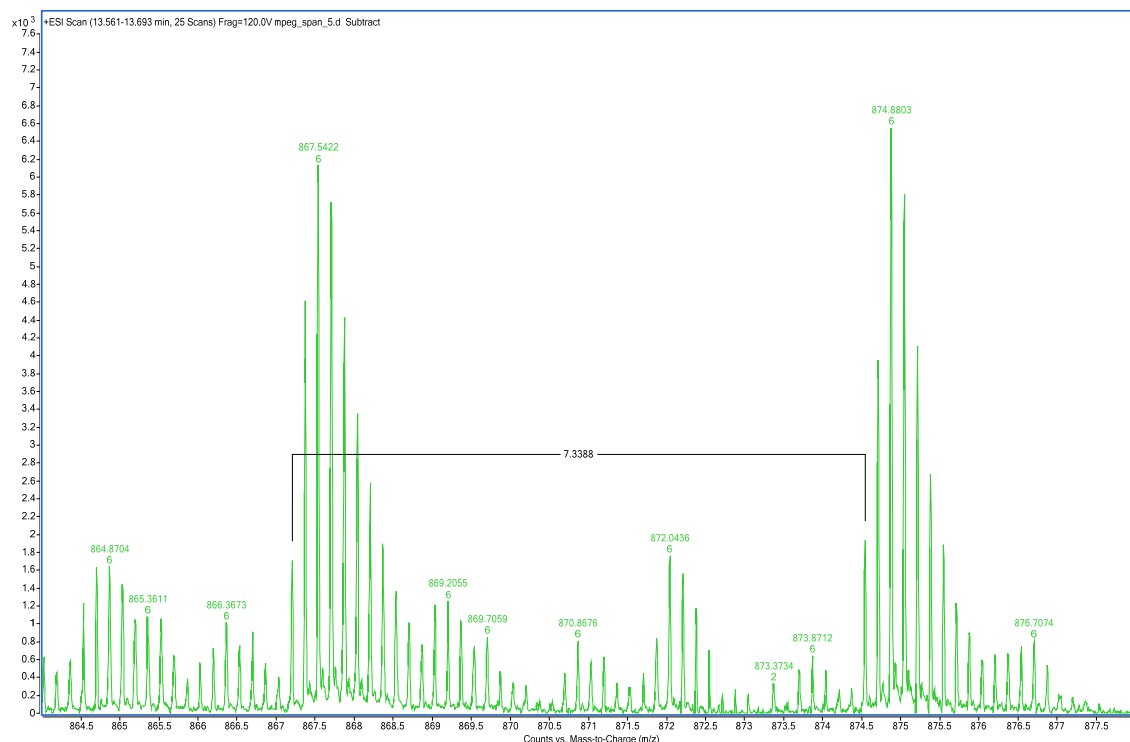
Figure 19: m/z distance of 7.3388 from C_{12} to C_{12} indicate the PEG repetition with atomic mass of 44.

Unmodified PEGylated QDs were tested in an aequorin based calcium assay to see if unspecific calcium signals are generated or if there is a reduction in agonist provoked signal. It was found, that no calcium signal is provoked by QDs itself, but the substance P-OMe generated calcium signal after 60 seconds incubation of QDs with the cells is also reduced in a concentration-dependent manner. Finally, an IC_{50} of 52.1 nM could be obtained by unmodified QDs (Figure 20). This is maybe because of bioluminescence quenching due to the generation of light at 488 nm, which ideally fits the excitation and absorbance spectra of QDs. Bioluminescence resonance energy transfer (BRET) as a radiationless option for minimizing not receptor mediated luminescence signals, is only possible if the distances between extracellular QDs and intracellular aequorin complex are small enough. This kind of luminescence resonance energy transfer is already described for aequorin and GFP (green fluorescent protein) [24]. Nevertheless, the obtained binding curves differ in a linear concentration range of 8.5-fold. The question here is, if this difference is obtained by present

free spantide I in the sample, because of inefficient nanoparticle purification or due to multivalent binding effects.
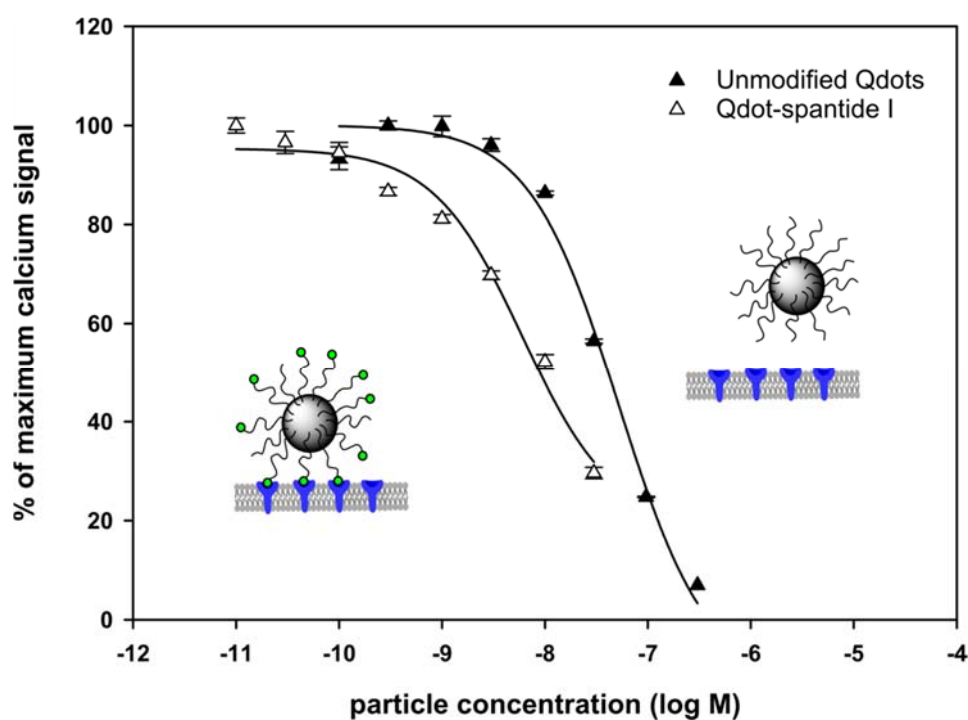

Figure 20: Unmodified QDs also show a decrease in bioluminescence with increasing particle concentration

References

[1]   Fichna J, Gach K, Piestrzeniewicz M, et al. Functional characterization of opioid receptor ligands by aequorin luminescence-based calcium assay. J. Pharmacol. Exp. Ther. 2006; 317: 1150–1154.

[2]   Fishburn C. The Pharmacology of PEGylation: Balancing PD with PK to Generate Novel Therapeutics. Journal of Pharmaceutical Sciences 2008; 97: 4167–4183.

[3]   Harris JM, Chess RB. Effect of pegylation on pharmaceuticals. Nat Rev Drug Discov 2003; 2: 214–221.

[4]   Molineux G. Pegylation: engineering improved pharmaceuticals for enhanced therapy. Cancer Treatment Reviews 2002; 28: 13–16.

[5]   Bailon P, Berthold W. Polyethylene glycol-conjugated pharmaceutical proteins. Pharmaceutical Science & Technology Today 1998; 1: 352–356.

[6]   Nischan N, Hackenberger, Christian P. R. Site-specific PEGylation of Proteins: Recent Developments. J. Org. Chem. 2014; 79: 10727–10733.

[7]   Morishige T, Yoshioka Y, Inakura H, et al. Creation of a lysine-deficient LIGHT mutant with the capacity for site-specific PEGylation and low affinity for a decoy receptor. Biochemical and Biophysical Research Communications 2010; 393: 888–893.

[8]   Bailey SJ, Jordan CC. A study of [D-Pro2, D-Phe7, D-Trp9]-substance P and [D-Trp7,9]-substance P as tachykinin partial agonists in the rat colon. British Journal of Pharmacology 1984; 82: 441–451.

[9]   Dutta AS. Small peptides: Chemistry, biology, and clinical studies. Amsterdam, New York: Elsevier 1993.

[10]   Nyberg F. Neuropeptides in neuroprotection and neuroregeneration. Boca Raton, FL: CRC Press 2012.

[11]   Hennig R, Veser A, Kirchhof S, Goepferich A. Branched Polymer–Drug Conjugates for Multivalent Blockade of Angiotensin II Receptors. Mol. Pharmaceutics 2015; 12: 3292–3302.

[12]   Hennig R, Ohlmann A, Staffel J, et al. Multivalent nanoparticles bind the retinal and choroidal vasculature. Journal of Controlled Release 2015; 220: 265–274.

[13]   Kelleher SM, Nooney RI, Flynn SP, et al. Multivalent linkers for improved covalent binding of oligonucleotides to dye-doped silica nanoparticles. Nanotechnology 2015; 26: 365703.

[14]   Brandl F, Hammer N, Blunk T, Tessmar J, Goepferich A. Biodegradable Hydrogels for Time-Controlled Release of Tethered Peptides or Proteins. Biomacromolecules 2010; 11: 496–504.

[15] Childs CE. The determination of polyethylene glycol in gamma globulin solutions. Microchemical Journal 1975; 20: 190–192.

[16] Schägger H. Tricine–SDS-PAGE. Nat Protoc 2006; 1: 16–22.

[17] THOMSEN W, FRAZER J, UNETT D. Functional assays for screening GPCR targets. Current Opinion in Biotechnology 2005.

[18] Janecka A, Poels J, Fichna J, Studzian K, Vanden Broeck J. Comparison of antagonist activity of spantide family at human neurokinin receptors measured by aequorin luminescence-based functional calcium assay. Regulatory Peptides 2005; 131: 23–28.

[19] Di Bello C, Scatturin A, D'Auria G, et al. Fluorescence, CD, and nmr studies on spantide, a bombesin and substance P antagonist. Biopolymers 1991; 31: 643–652.

[20] Josan JS, Handl HL, Sankaranarayanan R, et al. Cell-Specific Targeting by Heterobivalent Ligands. Bioconjugate Chem. 2011; 22: 1270–1278.

[21] Vauquelin G, Bricca G, van Liefde I. Avidity and positive allosteric modulation/cooperativity act hand in hand to increase the residence time of bivalent receptor ligands. Fundam Clin Pharmacol 2014; 28: 530–543.

[22] Jokerst JV, Lobovkina T, Zare RN, Gambhir SS. Nanoparticle PEGylation for imaging and therapy. Nanomedicine 2011; 6: 715–728.

[23] Mizrahi J, D'Orléans-Juste P, Drapeau G, Escher E, Regoli D. Partial agonists and antagonists for substance P. European Journal of Pharmacology 1983; 91: 139–140.

[24] Baubet V, Le Mouellic H, Campbell AK, Lucas-Meunier E, Fossier P, Brúlet P. Chimeric green fluorescent protein-aequorin as bioluminescent Ca2+ reporters at the single-cell level. Proceedings of the National Academy of Sciences of the United States of America 2000; 97: 7260–7265.

Chapter 6

Aprepitant, a small molecular weight antagonist for the neurokinin-1 receptor and its functionalization for nanoparticle coupling

Abstract

Because many NK_1R peptide antagonists, such as spantide I, suffer from poor metabolic stability and poor bioavailability, some small molecular weight antagonists for the neurokinin-1 receptor with high affinities were developed in the past [1,2]. Unfortunately, all of them lack suitable functional groups for common covalent nanoparticle coupling chemistries. The most popular representative NK_1R antagonist is aprepitant (MK-869), which is used as a BBB-passing antiemetic drug for chemotherapy afflicted patients. It is supposed that after covalent nanoparticle coupling, aprepitant is not able to pass the BBB anymore and therefore can be used as a specific receptor blocker on immune cells in inflamed and highly innervated tissues where NK_1Rs seem to be over-expressed. In this study, the chemical insertion of an alkyl-linker to aprepitant to make the drug molecule amenable to covalent nanoparticle coupling chemistry was shown. Since there is little information about the exact binding mode of aprepitant, the binding capacity of the alkyl-linker-modified aprepitant was also checked. Here, it was found that the molecule is still active to NK_1Rs after alkylation at its triazole group. This provided valuable information about its potential conformation within the NK_1R binding pocket. In addition, the linker-modified aprepitant represents, besides peptide antagonists, a promising small molecular weight ligand for further binding studies with aprepitant coated nanoparticles.

Introduction

Neuropeptides modulate stress responses by their communication between the cortex and peripheral tissues. A perfect example of such a neuropeptide related neuromodulator process is the emetic reflex of substance P through NK_1Rs, which are present in the brain in the CNS and the gastrointestinal tract with the enteric nervous system (ENS) along the so-called gut-brain axis [3]. One anti-emetic drug is aprepitant (MK-869), which was approved by the US Food and Drug Administration (FDA) in 2003 as an oral formulation and selectively antagonizes the human NK_1R [4]. It is distributed as hard capsules with various aprepitant concentrations (80 mg and 125 mg per capsule) under the trade name Emend®. A second pro-drug for intravenous injection is Fosaprepitant (dimeglumine), distributed as Ivemend® (Figure 1). Fosaprepitant is converted to aprepitant within 30 min after intravenous injection [5]. Both dosage forms are currently the only FDA approved NK_1R targeting ligands on the market and thus are used for administration in combination with other antiemetics (an $5-HT_3R$ antagonist and dexamethasone) in chemotherapy patients to prevent the negative acute and delayed side-effects of nausea and vomiting (CINV = chemotherapy-induced nausea and vomiting) [1,6]. Oral aprepitant administration leads to a peak concentration after 4 hours with a half-life of 9–13 hours [7]. The metabolization of aprepitant is complex, but it is primarily metabolized through the cytochrome P-450 pathway [6]. The plasma protein binding is about 95% and the bioavailability ranges between 60% and 65% [7]. Aprepitant has a poor water solubility with only 3–7 µg/ml within a broad pH range of pH 2–12 [8]. For that reason, the formulation of Emend® is based on drug loaded nanoparticles´ technology, to increase the surface area to optimize drug absorption in the upper gastrointestinal tract and increase bioavailability [9]. However, this technology does not address the aspect of cell or tissue specific NK_1R targeting. For this strategy, described in Chapter 4, our final goal is to covalently couple aprepitant to PEG-coated nanoparticles to obtain multivalent binding effects, only at target sites where the receptor density is high, which could be the case for either tumors or inflamed tissues. However, there are two major drawbacks. First, aprepitant and other commercially available NK_1R antagonists (a few of them are illustrated in Figure 1) do not exhibit a functional group for common PEG-coupling strategies. Second, there is little information about the exact binding mode of these drug molecules, which would help to predict negative influences on

the drug´s receptor binding affinity after the addition of a short alkyl linker or an even longer PEG chain. Here, the decision was to introduce a short alkyl linker with amine functionality at the triazole group of Emend® isolated aprepitant, which would make the drug molecule amenable for further PEGylation and nanoparticle coupling with well-established coupling chemistries. The effect on the binding properties of aprepitant upon triazole group modification was checked after alkyl linker addition reaction.
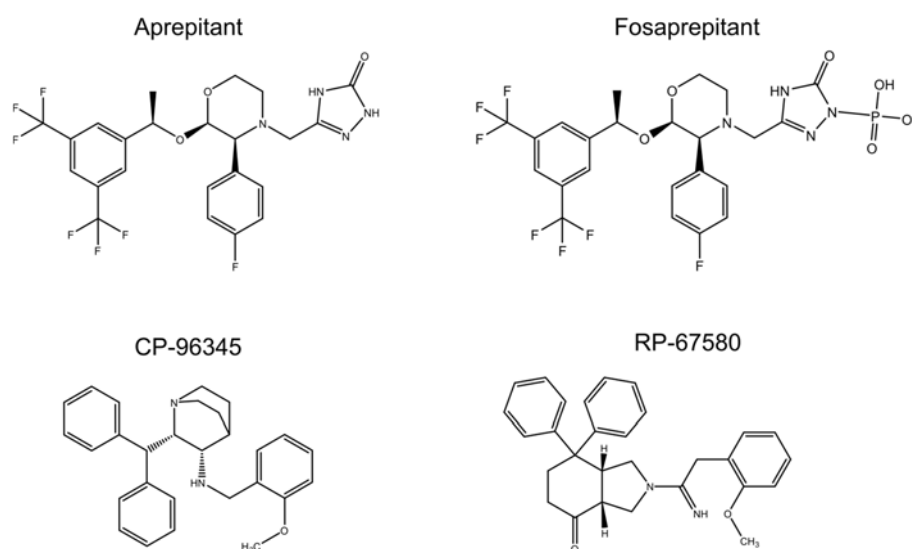

Figure 1: Showcase of small molecular antagonists for the neurokinin-1 receptor. Aprepitant and Fosaprepitant are two FDA approved antiemetic drugs, distributed by Merck MSD Sharp & Dohme GmbH under the trade names Emend® and Ivemend® for oral and intravenous application, respectively. CP-96345 was the first NK$_1$R non-peptide antagonist, developed by Pfizer, which served as the basis for later aprepitant synthesis [10]. RP-67580 was developed by Rhône-Poulenc, which could show inhibition of neurogenic inflammation in rats [11].

Materials and Methods

All chemicals were purchased from Sigma Aldrich (Taufkirchen, Germany) in analytical grade or higher if not stated otherwise. Emend® hard capsules with 125 mg aprepitant were purchased from MSD Sharp & Dohme GmbH (Haar, Germany). Pure aprepitant was purchased from Cayman Chemical Company (Ann Arbor, Michigan, USA). Thomas Dang-Lieu (Universität Regensburg, Lehrstuhl für Pharmazeutische Chemie, Prof. Sigurd Elz) synthesized Boc-protected alkyl linker (tert-Butyl-(3-bromopropyl) carbamate) (Figure 2). Sodium hydride as 60% suspension in paraffin oil was purchased from Merck (Darmstadt, Germany).

Isolation of aprepitant out of Emend® hard gelatin capsules

Emend® hard gelatin capsules contain pellets of nanocrystalline aprepitant [9]. The pellets further consist of sucrose, microcrystalline cellulose, hyprolose, and sodium dodecyl sulfate [12]. Aprepitant has good solubility in methanol, as well as other organic solvents. Compared to these, though, methanol is very easy to remove by vacuum evaporation. Therefore, the content of five Emend® capsules was levigated with mortar and pestle and subsequently suspended in 55 ml methanol and equally distributed into five 15 ml falcon tubes. After 15 min centrifugation at 10^4 x g, the supernatant was decanted and filtered through a 0.2 μm filter. The filter was washed with another 5 ml fresh methanol. All sediments were washed separately with 10 ml water and again centrifuged at 10^4 x g for 15 min. The supernatants were discarded and the sediments were each washed with 1 ml methanol and transferred in 2 ml Eppendorf tubes for a further centrifugation step under the same conditions. These supernatants were filtered through a fresh 0.2 μm filter. All drug containing methanol fractions were pooled in a 250 ml round bottom flask. The 65 ml methanol-drug solution was concentrated by vacuum evaporation at 40°C and 300 mbar to a final volume of 16 ml. The round bottom flask was fixed with a tripod sleeve over an ice water bath and a magnetic stirrer. With the help of a dropping funnel, twice the volume of methanol, which was 32 ml of water was dropped under gentle stirring into the ice cold methanol-drug solution for drug precipitation. The white precipitate was filtered through a

borosilicate glass frit with pore size 3 with the help of a vacuum pump. The pre-weighted frit was dried for several days in an exsiccator until a constant weight was observed. The dry weight was 578.3 mg, which represents a yield of 92.5% of the nominal drug content in the capsules.

Boc-alkyl linker (tert-Butyl-(3-bromopropyl) carbamate) synthesis

An amount of 3.45 g (15.5 mmol) of 3-Bromopropylamin hydrobromide was dissolved at 0°C in 25 ml methanol and mixed with 2.73 g triethylamine (27 mmol) in 1.75-fold molar excess. Then 27.5 mmol of Boc anhydride (di-tert-butyl dicarbonate) were dissolved in 15 ml methanol and added drop by drop under ice cooling. The solution was stirred for 2 hours at 0°C and dried afterwards under vacuum (Figure 2).
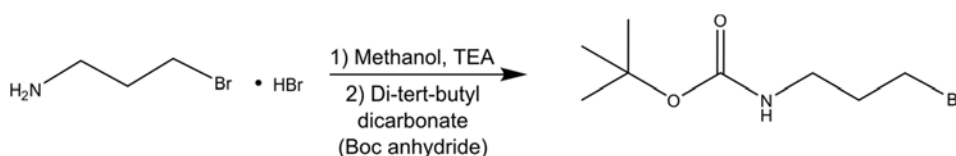
**Figure 2: Manufacture of Boc-protected alkyl linker for aprepitant modification**

The resulting product was resuspended in 35 ml DMF and transferred into 150 ml citric acid. A triple solvent extraction, using a separating funnel was performed by 75 ml ethyl acetate addition. The united organic phases were washed with diluted citric acid, saturated sodium chloride solution, saturated sodium hydrogen carbonate solution, and once again with saturated sodium chloride solution. The resulting solution was dried on sodium sulfate, filtered, and constricted under vacuum. The desired product was precipitated overnight in ethyl ether. The white crystals were obtained by drying under vacuum.

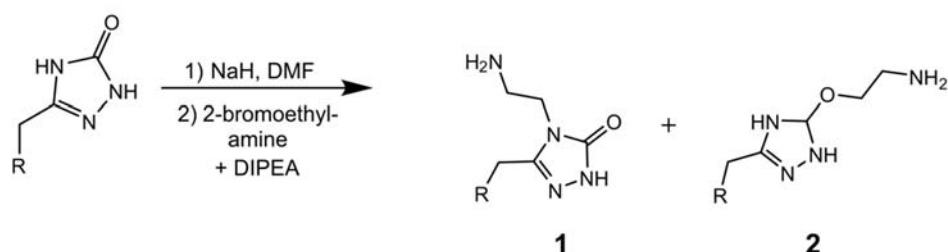## Boc-alkyl linker functionalization of aprepitant

Since there is no functional group for coupling in the original molecular structure of aprepitant, an alkyl linker was introduced to enable PEGylation and coupling to nanoparticles. The first synthesis strategy intended the addition of an unprotected alkyl linker

to deprotonated triazole group of aprepitant, either at the preferred nitrogen position, or the oxygen position (Figure 3). Because there was zero yield of the desired products in strategy 1, the base Diisopropylethylamine (DIPEA) was added in strategy 2 to reduce deprotonation of the drug molecule, which could be one reason for no product yield. However, this strategy also did not yield any alkylated aprepitant. Therefore, a third experiment commenced, where a Boc-protected alkyl linker (tert-Butyl-(3-bromopropyl) carbamate) was used. For all synthesis strategies, the respective work was performed under argon inert gas atmosphere to prevent oxidation of the easily inflammable sodium hydride in the first deprotonation step as well as oxidation of the aprepitant.
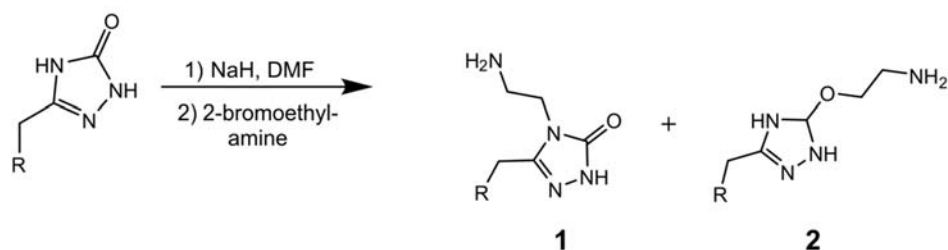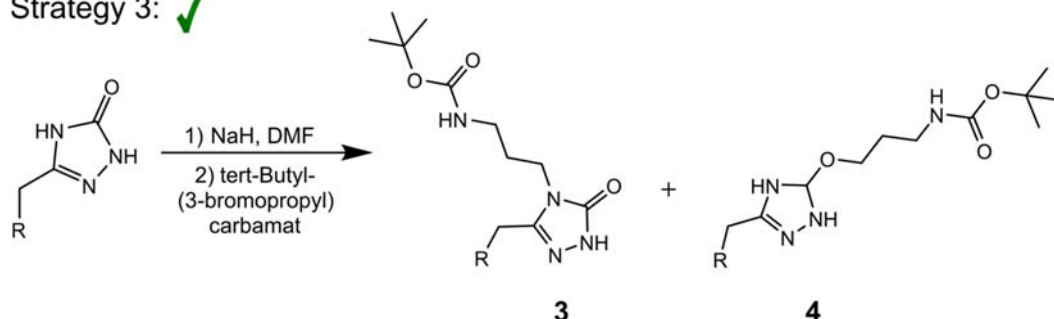

Figure 3: Tested synthesis strategies to introduce an alkyl linker to the 3-oxo-1,2,4 triazol-5-yl group of aprepitant for further chemical modification, such as PEGylation or covalent coupling to surface-functionalized nanoparticles. Alkyl linker addition was only observed for strategy 3 by using a Boc-protected alkyl linker.

For the third linker synthesis strategy (Figure 3), 200.15 mg Emend® isolate (aprepitant) were transferred in a baked out and argon-floated Schlenk plunger, dissolved in 10 ml anhydrous DMF, and subsequently transferred into the argon-floated dropping funnel of the experimental setup in Figure 4. Sodium hydride was used as deprotonation reagent in 1.65-fold molar excess to aprepitant. Therefore, 24.75 mg sodium hydride (60% suspension in paraffin oil) were transferred in the baked out and argon-floated Schlenk plunger of the experimental setup in Figure 4 and dissolved in 10 ml anhydrous DMF. Because of exothermal heating of the deprotonation reaction, the plunger was cooled by a freezing mixture, consisting of 115 g sodium chloride and 500 g crushed ice. The aprepitant solution was carefully added to the sodium hydride solution under thorough stirring for 15 min. The Boc-protected alkyl linker (tert-Butyl-(3-bromopropyl) carbamate) was used in 2-fold excess to the deprotonated aprepitant by dissolving 187.12 mg in a separate argon-floated Schlenk plunger in 10 ml water-free DMF and transferred in the dropping funnel for the second alkylation reaction step. The linker solution was added drop by drop to the deprotonated aprepitant.
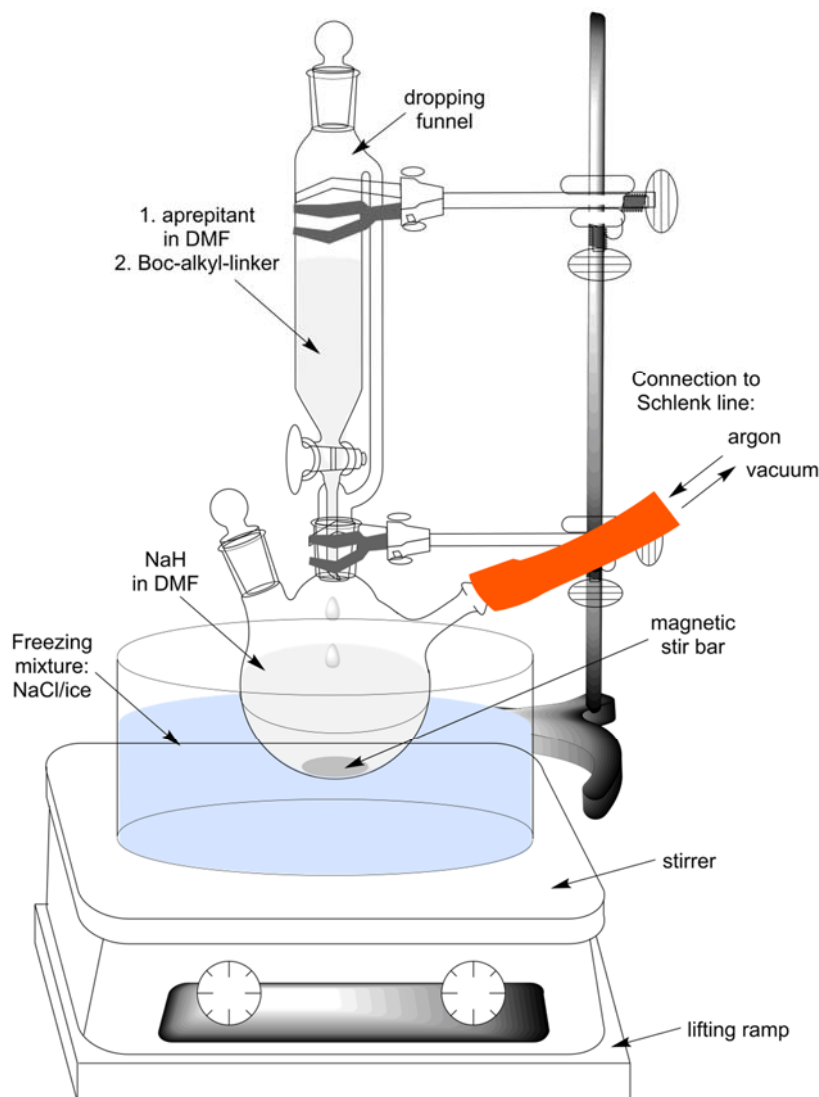
Figure 4: Experimental setup for water-free alkyl linker-aprepitant synthesis to prevent oxidation of sodium hydride and aprepitant.

The reaction was further stirred overnight at room temperature under argon atmosphere. The dropping funnel was replaced by an argon filled balloon. Then the product was precipitated under gentle stirring by the addition of 60 ml ice cold water, which is double the volume of the final reaction in anhydrous DMF, again using the dropping funnel. The crystallization was completed by further incubation at 4°C overnight. The precipitate was separated from the DMF:water mixture by filtration through a borosilicate glass frit with pore size 3 using a vacuum pump. The dry product was dissolved in ethanol (Uvasol®) for determining the concentration, using a calibration curve of pure aprepitant in ethanol.

Analysis of educt and product by HPLC-MS and ^{1}H-NMR

To confirm successful isolation and purification of aprepitant out of Emend capsules and subsequent alkyl linker addition, an HPLC-MS analysis was performed by an electrospray ionization mass spectrometer (Agilent Technologies, Waldbronn, Germany). For NMR analysis, 10 mg of dried substance before and after alkyl linker synthesis were each dispensed in 1 ml deuterated DMSO and filled in glass capillary tubes. ^{1}H-NMR spectra were recorded at room temperature on a Bruker Avance 300 spectrometer (Bruker BioSpin GmbH, Rheinstetten, Germany).

Confirmation of GPCR functionality of Boc-alkyl linker-aprepitant

Little is known about the exact binding of aprepitant to neurokinin-1 receptors, whether a modification at a special site within the molecule would influence the receptor binding properties, and if so, to which extent. Therefore, the binding efficiency of pure aprepitant, Emend-isolated aprepitant, and alkylated-Emend-isolated aprepitant was checked. For each aprepitant type, a 500 µM stock solution in DMF was prepared. Therefore, solvent was exchanged from ethanol to DMF by using a SpeedVac. Dilution series of all aprepitant types for the determination of IC_{50} values in an aequorin based luminescence calcium assay were made in DPBS, supplemented with 0.03% Pluronic F68. To exclude that DMF caused cytotoxicity, the highest used DMF concentration without antagonist was also tested for calcium signaling.

Binding studies via Aequorin calcium assay

Neurokinin-1 receptor ligand binding studies were performed with a stable transfected neurokinin-1 receptor expressing CHO cell line, which Dr. Ralf Schwandner (Amgen Research GmbH, BioPark Regensburg) kindly provided. The calcium based binding studies were performed according to the assay in Chapter 5. A frozen cell cryovial with 20^6 cells was thawed and washed and finally loaded for 2 hours 5 µg/ml coelenterazine under gentle shaking in the dark in 4 ml 8 mM L-glutamine and 1% PenStrep supplemented Leibovitz´s medium at room temperature. After dilution to $1*10^6$/ml with the same medium, the cells

were incubated for a further 2 hours. The calcium measurements were performed with a MicroLumat Plus luminescence microplate reader (Berthold Technologies, Bad Wildbad, Germany). Two 1:10 dilution series, starting from 10 µM and 3 µM final well concentrations, were prepared for aprepitant (reference substance), Emend-isolated aprepitant and Boc-alkyl linker-aprepitant and were filled in triplicate in separate wells of a white 96-well plate (Greiner Bio-One, Frickenhausen, Germany). The two pumps of the luminescence plate reader injection system were equilibrated respectively with the prepared CHO-NK$_1$R cell suspension and a 200 pM substance P-OMe competitive agonist solution. With a delay of 1.6 seconds, 50 µl cell suspension were injected into the well with 50 µl preload of antagonist and incubated for 1 min. Then 100 µl of competitive antagonist (final EC$_{80}$ substance P-OMe) was injected with the second pump to measure the literal antagonistic luminescence emission. The areas under the signal curves were calculated in triplicate for each antagonist concentration by integration and were plotted against the natural logarithm of used concentrations. All dose-response curves were normalized against the maximum calculated area in the calcium assay. The obtained dose-response points were fitted in SigmaPlot with an equation for sigmoidal dose-response with variable slope, to determine the ligand specific IC$_{50}$ values, which provide information about the binding affinity.

Results and discussion

HPLC-MS and ¹H-NMR analysis of Emend® capsule isolate

The success of aprepitant extraction out of Emend® hard capsules was verified by HPLC-MS analysis and ¹H-NMR. A dry yield of 92.5% could be obtained by the drug isolation procedure. In HPLC-MS analysis, no impurities or side products could be detected. The observed mass of 535.2 corresponded to the expected mass of pure aprepitant, and the UV spectrum of the extracted mass peak was identical to that obtained for the pure reference substance with two typical maxima at 264 nm and 272 nm (Figure 5).
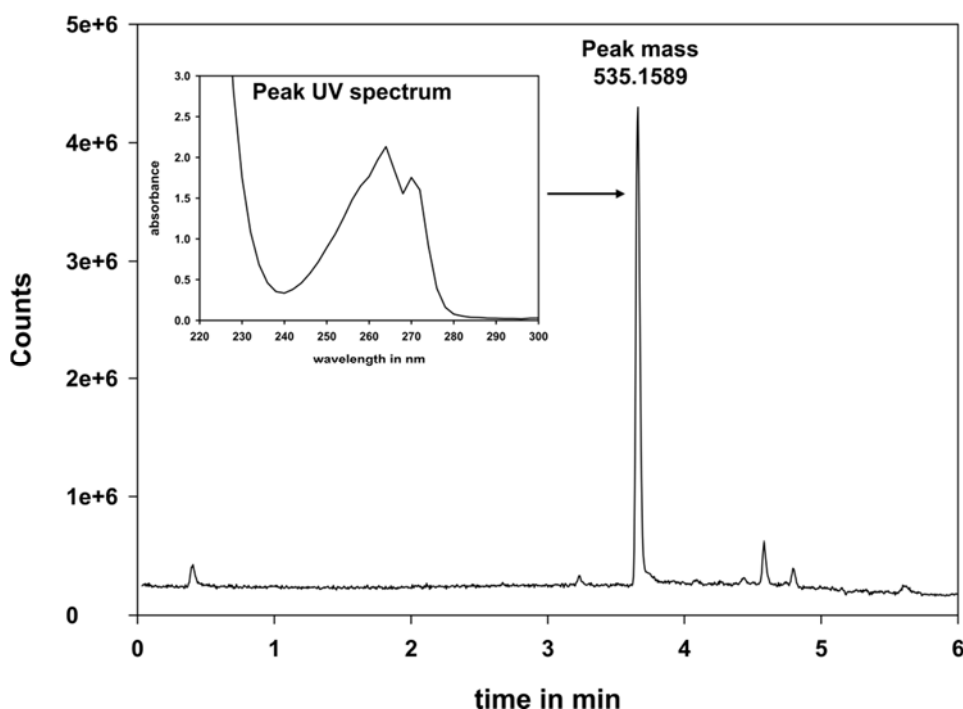

Figure 5: HPLC-ESI-MS chromatogram for Emend® isolate (TIC scan) and corresponding absorbance spectrum. The elution peak of aprepitant occured after 3.7 minutes. No impurities were detectable. The peak UV absorbance spectrum shows the typical shape for aprepitant with its maxima at 264 nm and 271 nm. The detected mass of 535.2 corresponds to the expected molecular weight of pure aprepitant.

The ^{1}H-NMR spectrum of Emend® isolate has shown the expected proton peaks for aprepitant. In total, 21 protons were detected (Figure 6). Typical solvent residual peaks of water and $(CD_3)_2SO$ were detected at 3.33 ppm and 2.50 ppm, respectively [13].
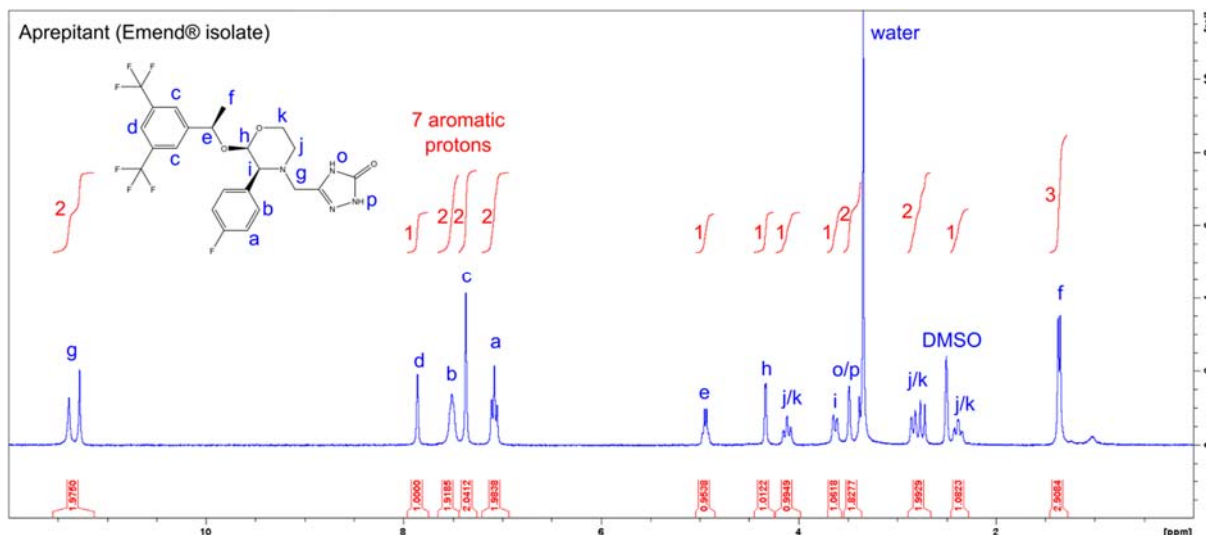

Figure 6: ^{1}H-NMR spectrum of isolated aprepitant (300 MHz, $(CD_3)_2SO$). Abbreviations: s = singulet, d = doublet, t = triblet, m = multiplet: δ = 1.36 (d, J = 407.7 Hz, 3 H, f-H), δ = 2.38 (t, J = 714.7 Hz, 1 H, j/k-H), δ = 2.79 (m, J = 837.1 Hz, 2 H, j/k-H), δ = 3.49 (d, J = 1046.1 Hz, 2 H, o/p-H), δ = 3.63 (d, J = 1088.4 Hz, 1 H, i-H), δ = 4.12 (t, J = 1235.0 Hz, 1 H, j/k-H), δ = 4.33 (d, J = 1300.3 Hz, 1 H, h-H), δ = 4.94 (m, J = 1482.4 Hz, 1 H, e-H), δ = 7.08 (t, J = 2124.9 Hz, 2 H, a-H), δ = 7.37 (s, J = 2211.4 Hz, 2 H, c-H), δ = 7.51 (t, J = 2253.8 Hz, 2 H, b-H), δ = 7.86 (s, J = 2358.39 Hz, 1 H, d-H), δ = 11.33 (d, J = 3399.9 Hz, 2 H, g-H).

HPLC-MS and NMR analysis of Boc-alkylated aprepitant

The correct mass of Boc-alkylated aprepitant was verified by HPLC-MS analysis and ^{1}H-NMR. For relative comparison of aprepitant peaks in HPLC-MS analysis, the UV detector was set at 264 nm (Figure 7). The observed mass of the main product was 692.3 g/mol and correlated with the expected mass of Boc-alkylated aprepitant. A later, much smaller eluting peak mass of 849.4 g/mol indicated a double-Boc-alkylated side product. Only negligible amounts of unreacted aprepitant were detected.
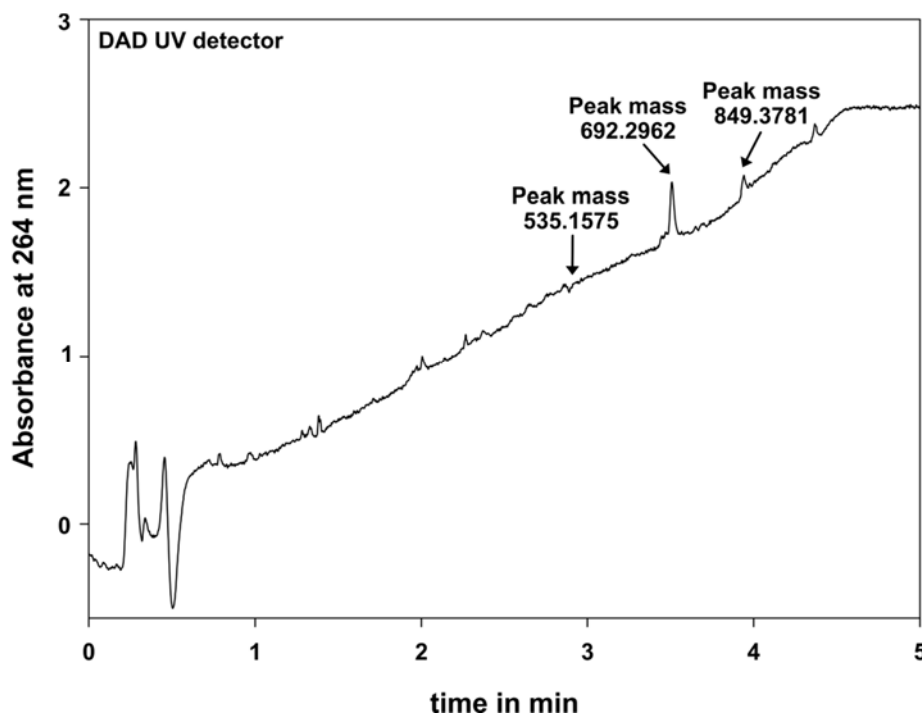
Figure 7: HPLC-ESI analysis of Boc-protected propylamine-aprepitant. The shown elution profile was detected with UV detector at 264 nm. The correct mass peak for Boc-alkylated aprepitant was detected at 3.5 min with a mass of 692.3. The mass of a second, less dominant peak at 4.0 min was 849.3781 and corresponds to the mass of a double-alkylated product. Only small amounts of non-alkylated aprepitant were detected at 2.9 min with an extracted mass of 535.2.

The ^{1}H-NMR analysis after tert-Butyl-(3-bromopropyl)carbamate addition could not be conclusively interpreted due to further proton peaks caused by either double-Boc-alkylated aprepitant side products or the alkylation at the less preferred oxygen position at the triazole ring. This was additionally indicated by a total of more than 36 protons (Figure 8). The typical solvent residual peaks of water and $(CD_3)_2SO$ were detected at 3.33 ppm and 2.50 ppm, respectively, and an additional DMF peak at 7.95 ppm [13].
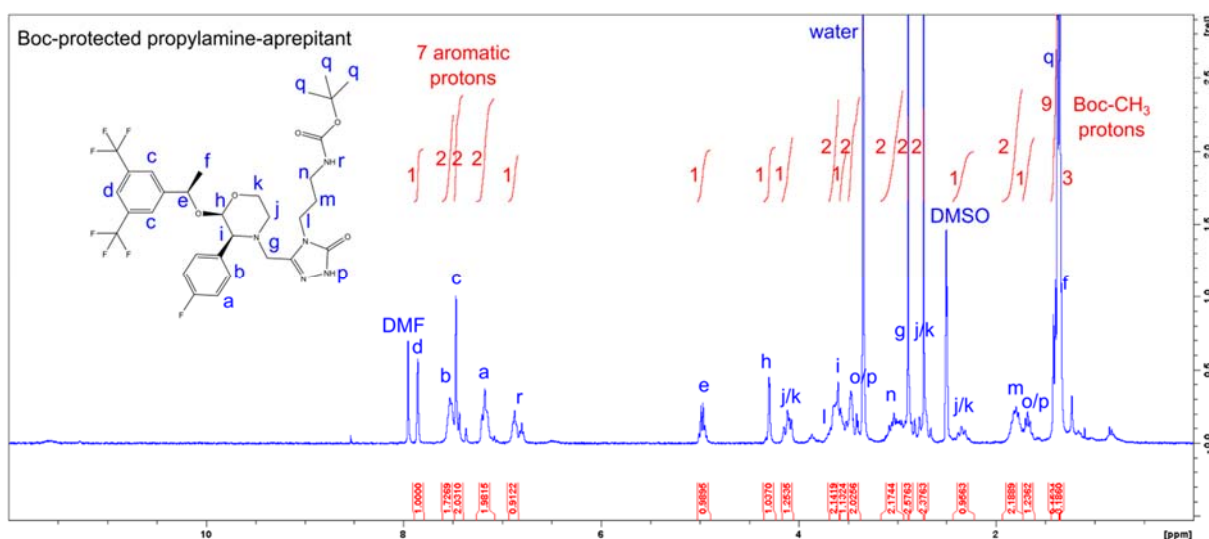
Figure 8: ^{1}H-NMR spectrum of Boc-protected amine-linker synthesis product (300 MHz, (CD$_3$)$_2$SO). Abbreviations: s = singulet, d = doublet, t = triblet, m = multiplet: δ = 1.35-1.36 (J = 406.7 Hz, 3 H, f-H), δ = 1.36-1.45 (J = 421.6 Hz, 9 H, q-H), δ = 1.68 (m, J = 503.6 Hz, 1 H, o/p-H), δ = 1.78 (m, J = 539.0 Hz, 2 H, m-H), δ = 2.35 (m, J = 704.9 Hz, 1 H, j/k-H), δ = 2.73 (s, J = 819.2 Hz, 2 H, j/k/g-H), δ = 2.89 (s, J = 867.3 Hz, 2 H, j/k/g-H), δ = 2.94-3.17 (m, J = 910.4 Hz, 2 H, n-H), δ = 3.37-3.50 (m, J = 1031.8 Hz, 2 H, o/p-H), δ = 3.50-3.58 (m, J = 1051.8 Hz, 1 H, i-H), δ = 3.59-3.69 (m, J = 1093.3 Hz, 2 H, l-H), δ = 4.11 (m, J = 1234.1 Hz, 1 H, j/k-H), δ = 4.30 (m, J = 1290.0 Hz, 1 H, h-H), δ = 4.97 (m, J = 1290.0 Hz, 1 H, e-H), δ = 6.87 (t, J = 2062.7 Hz, 1 H, r-H), δ = 7.18 (t, J = 2153.8 Hz, 2 H, a-H), δ = 7.44 (d, J = 2241.4 Hz, 2 H, c-H), δ = 7.53 (t, J = 2259.9 Hz, 2 H, b-H), δ = 7.85 (s, J = 2357.4 Hz, 2 H, d-H)

Binding studies via aequorin assay

The binding capacities of pure aprepitant as a reference substance, Emend® isolated aprepitant and Boc-alkylated aprepitant were tested in an aequorin luminescence-based calcium assay. It was found that the isolated aprepitant from Emend® capsules showed almost the same binding affinity as the pure substance, which confirmed the validity of the used isolation and purification procedure. After alkylation, the binding affinity was 3.9-fold reduced. Due to the quite high initial affinity of 35.4 nM of unmodified aprepitant, the affinity is still in the nanomolar concentration range with and IC$_{50}$ of 115.2 nM (Figure 9).
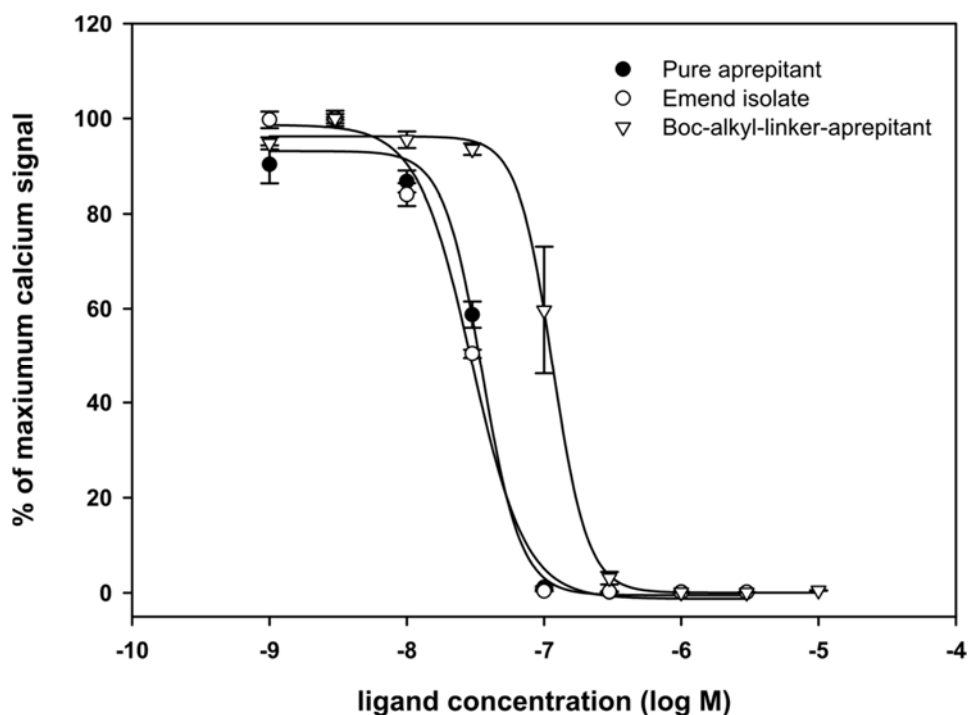
Figure 9: The determined affinity of the Emend® isolate with an IC_{50} = 29.7 is close to that of pure aprepitant with an IC_{50} = 35.4 nM. The addition of a Boc-alkyl linker for further chemical modification negatively influences the binding affinity in the form of a 3.9-fold drop-in affinity to an IC_{50} = 115.2 nM.

Conclusion

To overcome the limitations of post-synthetic modification of small molecular weight neurokinin-1 receptor antagonists due to the lack of functional groups, it could be shown that chemical modification of the triazole group of aprepitant is possible by using a strong deprotonation reagent and a tert-Butyl-(3-bromopropyl)carbamate as an alkyl linker with Boc-protected amine functionality. In a binding study with the final product, it was found that the affinity dropped 3.9-fold, but still has an acceptable IC_{50} of 115.2 nM and therefore represents a promising antagonist for nanoparticle functionalization and further multivalent receptor binding studies. One drawback of this Boc-protected antagonist was the Boc-group cleavage under conditions, which are strong enough for deprotection on the one hand, and mild enough to keep the basic morpholine-ring structure of aprepitant intact on the other hand [8]. A better option would have been the introduction of an alkyl linker without the Boc-protecting group, but there is currently no way to perform such an alkylation. Therefore, it is proposed that the best way to obtain an amine-alkyl-linker functionalized aprepitant is to start the design of the desired drug molecule by stepwise synthesis from the very beginning instead of post-synthetic linker addition.

References

[1]   Rojas C, Raje M, Tsukamoto T, Slusher BS. Molecular mechanisms of 5-HT3 and NK1 receptor antagonists in prevention of emesis. European Journal of Pharmacology 2014; 722: 26–37.

[2]   Watling KJ. Nonpeptide antagonists herald new era in tachykinin research. Trends in Pharmacological Sciences 1992; 13: 266–269.

[3]   Lembeck F, Donnerer J, Tsuchiya M, Nagahisa A. The non-peptide tachykinin antagonist, CP-96,345, is a potent inhibitor of neurogenic inflammation. British Journal of Pharmacology 1992; 105: 527–530.

[4]   Hargreaves R, Ferreira, Juan Camilo Arjona, Hughes D, et al. Development of aprepitant, the first neurokinin-1 receptor antagonist for the prevention of chemotherapy-induced nausea and vomiting. Annals of the New York Academy of Sciences 2011; 1222: 40–48.

[5]   Navari RM. Fosaprepitant (MK-0517): a neurokinin-1 receptor antagonist for the prevention of chemotherapy-induced nausea and vomiting. Expert Opin Investig Drugs 2007; 16: 1977–1985.

[6]   Navari RM. Aprepitant: a neurokinin-1 receptor antagonist for the treatment of chemotherapy-induced nausea and vomiting. Expert Review of Anticancer Therapy 2014; 4: 715–724.

[7]   Bhandari P. Recent advances in pharmacotherapy of chemotherapy-induced nausea and vomiting. J Adv Pharm Tech Res 2012; 3: 202.

[8]   Liu J, Zou M, Piao H, et al. Characterization and Pharmacokinetic Study of Aprepitant Solid Dispersions with Soluplus®. Molecules 2015; 20: 11345–11356.

[9]   Müller R, Junghanns. Nanocrystal technology, drug delivery and clinical applications. IJN 2008: 295.

[10]   Li B, Berliner M, Buzon R, et al. Aqueous Phosphoric Acid as a Mild Reagent for Deprotection of tert -Butyl Carbamates, Esters, and Ethers. J. Org. Chem. 2006; 71: 9045–9050.

[11]   Moussaoui SM, Montier F, Carruette A, Blanchard JC, Laduron PM, Garret C. A non-peptide NK1-receptor antagonist, RP 67580, inhibits neurogenic inflammation postsynaptically. British Journal of Pharmacology 1993; 109: 259–264.

[12]   Merck. Drug Information Emend; 2004.

[13]   Gottlieb HE, Kotlyar V, Nudelman A. NMR Chemical Shifts of Common Laboratory Solvents as Trace Impurities. J. Org. Chem. 1997; 62: 7512–7515.

- 125 -

Chapter 7

Enzymatic ligand activation on the surface of nanoparticles

Abstract

For peptide ligands, immobilized on the surface of nanoparticles for multivalent GPCR targeting, the question arises as to whether these ligands are susceptible to enzymatic cleavage even though there is a shielding against macrophages and enzyme attack by the flexible nanoparticle´s PEG corona, in which coupled ligands are able to isolate themselves. Especially if the cutting site within a peptide sequence is localized a favorable distance away from the PEG anchor position, a ligand cleavage seems to be possible. However, is it possible to process a ligand specifically at a target site, where a special enzyme is produced in high rates and if this is so, is the particle still able to bind to a specific GPCR? As a model for such a ligand conversion into its active form, angiotensin I was chosen, which is processed by ACE to angiotensin II. Angiotensin II is the preferred ligand for AT_1 receptors (AT_1Rs), which is expressed, for example, in rat mesangial cells. In the first part of this work, a renal cell line was sought, expressing both ACE and AT_1R at high levels. In the second part, we investigated the mechanistic principle of enzymatic ligand activation on the surface of nanoparticles in general. In the performed PCR experiments, only rat and human mesangial cells, but not rat tubule cells, were identified as AT_1R positive cell types. However, in a functional calcium assay, only the rat mesangial cells gave a positive signal for the AT_1R. According to PCR results, ACE is only expressed by human mesangial cells and tubule cells. In a functional Förster Resonance Energy Transfer (FRET) based assay, where Captopril was used as an ACE specific inhibitor, it was observed that ACE is most selectively expressed by the renal tubule cell line NRK-52E. The enzymatic cleavage mechanism of angiotensin I ligands on QDs was examined using highly efficient recombinant human ACE. In a Fura-2 calcium assay, a significantly different calcium mobilization of enzyme incubated angiotensin I-modified QDs was measured, which was the first hint for successful nanoparticle activation. In contrast, in FACS binding studies, no significant greater binding was observed for enzymatically activated QDs.

Intoduction

Angiotensin II is degraded within seconds by peptidases in the blood [1]. Sensitivity to enzymatic cleavage processes and opsonization after they were administered are chief causes [2]. Most cleavage mechanisms are driven by the recognition from immune system and reticuloendothelial system (RES) affiliated cells [3]. For better resistance against these clearance causes, nanoparticles used for drug delivery are shielded by so-called stealth coatings, which are, in most cases, hydrophilic and non-charged polymers such as PEG and polysaccharides or zwitterionic polymers or even biomimetic red blood cell (RBC) membranes [4–6]. However, in some cases cleavage processes are not unwanted. There are many cleavage mechanisms of precursor peptides and proteins that are essential to bring them into an active form, as is the case for the Renin-Angiotensin-System (RAS) involved in the regulation of blood pressure [7]. The RAS can be described as a kind of cleavage cascade, where the liver and renal derived precursor angiotensinogen is cleaved by renin in the kidney to angiotensin I, which itself is further shortened by ACE to angiotensin II [8]. Although ACE is not the best example for producing beneficial therapeutic effects—rather the opposite is the case since angiotensin II is known to cause hypertension [9,10]. Also, in diabetic nephropathy, intrarenal angiotensin II production is increased because of higher local ACE activity. However, this kind of enzyme driven activation can be one further key mechanism to overcome the problem of off-target cell and tissue targeting. To date, only highly selective ligands, multiple selective ligands, and some enzyme driven shielding mechanisms were taken into account, when ligands are immobilized on the surface of nanoparticles [11–13]. According to our current state of knowledge, there is no evidence that the ligand itself is activated by an enzyme driven cleavage mechanism to obtain multivalent GPCR targeting through a peptide ligand decorated nanoparticle. This study was performed to investigate whether it is possible to activate angiotensin I coated QDs *in vitro* by human recombinant ACE. Therefore ACE-incubated QDs were added to AT_1R positive mesangial cells to examine their binding ability by GPCR triggered calcium mobilization measurements, fluorescence microscopy, and flow cytometry. In parallel, there was a search for an appropriate cell line that expresses both targets, ACE and the AT_1R. Therefore, we performed RT-PCR experiments, calcium measurements as a proof for the presence of functional AT_1 receptors, and a FRET-based assay for ACE detection.

Materials and methods

All chemicals were obtained from Sigma Aldrich (Taufkirchen, Germany) in analytical grade unless stated otherwise. Dulbecco's phosphate-buffered saline (DPBS) pH 7.4 consisting of 1.5 mM KH_2PO_4, 8 mM Na_2HPO_4, 2.7 mM KCl and 138 mM NaCl was purchased from Life Technologies/Thermo Scientific (Darmstadt, Germany). Ultrapure water was obtained from a Milli-Q water purification system (Millipore, Billerica, MA, USA). Rat mesangial cells were a gift from Prof. Armin Kurtz (Department of Physiology, University of Regensburg, Germany). NRK-52E tubule cells were obtained from Prof. Joachim Wegener (Department of Analytical Chemistry, University of Regensburg, Germany). The human mesangial cells were a gift from Dr. Miriam Banas (Internal Medicin II/Nephrology, University of Regensburg). Rat mesangial cells were cultured in RPMI 1640 + glutamate, 2 g/l $NaHCO_3$, 100 nM Hydrocortisone, 10 ml/l Insulin-Transferrin-Natriumselenit (ITS), 1% Penicillin/ Streptomycin, 10% FCS. NRK-52E; tubule cells were cultured in DMEM, 5% FCS; and human mesangial cells were cultured DMEM, supplemented with 4 mM L-Glutamine, 1% Penicillin/Streptomycin, 10% FCS.

Determination of renal cell lines for AT_1 receptor and ACE expression by RT-PCR

Various renal cell types, such as mesangial cells and tubule cells, were examined for AT_1R and ACE expression by RT-PCR. The peqGOLD Total RNA Kit and the peqGOLD DNase I Digest Kit were used for mRNA extraction and to remove potentially present DNA. Both kits were used according to the manufacturer´s instructions. The RNA content was determined at a NanoDrop UV meter. Then 2 μg RNA were reverse-transcribed with the peqGOLD cDNA Synthesis Kit H Minus, using an oligo(dT) primer and random primer mix of 170 ng to 30 ng. The resulting cDNAs were used as templates for amplification in PCRs. For PCR, the peqGOLD Taq-DNA-Polymerase was used. For each reaction, a total volume of 25 μl with a primer content of 10 pmol and 1 μl of cDNA template were used. As reaction buffer, 10x reaction buffer S was chosen with a $MgCl_2$ content of 15 mM. All other components were applied according the manufacturer´s instructions. The primers were ordered from Eurofins Genomics, Ebersberg, Germany (Table 1).

Table 1: Primer sequences

Target	Sequence (5´-> 3´)	T_m in °C	GC content in %
Human ACE [14]	Forw.: GGTGGTGTGGAACGAGTATG	59.4	55.0
	Rev.: TCGGGTAAAACTGGAGGATG	57.3	50.0
Rat ACE [15]	Forw.: TCCTGCTAGACATGGAGACGA	59.8	52.4
	Rev.: CAGCTCTTCCACACCCAAAG	59.4	55.0
Human AT$_1$R [16]	Forw.: GCTTTCCTACCGCCCCTCAGA	63.9	61.9
	Rev.: TTTCGAACATGTCACTCAACCTCAA	61.1	40.0
Human AT$_1$R (used for rat) [17]	Forw.: GGCCAGTGTTTTTCTTTTGAATTTAGCAC	62.8	37.9
	Rev.: TGAACAATAGCCAGGTATCGATCAATGC	63.6	42.9

The following PCR programs were used:

1. Denaturation	94°C	2 min	
2. Denaturation	94°C	30 sec	
3. Annealing	60°C[1)]/57°C[2)]	60 sec[1)]/30 sec[2)]	40[1)]/35[2)] cycles
4. Elongation	72°C	30 sec	
5. Final elongation	72°C	7min	
6.	4°C	∞	

[1)] NRK-52E tubule cells, [2)] human and rat mesangial cells

The amplified cDNA was visualized by gel electrophoresis with 2% agarose (Invitrogen/Thermo Scientific, Darmstadt, Germany) in 1x TAE buffer. The bands were visualized by adding 0.4 µg/ml ethidium bromide to pre-solid gel. For sample load, 20 µl of PCR reaction product was mixed with 4 µl 6x Loading Dye (Peqlab, Erlangen, Germany). For fragment size determination the peqGOLD 50 bp DNA ladder was used.

Examination of supernatants of NRK-52E rat tubule cells for peptidase activity

In calcium measurements of CCM supernatants, supplemented with angiotensin I for cell-derived ACE conversion to angiotensin II, the renal rat tubule cell line NRK-52E was examined for functional ACE expression. Angiotensin I was incubated in a time range of 25 hours and the influence of zinc addition to the medium was evaluated. The NRK-52E cells were grown to 85% confluency in 1x DMEM with phenol red and 5% FCS in T25 cell culture flasks. Then the medium was replaced by differently concentrated angiotensin I containing 1xDMEM media (1 µM and 2 µM) without phenol red and without FCS, but either with or without 10 µM $ZnCl_2$. As a control for successful angiotensin I conversion, the ACE inhibitor Captopril was used in 25-fold excess to angiotensin I. At time points 2 h, 4 h, 6 h and 25 h, a supernatant volume of 155 µl was sampled and frozen at -20°C until calcium measurement.

Fura-2 calcium assay

AT_1 receptor positive mesangial cells were grown until confluency, washed twice with warm DPBS, and loaded for 1 hour at room temperature with 5 µM calcium chelator Fura-2 acetoxy methyl ester (Life Technologies/Thermo Scientific, Darmstadt, Germany) in the presence of 2.5 mM ABC transporter inhibitor probenecid (Santa Cruz, Heidelberg, Germany) in Leibovitz medium. Due to acetoxy methyl ester cleavage, Fura-2 can penetrate cells and is trapped there by the action of probenecid. The excess of Fura-2 was removed by 5 min centrifugation at 200 x g, two washing steps in probenecid containing Leibovitz medium, and further centrifugal steps. Finally, the cells were resuspended in probenecid containing medium to a cell density of $1*10^6$ cells/ml. In a 96-well plate (Greiner Bio-One, Frickenhausen, Germany), 50 µl of each medium supernatant, collected from NRK-52E cells were provided. Medium without cell contact was used as a control. All other samples for calcium measurements, such as free angiotensin I or angiotensin I-modified QDs, were diluted in DPBS. With the help of a BMG Omega Microplate reader and its injector system, 150 µl of the Fura-2 loaded mesangial cell suspension was injected to mix with the tubule supernatants to measure calcium influx in dual excitation mode. Therefore, excitation filters

340/20 nm and 380/nm were used. For both, excitations the emissions were detected using a 510/20 nm band-pass filter. The calcium influx into cells was calculated based on the Grynkiewitcz equation, which is proportional to the 510 nm emission ratio by excitation at 340 nm and 380 nm. The maximum and minimum calcium signals were obtained by complete cell lysis after 0.1 % Triton X 100 without (max) and with 4.5 mM EGTA (min) for total calcium complexation in two separate wells.

The binding affinity of angiotensin I to AT$_1$ receptors

To determine whether angiotensin I is also able to bind to AT$_1$ receptors, a dose-response curve was recorded in a calcium assay. As a control for selective angiotensin I binding to solely AT$_1$ receptors, the highly selective AT$_1$ receptor antagonist EXP3174 (Santa Cruz, Heidelberg, Germany) was used, which is a Losartan derivative.

Determination of enzyme activity by a FRET-based cleavage assay

As a fluorogenic protease substrate Mca-Arg-Pro-Pro-Gly-Phe-Ser-Ala-Phe-Lys(Dnp)-OH[Mca=(7-methoxycoumarin-4-yl)acetyl;Dnp=2,4-dinitrophenyl] (Enzo Life Sciences GmbH, Lörrach, Germany) was used. It is substrate for ECE-1 and ECE-2, ACE1 and ACE2, neprilysin, MMP-2 and MMP-9, and thimet oligopeptidase, as well as cathepsin A, cathepsin X/Z, BACE, and insulinase, but not MMP-1. The fluorescence of Mca at 390 nm is efficiently quenched by the Dnp group in the peptide sequence by its proximity until enzymatic cleavage separates them. In presence of an enzyme, this FRET state becomes interrupted and donor emission at 390 nm can be measured after excitation at 340 nm. Therefore, this peptide is a valuable tool for time related enzyme activity studies (Figure 1).
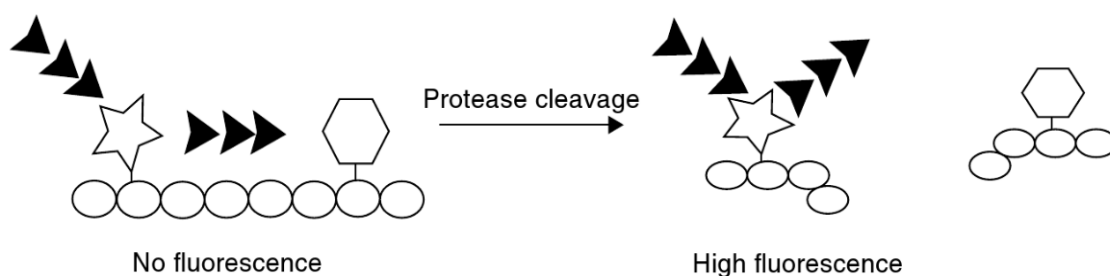
Figure 1: Principle of FRET assay for the determination of ACE activity. Before a peptide is cleaved, FRET-based transfer of donor emitting fluorescence is absorbed by a donor in tight proximity, within the so-called Förster distance. After protease cleavage, the quenching is interrupted so that direct donor emission can be measured.

For standard curve preparation, various FRET substrate concentrations from 2.5 to 12.5 µM were converted by 0.2 ng/µl recombinant human ACE (R&D Systems, Bio-Techne GmbH, Wiesbaden-Nordenstadt, Germany). Therefore, 10 µg of ACE were diluted to a final stock concentration of 1 µM (0.143 µg/µl) in a sterile buffer, consisting of 12.5 mM Tris, 75 mM NaCl, 0.5 µM $ZnCl_2$, pH 7.5. ACE stock solution aliquots of 5 µl were stored at -20°C in sterile Protein LoBind Tubes (Eppendorf AG, Hamburg, Germany) until use. For the FRET measurement, the enzyme was diluted in the same buffer to 0.4 ng/µl. This enzyme solution was kept on ice until use. For the assay, 50 µl of the enzyme solution was preloaded into a black 96-well plate (Greiner Bio-One, Frickenhausen, Germany) and 50 µl of substrate, diluted in Leibovitz medium was added. For ACE specific enzyme inhibition, another equivalent substrate dilution series, supplemented with a constant Captopril concentration of 10 µM was prepared. The enzyme kinetics were immediately captured with a BMG Omega Microplate reader, heated at 37°C within 6 hours.

For measuring the ACE activity of cells were seeded in a cell type dependent ideal density from 10,000 to 25,000 in a black 96-well plate with clear bottom and CellBIND surface (Corning, Wiesbaden, Germany) and were grown for 24 h at 37°C and 5% CO_2 atmosphere. The medium was removed and cells were washed once with warm DPBS. Then various FRET substrate concentrations from 2.5 µM to 10 µM either without or with competitive 10 µM Captopril addition, all diluted in Leibovitz were added and the kinetic measurements over 6h at 37°C were started immediately.

In vitro ACE driven activation of angiotensin I-modified quantum dots

The synthesis of angiotensin I-modified QDs is described in Chapter 3. For the *in vitro* conversion of angiotensin I decorated QDs, human recombinant ACE was used (Figure 2).
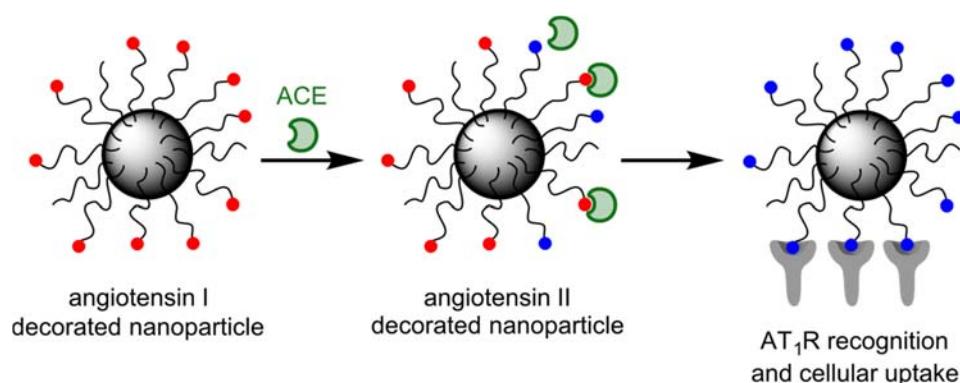

Figure 2: Principle of enzymatic activation of ligand decorated nanoparticles. Angiotensin I is attached to the PEG chains on the surface of QDs. The particles are then incubated with soluble ACE and subsequently tested for their interaction with AT1R positive cells.

The QDs were mixed in Protein LoBind Bind Tubes to a final concentration of 40 nM or 80 nM with 5 nM ACE in DPBS and were supplemented with or without either 8 µM Captopril or 24 µM EXP3174. The tubes were incubated for 1.5 hours at 37°C to start enzymatic angiotensin I conversion. For a following Fura-2 calcium assay, 50 µl of each sample was loaded in a 96-well plate and mixed by an injection of 150 µl AT_1R positive mesangial cell suspension, leading to a final QDs concentration of 10 nM or 20 nM and 6 µM of AT_1R inhibitor EXP3174.

Fluorescence microscopy

Angiotensin I functionalized QDs were enzymatically activated by human recombinant ACE before they were used in 2D cell culture studies. 1 pmol QDs were converted in a 5 nM solution of ACE in DPBS at 37°C for 2 hours. After this enzymatic ligand conversion step, the QDs were further diluted to a final concentration of 10 nM with Leibovitz´s medium, containing final 0.3% BSA. This solution was administered to AT_1 receptor positive rat

mesangial cells, seeded into 8-well µ-slides (Ibidi, Martinsried, Germany) and incubated for 80 min at 37°C, 5% CO_2 atmosphere to assess nanoparticle binding. Unbound nanoparticles were removed by two consecutive washing steps with pre-warmed DPBS and the cells were covered with warm Leibovitz´s medium. The enzyme driven nanoparticle binding upon peptide ligand conversion was examined by fluorescence microscopy, using a 63x Plan-Apochromat (NA 1.4) oil immersion objective with a Zeiss Axiovert 200 microscope equipped with an LSM 510 laser-scanning device (Zeiss, Jena, Germany). The QDs were excited with an argon-ion laser at 488 nm, and fluorescence emission was recorded using a 560–615 nm band-pass filter. For image acquisition, AIM 4.2 software (Zeiss, Jena, Germany) was used. Images were processed using ImageJ software.

Flow cytometry analysis

Rat mesangial cells of passage 92 were seeded in a density of 10^5 cells per well in a 24-well plate (Corning, Wiesbaden, Germany) and were grown for 48 hours. An amount of 2 pmol angiotensin I-modified QDs were pre-incubated for 2 hours at 37°C with 5 nM human recombinant ACE in DPBS either with or without 10 µM Captopril. Then the solutions were diluted to a final QD concentration of 10 nM in Leibovitz´s medium, containing final 0.3% BSA. As a second inhibitor control, 2.5 µM EXP3174 was included. In each well, 200 µl of QD sample solution was added after washing the cells once with warm DPBS. The cells were incubated for 1 hour with the nanoparticles at 37°C and 5% CO_2, before the solutions were aspirated. The cells were washed with warm DPBS and detached by trypsinization for 5 min at 37°C. The enzyme was inactivated by addition of warm 10% FCS containing Leibovitz´s medium. The cell suspensions were transferred in 1.5 ml Eppendorf tubes and kept on ice. The cells were spun down at 4°C and 200*g. The resulting pellets were washed in ice cold DPBS and centrifuged again under the same conditions. Finally, the pellets were resuspended in 200 µl DPBS for FACS analysis with a FACSCalibur flow cytometer (Becton Dickinson, Franklin Lakes, NJ, USA). Cell bound QDs were excited at 488 nm and detected in the FL-2 channel with band-pass filter 585/42 nm. The voltage was set at 702 and 10^4 events were detected. Flow cytometry data were analyzed by Flowing Software version 2.5 (Turku Centre for Biotechnology, Turku, Finland). Only the population of viable cells was gated and used for GeoMean fluorescence intensity determination.

Results and discussion

RT-PCR to determine AT$_1$ receptor and ACE expression in renal cell lines

With the help of reverse transcription PCR, the cell types that express mRNA for either ACE or the AT$_1$ receptor, or both in the best case, could be shown. It was found that human mesangial cells showed expected bands for AT$_1$R and ACE at 84 bp and 428 bp, respectively (Figure 3A). The rat tubule cell line NRK-52E exhibits only ACE expression, indicated by a band at 142 bp, but no receptor expression (Figure 3B). Rat mesangial cells express the AT$_1$R due to a band at 210 bp but not ACE, even if cells were stimulated with high glucose concentrations (Figure 3C). In the pathogenesis of diabetic nephropathy, high extracellular glucose also seems to be directly involved in the subsequent production of cytokines and growth factors by glomerular, tubular, vascular, and interstitial cells [7]. The stimulation of cells in 2D culture with glucose is recommended in the literature to influence the AT$_1$R and ACE expression with increasing glucose concentration [18]. The normal glucose concentration is 10 mM, high glucose is 30 mM, and very high is 60 mM.
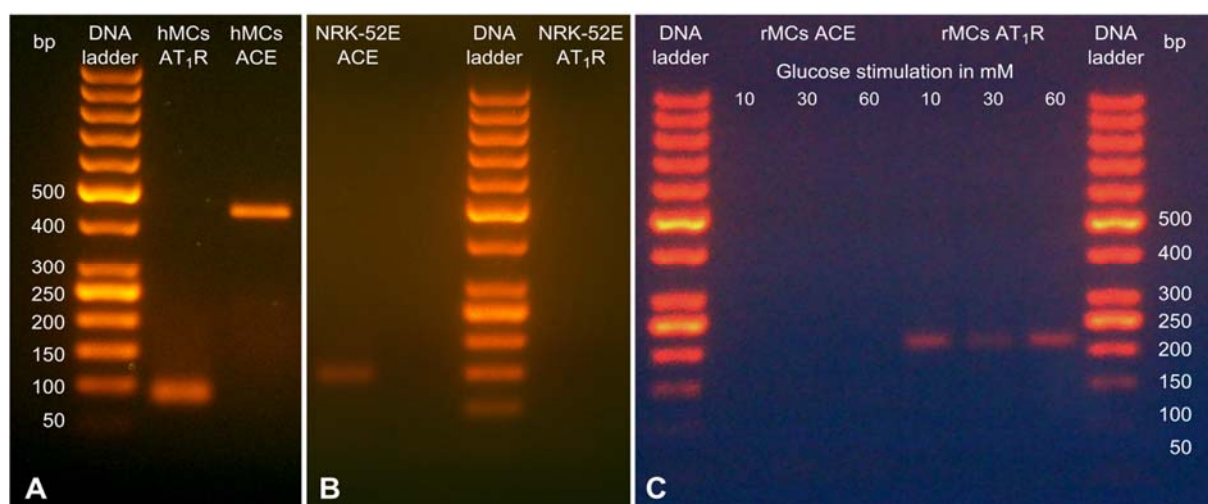

Figure 3: RT-PCR amplified cDNA products, separated in 2% agarose gels

Therefore, the human mesangial cells seemed to be a promising target cell line for further experiments. Unfortunately, these human mesangial cells did not show a clearly positive response to angiotensin II in calcium measurements, which indicates that only a few

functional receptors are present on the cell surface. For the NRK-52E tubule cells, no calcium signal could be measured, which corresponds to the data obtained by RT-PCR (Figure 4).
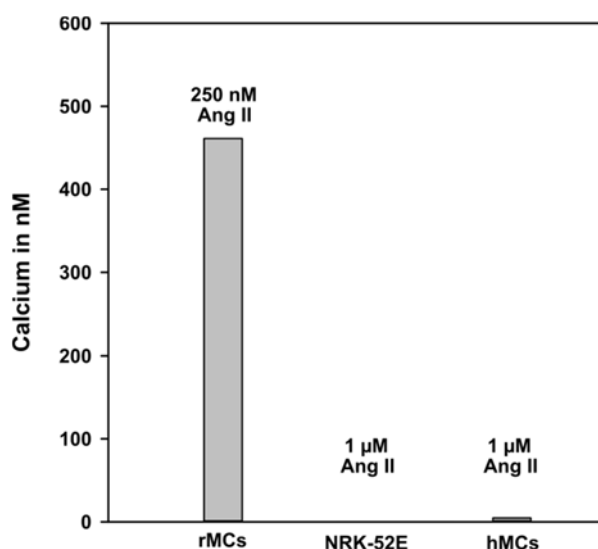

Figure 4: Comparison of calcium signals for different cell types

The binding affinity of angiotensin I to AT_1 receptors

Besides angiotensin II, angiotensin I is also likely to bind to the AT_1 receptors. However, compared to angiotensin II, angitoensin I binds with about a 54-fold lowered affinity to the AT_1 receptor (Figure 5). In regard of this fact, for further experiments concerning the effects of ACE dependent angiotensin I conversion, only substrate concentrations lower than 300 nM were used. A 10-fold excess of EXP3174 could markedly suppress the generated calcium signal, which indicates the selective binding of angiotensin I to AT_1 receptors.
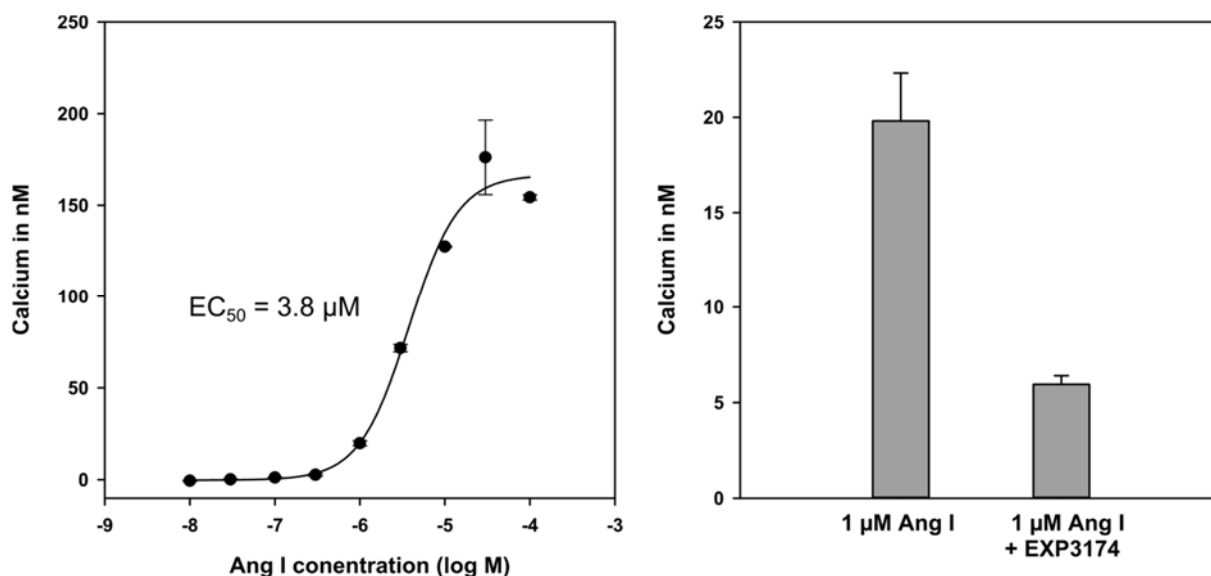
Figure 5: Angiotensin I shows selective affinity to AT1 receptors in a concentration-dependent manner, which can be suppressed by EXP3174.

Examination of supernatants of NRK-52E rat tubule cells by calcium measurements

The medium supernatants of NRK-52E tubule cells produced an increase in calcium signal, dependent on the applied angiotensin I concentration and incubation time (Figure 6). Contrary to the expectation, the administration of additional zinc in the form of $ZnCl_2$ supplemented medium did not improve the cell-derived enzymatic angiotensin I to angiotensin II conversion. The signals with zinc including samples show lowered calcium signals (Figure 7). One explanation could be that Zn^{2+} is likely to bind to Fura-2 when it is internalized into cells and will therefore compete with Ca^{2+} ions for chelator binding sites.
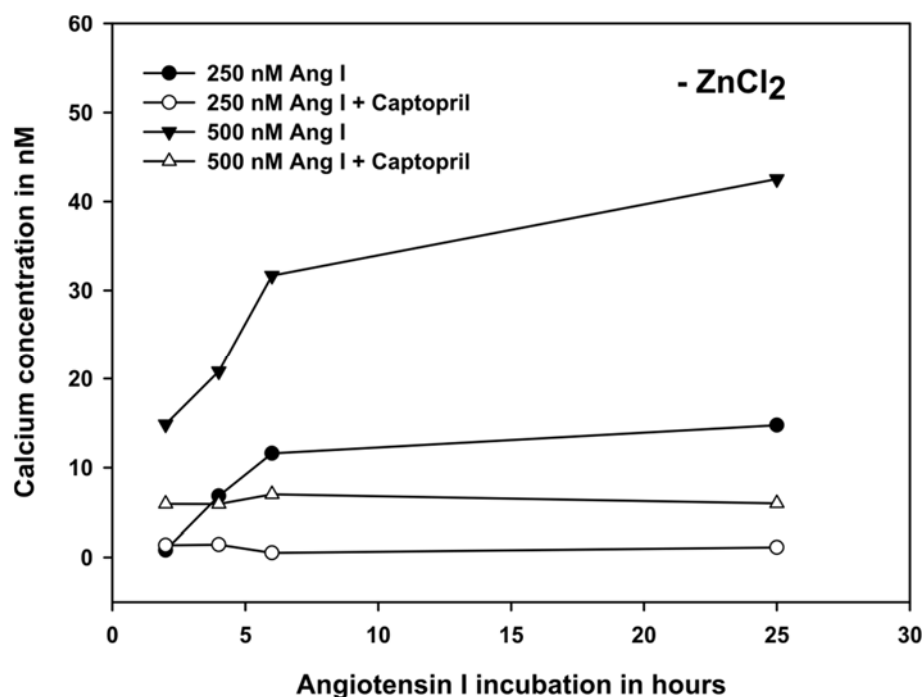
Figure 6: Calcium measurements of NRK-52E cell medium supernatants after angiotensin I incubation. Over time, angiotensin I is converted into angiotensin II, which leads to an AT1R mediated increase in intracellular calcium.
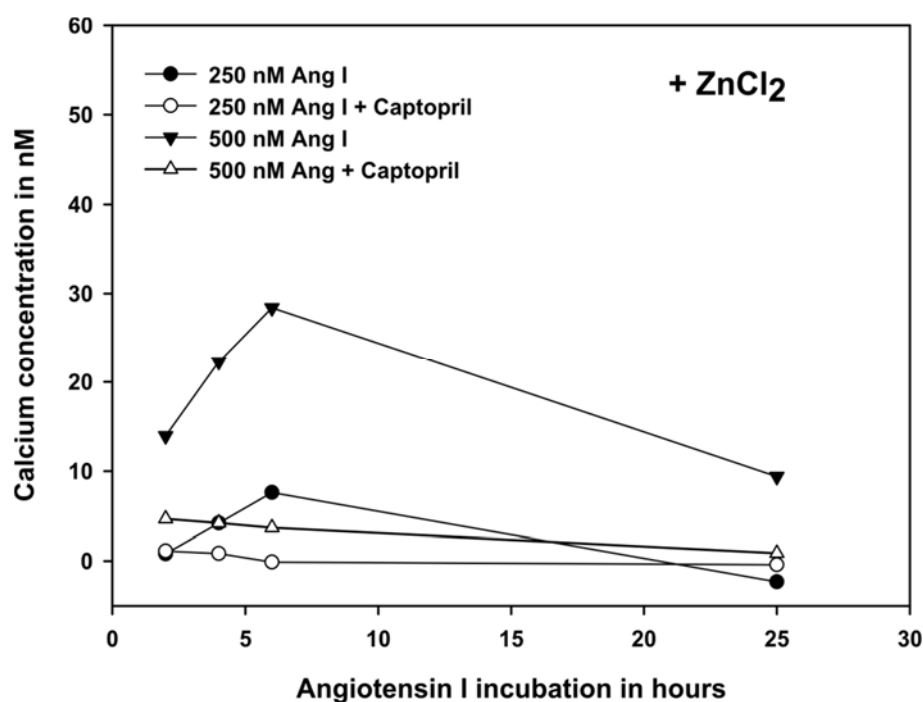

Figure 7: The addition of zinc in the CCM leads to decreased calcium levels, perhaps because of zinc complexation with Fura-2 calcium chelator.

Determination of enzyme activity by a FRET-based cleavage assay

The FRET substrate Mca-Arg-Pro-Pro-Gly-Phe-Ser-Ala-Phe-Lys(Dnp)-OH was completely converted by 0.02 µg of human recombinant ACE in a substrate concentration range of 2.5 to 12.5 µM. There is a steep increase in substrate conversion for very high substrate concentrations. After 1 hour of substrate incubation, a saturation plateau occurs (Figure 8).
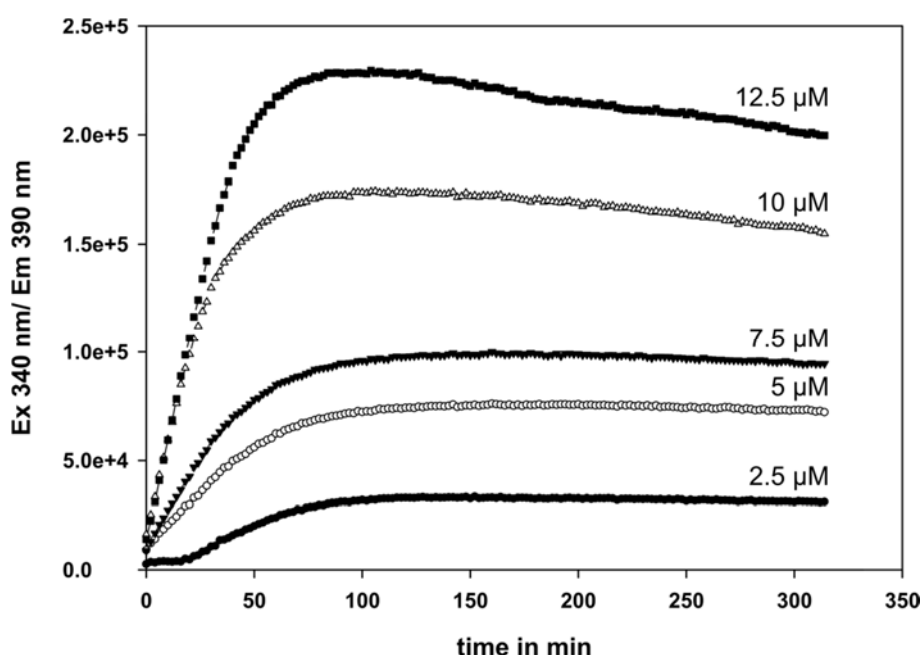

Figure 8: Cleavage of different FRET substrate concentrations by 0.02 µg human recombinant ACE: Increasing FRET substrate concentrations generates higher fluorescence intensities by enzyme triggered dequenching of peptide FRET pairs.

The inhibition of the human recombinant ACE with 10 µM Captopril was particularly successful for FRET substrate concentrations ≤ 5 µM. Therefore, using Captopril in 2-fold excess to substrate or higher (Figure 9) is recommended.
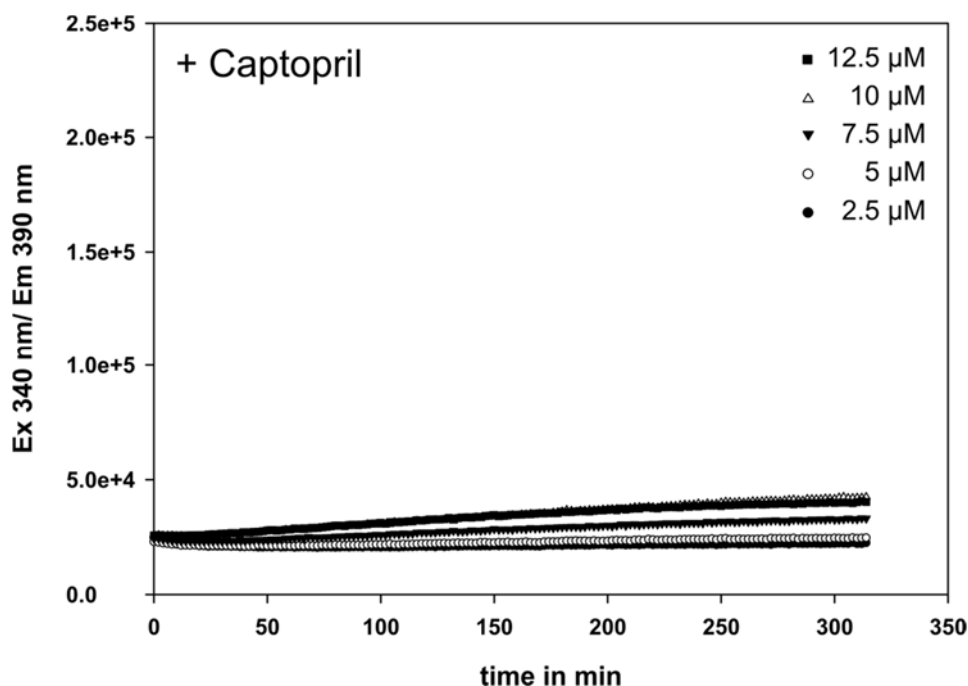
Figure 9: Captopril is an efficient inhibitor for human recombinant ACE. It is necessary to use Captopril in a 2-fold excess to substrate used, to accomplish total ACE inhibition or to block 2 ng/µl ACE.

For quantitative analysis, enzyme kinetic parameters like V_{max} and K_M were determined by double reciprocal representation of the Michaelis-Menten enzyme kinetic in the form of a Lineweaver-Burk-Plot linearization, using a standard curve for FRET substrate conversion by human recombinant ACE (Figure 11). All obtained enzyme kinetic curves of various cell types for the various FRET substrate concentrations used were fitted with a nonlinear polynomial quadratic regression function ($f = y0 + a*x + b*x^2$) in SigmaPlot to determine the initial velocity V_0, which corresponds to a in the equation (Figure 10). The Lineweaver-Burk-Plot illustration also offers information about the kind of enzymatic inhibition of ACE by Captopril. For example, whether it is competitive (Figure 12–14). The experimental data were not shown due to the linear extrapolation to x-axis intercept, which led to overlapping data points.
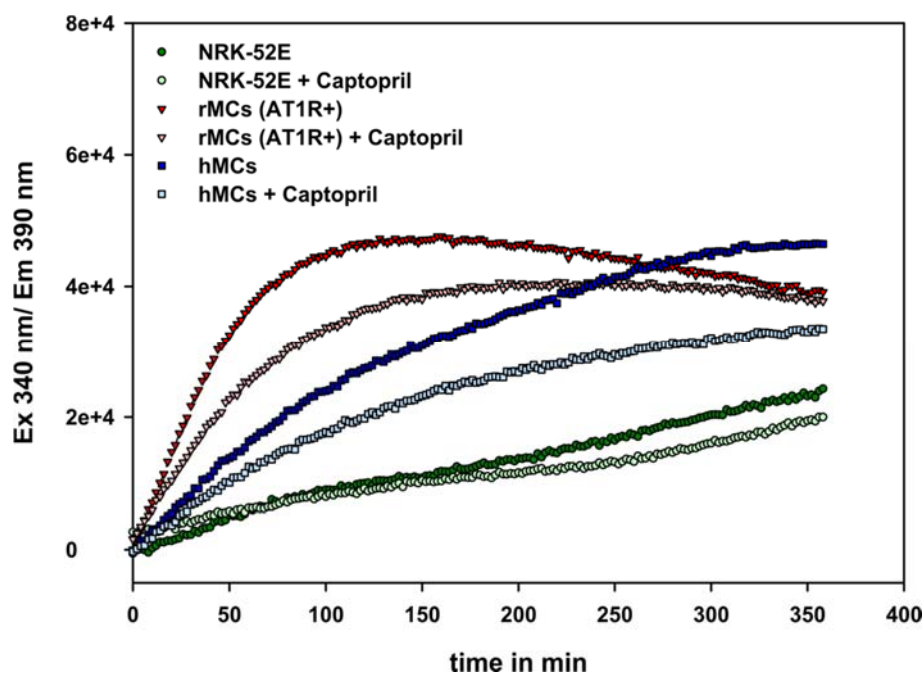
Figure 10: FRET kinetics for various tested renal cell lines with and without ACE inhibitor Captopril under substrate incubation.
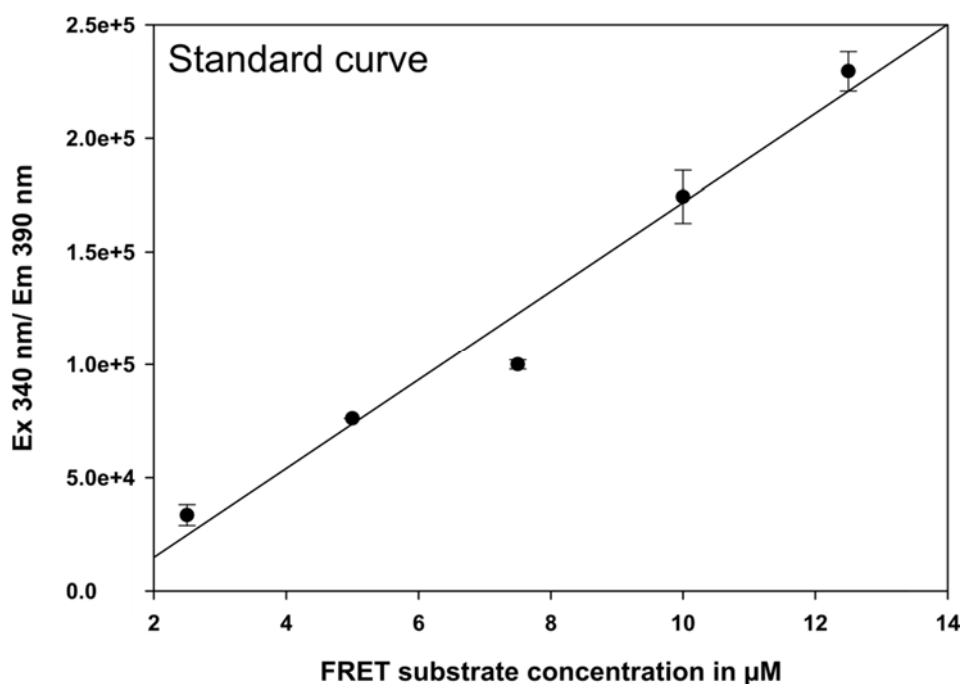

Figure 11: Standard curve of human recombinant ACE: Increasing FRET substrate concentrations were converted by 0.02 µg human recombinant ACE (n=2), shown in Figure 8. The maximum fluorescence emission was used for standard curve formation.
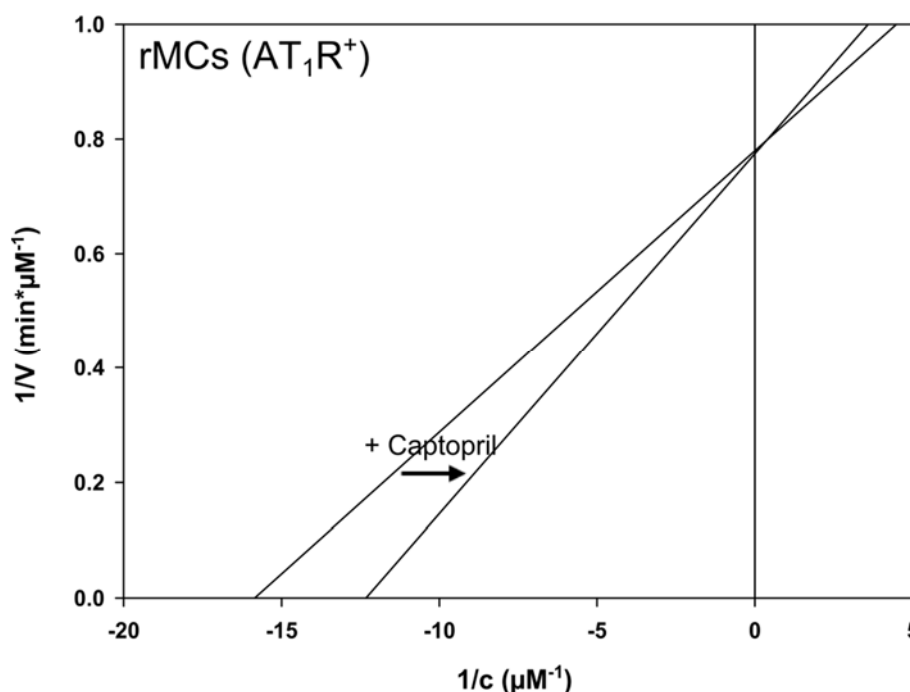
Figure 12: Lineweaver-Burk-Plots (double reciprocal plots of enzyme kinetics) of rMCs. After Captopril administration, an increase in slope is visible, which is an indicator for competitive inhibition of ACE by Captopril.

Figure 13: Lineweaver-Burk-Plots (double reciprocal plots of enzyme kinetics) of rat NRK-52E renal tubule cells. The effect of slope increase is most clearly visible for NRK-52E cells, which is an indication for the most selective FRET substrate conversion due to ACE.
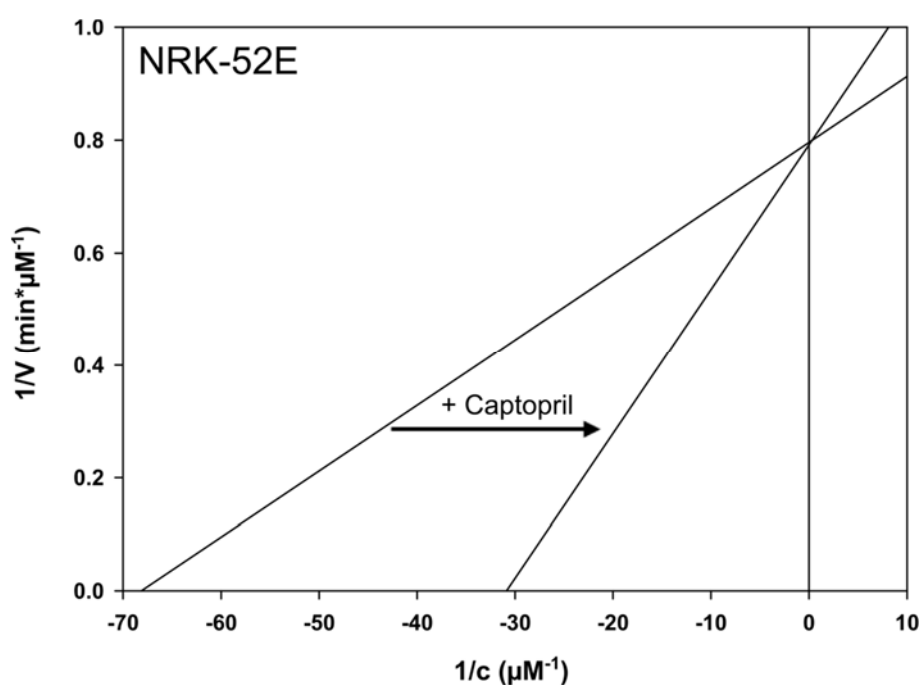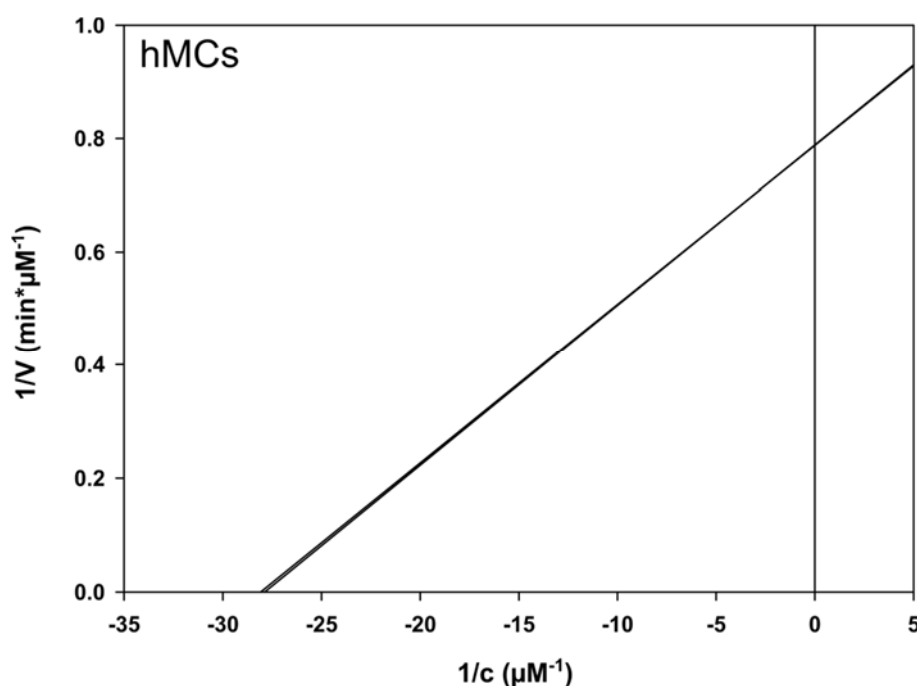
Figure 14: Lineweaver-Burk-Plots (double reciprocal plots of enzyme kinetics) of hMCs. The Lineweaver-Burk-Plot slopes with and without Captopril overlap each other and therefore suggest that the FRET substrate conversion may not be ACE-derived.

Increasing K_M values represent the substrate concentration, which is necessary to reach the half-maximum velocity. After inhibitor addition, an increasing K_M value suggests that there must be an inhibitor specific blockade of the enzyme, which is targeted by the used substrate. This was the case for rat NRK-52E tubule cells and rat mesangial cells, but surprisingly not for human mesangial cells. The initial substrate concentration is lower for NRK-52E tubule cells, compared to both mesangial cell types, which indicates a higher enzymatic activity of the tubule cells. Also, the literature explains that the conversion of angiotensin I via ACE is localized on the proximal tubule cell brush border [19]. For the rat mesangial cells, 4.2-fold more FRET substrate must be converted, compared to tubule cells. Here, the human mesangial cells show no ACE-derived enzyme activity (Figure 14). In the case of a competitive inhibitor, V_{max} remains unchanged, which is the case for all tested cell types (Table 2).

Table 2: Calculated parameters

Cell type	V_{max} No inhibitor	V_{max} (+ Captopril)	K_M (µM) No inhibitor	K_M (µM) (+ Captopril)	fold K_M increase
NRK-52E	1.26	1.26	0.015	0.032	2.1
rMCs (AT$_1$R$^+$)	1.28	1.29	0.063	0.081	1.3
hMCs	1.27	1.27	0.036	0.036	1.0

In general, such linearization methods for gaining insight into enzyme kinetics and inhibition mechanisms are controversial, particularly with respect to their reliability. This is especially true in this case, where the enzyme specificity of the FRET substrate is not warranted, and the kinetics of cell-derived enzymes differ quite strongly to that of rhACE, which was used for standard curve preparation. To obtain a more reliable linear extrapolation, more than four data points and more inhibitor concentrations should be tested. Another parameter for improvement is the cell density, which also determines enzyme concentration.

In vitro enzymatic conversion of angiotensin I functionalized quantum dots

The buffer corrected calcium signals, measured for ACE activated QDs for 10 nM and 20 nM QDs, differ significantly from these obtained by control QDs, which were unmodified QDs (only data for 10 nM QDs) and angiotensin I-modified QDs without ACE or including Captopril as enzyme inhibitor (Figure 15). Enzyme activated QD binding to AT$_1$R can be blocked by EXP3174 (data only for 10 nM QDs).
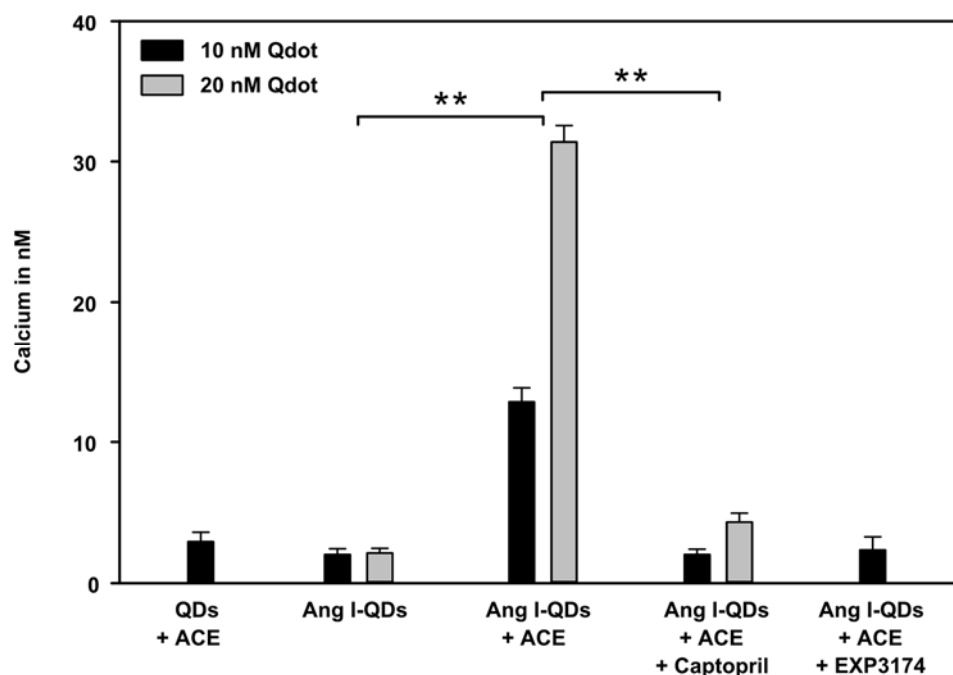
Figure 15: Fura-2 calcium signaling for ACE activated QDs. The GPCR binding of enzyme activated QDs results in higher calcium signals, than the control groups. Data were obtained by two independent experiments with dilutions in triplicate with QDs of different distributors (Life Technologies and Strem Chemicals). Levels of statistical significance are indicated as $p < 0.01$.

Fluorescence microscopy

In fluorescence microscopy studies, a higher QD binding was observed if angiotensin I-modified particles were processed by human recombinant ACE before administration to AT_1R positive rat mesangial cells (Figure 16 A). The binding of particles was reduced by Captopril (Figure 16 B).
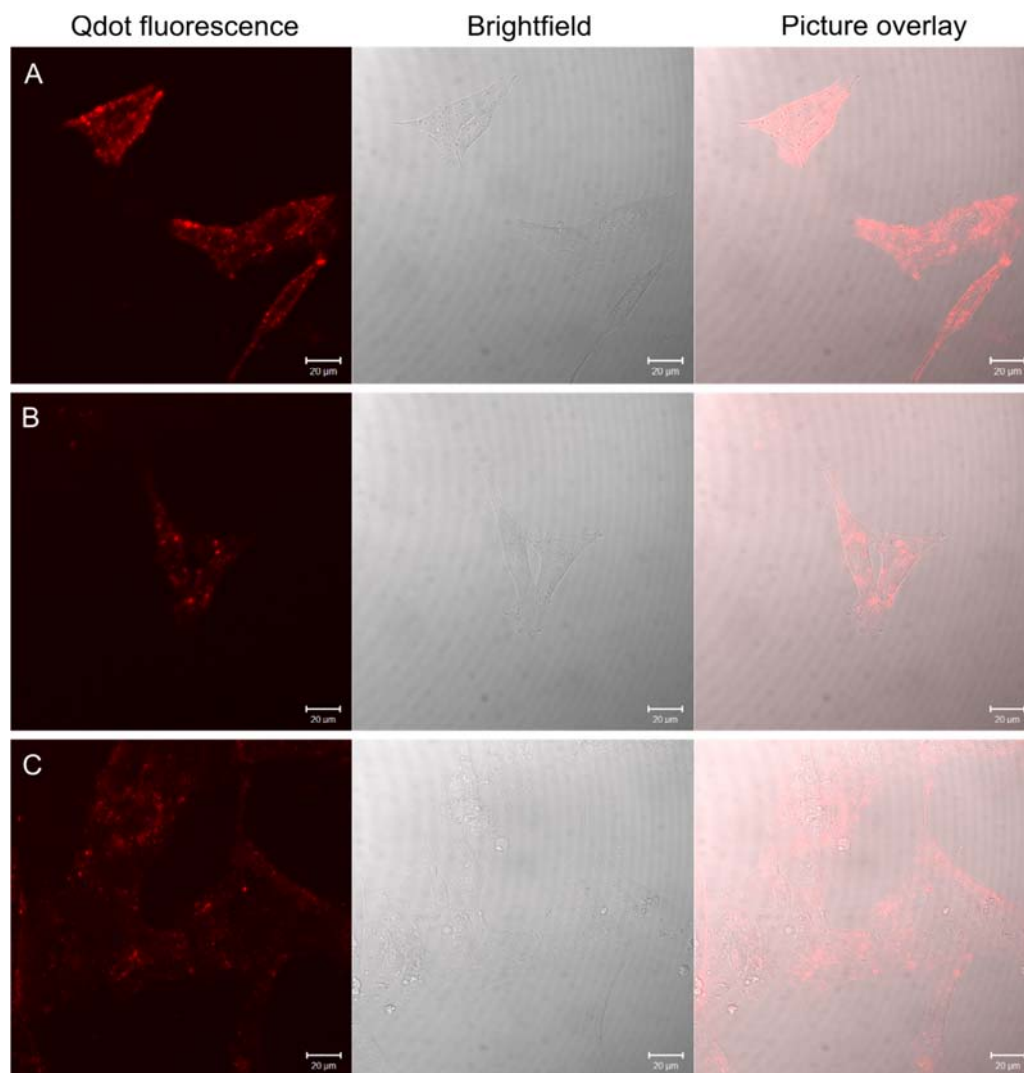
Figure 16: Fluorescence microscopy pictures of mesangial cells incubated with ACE activated angiotensin I-QDs (A), Captopril-inhibited angiotensin I-QDs (B), and not activated angiotensin I-QDs (without ACE) (C). Compared to not activated QD controls (B,C), the ACE converted angiotensin I-QDs show AT_1 receptor mediated binding and uptake (A).

Flow cytometry analysis

As proof of the conclusions drawn based on the microscopic images, the angiotensin I-modified QD binding to AT_1R positive mesangial cells was also checked after pre-incubation of the particles with rhACE and in the presence of Captopril and EXP3174 inhibitors. During this experiment, no significant differences were found between ACE-incubated angiotensin I-modified QDs and the controls, without either ACE or

enzyme/receptor competing antagonists. A high unspecific binding was observed for unmodified amino-PEG QDs (Figure 17).

Figure 17: FACS analysis showed no significant differences between angiotensin I-modified QDs. There is a high unspecific binding of unmodified QDs.

Conclusion

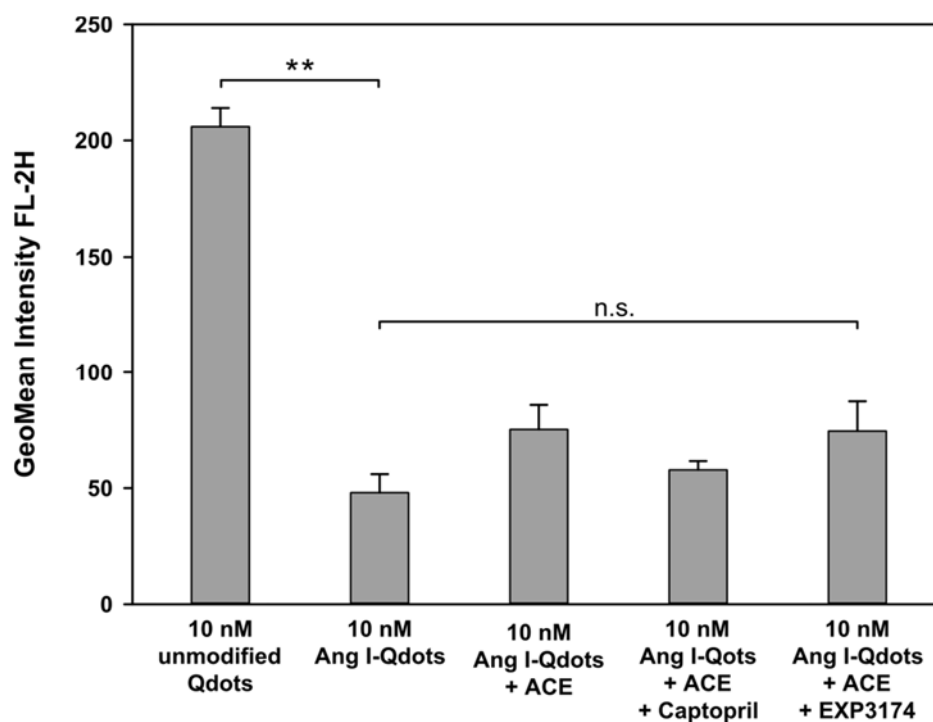The present experiments show that enzymatically processed angiotensin I coated nanoparticles can selectively bind to AT_1R positive mesangial cells. To date, it is not clear whether multivalent receptor binding is induced after enzymatic processing of angiotensin I-modified QDs, because the measured calcium responses were very low and because microscopy pictures and flow cytometry data did not clearly show strong differences in receptor binding between enzymatically converted nanoparticles and the respectively used controls with either enzyme inhibitor or receptor blocker. There may be multiple reasons for this. The coupling efficiency of angiotensin I to QDs is too low and/or the ligand conversion efficiency by ACE is too low. A further reason may be that free unbound angiotensin I is not completely removed from the QD sample. Thus, free converted angiotensin I can compete with angiotensin I-modified QDs for receptor binding sites. Nevertheless, in each experiment the binding of angiotensin I coated nanoparticles before ACE-derived processing is lower compared to converted QDs, indicating a certain conversion, which may be insufficient to reach multivalent particle binding. Such an enzyme driven nanoparticle binding could be one step further towards preventing unspecific nanoparticle binding and uptake to and from off-target cells. In future experiments, artificial human recombinant ACE should be replaced by natural cell-derived ACE, expressed ideally by one cell type. Particularly in diabetic nephropathy, this kind of particle can be used as a probing system to better understand the sites of action and interaction of ACE and AT_1R in renal tissues. Therefore, the parallel injection of the inhibitors Captopril and EXP3174 is recommended to avoid enzymatic cleavage of ligands by enzymes in the blood stream and nanoparticle binding to off-target cells before they arrive at the target site in the kidney.

Since it is known that in addition to synovium derived cells, bovine chondrocytes in 2D cell cultures also express AT_1 receptors for angiotensin II, independent from interleukin-1 stimulation, cartilage cells could be a potential target for antiangiogenic drugs (Supplementary information, Figure 20). Therefore, angiotensin I-modified QDs could also be an effective tool to investigate the influence of ACE in the progression of RA. Moreover, these QDs could be used as a diagnostic marker for various disease states.

Supplementary information

TEM images of quantum dots

A volume of 1 µl of a 60 mM QD solution in water was fixed on TEM grids. Although QDs show high self-contrast, they were stained with phosphotungstic acid, pH 7. With the staining, a light corona is visible for the PEGylated QDs, which could be due to the dense PEG shell surrounding the dark QD core. The TEM images did not show significant aggregation for amino-PEG QDs, neither before nor after ligand coupling. They are in the expected core size range of 10 nm (Figure 18).
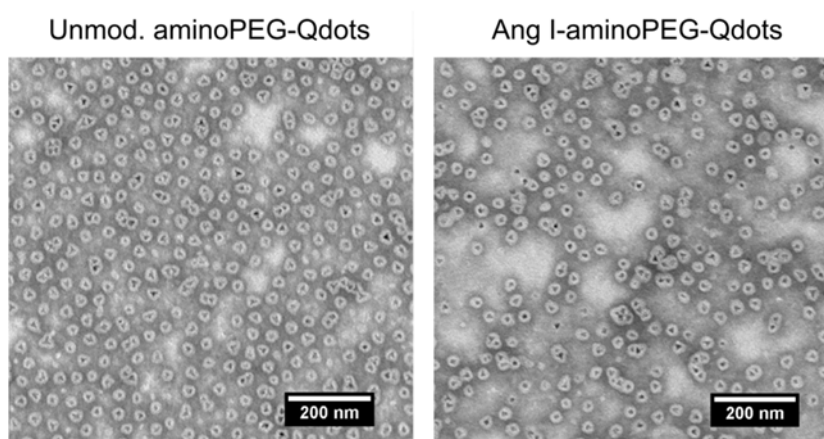
Figure 18: TEM images of QDs before and after angiotensin I modification.

Investigation of ACE-2 expression

The expression of ACE-2, another angiotensin-converting enzyme, which seems to have adverse renoprotective effects compared to ACE in diabetic nephropathy was also investigated [20,21]. This enzyme catalyzes two steps in the renin-angiotensin system: Angiotensinogen to angiotensin I and subsequently to angiotensin (1–9), ACE-derived angiotensin II to the shorter peptide fragment angiotensin (1–7) [7]. Therefore, the presence of this enzyme is not useful or beneficial for our experiments, since it degrades angiotensin II as the targeting ligand for the AT_1R. In an RT-PCR, it was found that the NRK-52E tubules cell line used, as well as rat mesangial cells do not express ACE-2. In human mesangial cells,

a band at 238 bp for ACE-2 was observed in addition to other unspecific bands. Human ACE-2 primer sequence was used from [22] and rat ACE-2 primer sequence was used from [15] (Figure 19).
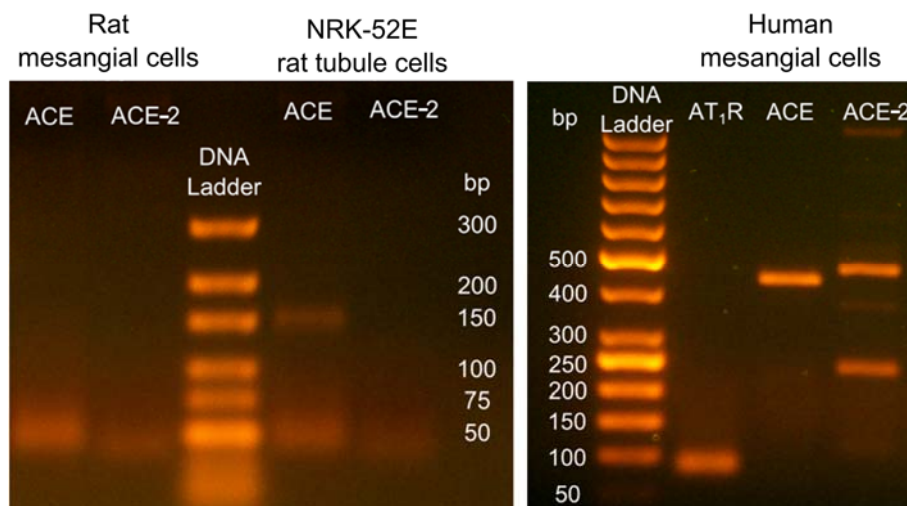
Figure 19: RT-PCR ACEs of different cell lines. Only human mesangial cells express both converting-enzymes: ACE (428 bp) and ACE-2 (238 bp). The rat mesangial and tubule cells used do not express ACE-2 (129 bp).

IL-1α and IL-1β stimulation of bovine chondrocytes in 2D culture

Besides the kidney, which is, in the disease state of diabetic nephropathy, an AT_1R and ACE positive target site, cartilage cells were also tested for AT_1R expression. To evaluate whether the AT_1R is expressed in general and whether there is a change in expression in the state of inflammation, primary bovine chondrocytes were stimulated in 2D culture with two different interleukins and the mRNA for RT-PCR was subsequently isolated. Therefore, bovine chondrocytes of the first passage were cultured in T25 cell culture flasks (Corning, Wiesbaden, Germany) in CCM, consisting of DMEM (Gibco/Thermo Scientific, Darmstadt, Germany), 10 mM HEPES, non-essential amino acid (Gibco/Thermo Scientific, Darmstadt, Germany), 46 µg/ml proline, 50 µg/ml ascorbic acid, 1% Penicillin/Streptomycin (Gibco/Thermo Scientific, Darmstadt, Germany), and 10% FCS. Confluent cells were washed with warm DPBS and then stimulated with interleukins, either 10 ng/ml IL-1α or

IL-β (PreproTech, Hamburg, Germany) in phenol red free CCM without FCS and 0.1% BSA and incubated for 24 h at 37°C and 5% CO_2 atmosphere. The isolation of RNA, reverse transcription, and PCR were performed with Peqlab kit systems. AT_1R mRNA expression was detected before and after interleukin stimulation by the expected band 210 bp. The sample without interleukin stimulation exhibited even more expression (Figure 20). These results are consistent with those in the literature for human chondrocytes [23].

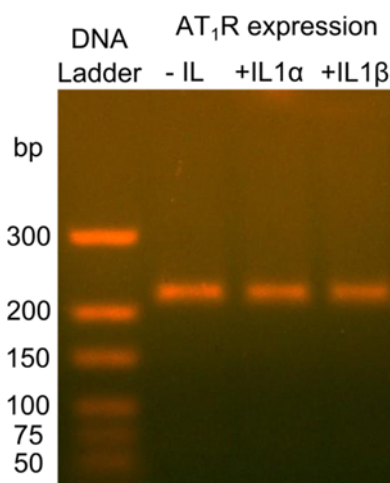
Figure 20: AT_1 receptor expression in bovine chondrocytes in 2D culture. Cells were stimulated with either human IL-1α or IL-1β for 24 hours to mimic an inflammatory state. AT_1R is expressed independently from interleukin-1 stimulation.

References

[1]   Moskowitz DW. Is "Somatic" Angiotensin I-Converting Enzyme a Mechanosensor? Diabetes Technology & Therapeutics 2002; 4: 841–858.

[2]   Bruno BJ, Miller GD, Lim CS. Basics and recent advances in peptide and protein drug delivery. Therapeutic Delivery 2013; 4: 1443–1467.

[3]   Huynh NT, Roger E, Lautram N, Benoît J, Passirani C. The rise and rise of stealth nanocarriers for cancer therapy: passive versus active targeting. Nanomedicine 2010; 5: 1415–1433.

[4]   Amoozgar Z, Yeo Y. Recent advances in stealth coating of nanoparticle drug delivery systems. WIREs Nanomed Nanobiotechnol 2012; 4: 219–233.

[5]   Ding H, Ma Y. Design strategy of surface decoration for efficient delivery of nanoparticles by computer simulation. Sci. Rep. 2016; 6: 26783.

[6]   Rao L, Xu J, Cai B, et al. Synthetic nanoparticles camouflaged with biomimetic erythrocyte membranes for reduced reticuloendothelial system uptake. Nanotechnology 2016; 27: 85106.

[7]   Carey RM, Siragy HM. The intrarenal renin–angiotensin system and diabetic nephropathy. Trends in Endocrinology & Metabolism 2003; 14: 274–281.

[8]   Iwai M, Horiuchi M. Devil and angel in the renin–angiotensin system: ACE–angiotensin II–AT1 receptor axis vs. ACE2–angiotensin-(1–7)–Mas receptor axis. Hypertens Res 2009; 32: 533–536.

[9]   Giani JF, Janjulia T, Taylor B, et al. Renal Generation of Angiotensin II and the Pathogenesis of Hypertension. Curr Hypertens Rep 2014; 16.

[10] Gonzalez-Villalobos RA, Janjoulia T, Fletcher NK, et al. The absence of intrarenal ACE protects against hypertension. J. Clin. Invest. 2013; 123: 2011–2023.

[11] de la Rica, Roberto, Aili D, Stevens MM. Enzyme-responsive nanoparticles for drug release and diagnostics. Advanced Drug Delivery Reviews 2012; 64: 967–978.

[12] Dudani JS, Jain PK, Kwong GA, Stevens KR, Bhatia SN. Photoactivated Spatiotemporally-Responsive Nanosensors of in Vivo Protease Activity. ACS Nano 2015; 9: 11708–11717.

[13] Li H, Miteva M, Kirkbride KC, et al. Dual MMP7-Proximity-Activated and Folate Receptor-Targeted Nanoparticles for siRNA Delivery. Biomacromolecules 2015; 16: 192–201.

[14] Liebau MC. Functional expression of the renin-angiotensin system in human podocytes. AJP: Renal Physiology 2005; 290: F710.

[15] Klimas J, Olvedy M, Ochodnicka-Mackovicova K, et al. Perinatally administered losartan augments renal ACE2 expression but not cardiac or renal Mas receptor in spontaneously hypertensive rats. J. Cell. Mol. Med. 2015; 19: 1965–1974.

[16] Rhodes DR, Ateeq B, Cao Q, et al. AGTR1 overexpression defines a subset of breast cancer and confers sensitivity to losartan, an AGTR1 antagonist. Proceedings of the National Academy of Sciences 2009; 106: 10284–10289.

[17] Ikhapoh I, Pelham CJ, Agrawal DK. Synergistic effect of angiotensin II on vascular endothelial growth factor-A-mediated differentiation of bone marrow-derived mesenchymal stem cells into endothelial cells. Stem Cell Res Ther 2015; 6: 4.

[18] Vidotti DB. High glucose concentration stimulates intracellular renin activity and angiotensin II generation in rat mesangial cells. AJP: Renal Physiology 2004; 286: F1039.

[19] Navar LG, Inscho EW, Majid SA, Imig JD, Harrison-Bernard LM, Mitchell KD. Paracrine regulation of the renal microcirculation. Physiological Reviews 1996; 76: 425–536.

[20] Batlle D, Soler MJ, Wysocki J. New aspects of the renin–angiotensin system: angiotensin-converting enzyme 2 – a potential target for treatment of hypertension and diabetic nephropathy. Current Opinion in Nephrology and Hypertension 2008; 17: 250–257.

[21] Liu CX, Hu Q, Wang Y, et al. Angiotensin-converting enzyme (ACE) 2 overexpression ameliorates glomerular injury in a rat model of diabetic nephropathy: a comparison with ACE inhibition. Molecular medicine (Cambridge, Mass.) 2011; 17: 59–69.

[22] Jia HP, Look DC, Shi L, et al. ACE2 Receptor Expression and Severe Acute Respiratory Syndrome Coronavirus Infection Depend on Differentiation of Human Airway Epithelia. Journal of Virology 2005; 79: 14614–14621.

[23] Kawakami Y, Matsuo K, Murata M, et al. Expression of Angiotensin II Receptor-1 in Human Articular Chondrocytes. Arthritis 2012; 2012: 1–7.

Chapter 8

Summary and Conclusions

The goal of this thesis was to investigate the neurokinin-1 receptor (NK_1R) as a potential target site for multivalent receptor blockade. Since the NK_1R is peripherally expressed on various cell types of the human body and its expression increases when an immune response occurs, this receptor seems to offer great potential for selective and specific antagonistic surface receptor targeting with a minimizing effect of inflammation and pain.

In the experiments described in **Chapter 3,** it was found that the inflammatory factor IL-1β has a direct influence on NK_1R expression levels in U87 MG glioblastoma and MDA-MB-231 breast cancer cell lines and primary bovine chondrocytes in 2D cell culture. For U87 MG and MDA-MB-231 cells, it was found that the NK_1R mRNA is upregulated within the first 3 hours of IL-1β stimulation, but down-regulated for long-term IL-1β stimulation. Here, less NK_1R expression at the mRNA level was observed for MDA-MB-231 cells than for U87 MG cells. In receptor binding experiments, approximately 2% of the maximum intracellular calcium signals were reached, compared to NK_1R positive transfected CHO cells, indicating only a low NK_1R density on these cell types. These results were quite disappointing because these non-transfected cells could not be used for further receptor binding studies of antagonist modified multivalent binding nanoparticles in fluorescence-based calcium assays. Nevertheless, NK_1R mRNA was found in bovine chondrocytes and the results of NK_1R immunostaining in bovine cartilage tissue sections were quite promising. In addition, it could be demonstrated in 2D cell cultures that IL-1β and substance P together contribute to the regulation of the chondrocytes´ surrounding extracellular matrix (ECM) behavior by the selective regulation of matrix-metalloproteinases´ (MMPs) gene expression. In this context, it could be shown that MMP-13 in particular is regulated in a time and concentration-dependent manner by substance P and can be antagonized by the specific NK_1R antagonist spantide I, which allows us to assume that this intracellular signaling pathway is triggered via NK_1Rs. This aspect is intriguing since the literature also mentions that MMP-13 has an impact on the progression of arthritis. Finally, it is concluded that the short version of the NK_1R may be more prominent on the surface of all tested cell types and may offer the opportunity for NK_1R targeting, particularly due to the impact on MMP regulation. Due to the lack of the C-terminal G_q-protein binding site of this truncated NK_1R splice variant, no intracellular calcium signals

were detectable. For this reason, the NK$_1$R transfected CHO cells were used for further studies to predict the affinity of generated multivalent ligands.

In Chapter 4, fluorescent PEGylated QDs were used for ligand coupling to the surface of nanoparticles and to study their interactions with neurokinin-1 receptor positive cells. The introduction of thiol groups into cysteine-free peptide ligands is a common strategy for coupling well water-soluble ligands to maleimide functionalized nanoparticles such as QDs. It was found that thiolation reaction is quite efficient for the very hydrophilic angiotensin I, which was used in Chapter 7, whereas it is highly reduced for spantide I, although there are two different modification sites for 2-iminothiolane. In nanoparticle uptake experiments with receptor positive CHO-NK$_1$R cells, a high unspecific nanoparticle binding for amino-PEG modified QDs was examined. Here, free amino-PEG groups showed high unspecific binding to cells. In general, unspecific nanoparticle binding strongly hampers the argument of receptor mediated multivalent nanoparticle binding and uptake by GPCR. However, it was shown in FACS displacement experiments with high concentrations of free competing antagonists that nanoparticle binding was inhibited. This indicated receptor mediated nanoparticle binding. However, the previous low thiolation efficiency for the peptide may be the main reason for a low nanoparticle coupling propensity. In addition, double thiolated peptides may cause low ligand densities on the surface of nanoparticles. This also minimizes the chance for multivalent interactions. Since the C-terminal receptor interacting part of the peptide mainly consists of hydrophobic amino acids, there is also the chance for ligand inversion inside the PEG shell, a phenomenon that is also discussed for highly hydrophobic small non-peptide receptor antagonists.

Besides PEGylated QDs, branched 8-arm PEGs were used in **Chapter 5** for multivalent cell interaction studies. In contrast to QDs, PEGs are classified as non-toxic biomaterials; additionally, they do not interfere with luminescence-based calcium assays. It was found that there is a high concentration requirement of PEGylated spantide I species because N-terminal PEGylation decreases binding to membrane receptors but has the advantage of reduced clearance and immunogenicity. Double PEGylation of spantide I further increases the affinity loss to neurokinin-1 receptors because a higher PEG to peptide ratio sterically reduces receptor binding at the cell surface, although binding is sufficient at very high ligand concentrations. Furthermore, simple N-terminal truncation of the peptide sequence leads to

a great affinity loss. This indicates that the N-terminus sequence itself seems to be involved in receptor recognition and binding. Therefore, N-terminal truncation of the peptide sequence of spantide I is not an option to simplify the mono-PEGylation by elimination of amino acids, which are responsible for double PEGylation. The agonistic activity of some peptide antagonists makes it difficult to determine true IC_{50} values in the aequorin based calcium assay because of the consumption of bioluminescent aequorin complex. However, it was shown that there is a gain in affinity for 8armPEG-20k-spantide I due to multivalent receptor binding.

In **Chapter 6**, a small molecular weight antagonist, aprepitant, was modified to make it amenable for further PEG coupling, either to branched PEGs or PEG-coated nanoparticles. To overcome the limitations of post-synthetic modification of small molecular weight neurokinin-1 receptor antagonists due to the lack of functional groups, it could be shown that chemical modification of the triazole group of aprepitant is possible by using a strong deprotonation reagent and a tert-Butyl-(3-bromopropyl)carbamate as an alkyl linker with Boc-protected amine functionality. In a binding study with the final product, it was found that the affinity dropped 3.9-fold but still has an acceptable IC_{50} of 115.2 nM and therefore represents a promising antagonist for nanoparticle functionalization and further multivalent receptor binding studies. One drawback of this Boc-protected antagonist was the Boc-group cleavage under conditions, which are strong enough for deprotection on the one hand and mild enough to keep the basic morpholin-ring structure of aprepitant intact on the other hand. A better option would have been the introduction of an alkyl linker without a Boc-protecting group, but to date, there is no way to perform such an alkylation. Therefore, it is proposed that the best way to obtain an amine-alkyl-linker functionalized aprepitant would be to start the design of the desired drug molecule by stepwise synthesis from the very beginning instead of post-synthetic linker addition.

Another new strategy for site-specific multivalent nanoparticle targeting is presented in the final chapter, **Chapter 7**. This strategy is based on an enzyme driven activation mechanism of ligands which are immobilized on the surface of nanoparticles. For these studies, the ACE driven angiotensin I to angiotensin II conversion was used and the successful conversion was checked by AT_1 receptor binding studies. The results of these experiments have shown that enzymatically processed angiotensin I coated nanoparticles are able to selectively bind

to AT_1R positive mesangial cells. To date, it is not clear whether multivalent receptor binding is induced after enzymatic processing of angiotensin I-modified QDs because the measured calcium responses were very low, and microscopy pictures and flow cytometry data did not clearly show strong differences in receptor binding between enzymatically converted nanoparticles and the respectively used controls with either enzyme inhibitor or receptor blocker. There may be multiple reasons. The coupling efficiency of angiotensin I to QDs is too low and/or the ligand conversion efficiency by ACE is too low. A further reason may be that free unbound angiotensin I is not completely removed from the QD sample. Thus, free converted angiotensin I can compete with angiotensin I-modified QDs for receptor binding sites. Nevertheless, in each experiment, the binding of angiotensin I coated nanoparticles before ACE-derived processing is lower, compared to converted QDs, which indicates a certain conversion. Such an enzyme driven nanoparticle binding could be one step further in preventing unspecific nanoparticle binding and uptake to and from off-target cells. In future experiments, artificial human recombinant ACE should be replaced by natural cell-derived ACE, expressed ideally by one cell type. Particularly in diabetic nephropathy, this kind of particle can be used as a probing system to better understand the sites of action and interaction of ACE and AT_1R in renal tissues. Therefore, the parallel injection of the inhibitors Captopril and EXP3174 is recommended to avoid enzymatic cleavage of ligands by enzymes in the blood stream and nanoparticle binding to off-target cells before they arrive at the target site in the kidney.

Since it is known that in addition to synovium derived cells, bovine chondrocytes in 2D cell cultures also express AT_1 receptors for angiotensin II, independent from interleukin-1 stimulation, cartilage cells may also be a potential target for antiangiogenic drugs. Therefore, the present angiotensin I-modified QDs may also be an effective tool for investigating the influence of ACE in the progression of RA. Moreover, these QDs might be used as a diagnostic marker for different disease states.

Appendix

Abbreviations

^{1}H-NMR	proton nuclear magnetic resonance spectroscopy
2D/ 3D	two-dimensional/ three-dimensional
ACE	angiotensin-converting enzyme
Ang I/Ang II	angiotensin I/ angiotensin II
aprepitant	neurokinin-1 receptor antagonist (MK-869)
APS	Ammonium persulfate
AT$_1$R	angiotensin II receptor
ATCC	American Type Culture Collection
BBB	blood–brain barrier
bp	base pairs
BSA	bovine serum albumin
CCM	cell culture medium
CD	circular dichroism
cDNA	copy deoxyribonucleic acid
Cd	cadmium
CdSe	cadmium selenide
CGRP	calcitonin gene-related peptide
CHO cells	chinese hamster ovary cell line
CLSM	confocal laser scanning microscopy
CNS	central nervous system
COX	cyclooxygenase
DABCO	1,4-Diazabicyclo[2.2.2]octane
DAPI	2-(4-Amidinophenyl)-1H-indole-6-carboxamidine
DBA-1J mice	mice with type II collagen-induced arthritis
DMEM	Dulbecco´s modified Eagle´s medium
DMF	dimethylformamide

DMSO	dimethylsulfoxide
DNA	deoxyribonucleic acid
DPBS	Dulbecco´s phosphate-buffered saline
DTNB	5,5'-dithio-bis-[2-nitrobenzoic acid], (Ellman´s reagent)
ECM	extracellular matrix
EDTA	ethylendiaminetetraacetic acid
EDC	1-ethyl-3-3(3-dimethylaminopropyl) carbodiimide
EMEM	minimum essential medium containing Earl´s salts
ENS	enteric nervous system
EPR	enhanced permeability and retention
FACS	fluorescence activated cell sorting
FCS	fetal calf serum
FDA	Food and Drug Administration
FITC	fluorescein isothiocyanate
Fura-2 AM	fura-2-acetoxymethyl ester (ratiometric calcium indicator)
GAPDH	glyceraldehyde 3-phosphate dehydrogenase
GFP	green fluorescent protein
GPCR	G protein-coupled receptor
GRK	G protein-coupled receptor kinases
HEPES	2-[4-(2-hydroxyethyl)piperazin-1-yl]ethanesulfonic acid
HPLC	High-performance liquid chromatography
IBD	inflammatory bowel disease
IL	interleukin
IL-1ra	interleukin-1 receptor antagonist
MCF-7	human breast cancer cell line
MDA-MB-231	human breast cancer cell line
MMP	matrix metalloprotease
mRNA	messenger ribonucleic acid

MS	multiple sclerosis
MWCO	molecular-weight cutoff
NFκB	nuclear factor 'kappa-light-chain-enhancer' of activated B-cells
NHS	N-hydroxysuccinimide
$NK_1R/NK_2R/NK_3R$	neurokinin receptors
NSAIDs	nonsteroidal anti-inflammatory drugs
OA	osteoarthritis
OSM	oncostatin M
PBS	Phosphate-buffered saline
PCR	polymerase chain reaction
qPCR	quantitative real-time PCR
RA	rheumatoid arthritis
RT-PCR	reverse transcription PCR
PEG	polyethylene glycol
PD-ECGF	platelet-derived endothelial cell growth factor
PFA	Paraformaldehyde (Polyoxymethylene)
QD	quantum dot
rcf	relative centrifugal force
SDS	sodium dodecyl sulfate
SEC	size-exclusion chromatography
SP	substance P, neurokinin-1 receptor agonist
SP I	spantide I, neurokinin-1 receptor antagonist
Sulfo-SMCC	sulfosuccinimidyl-4-(N-maleimidomethyl)-cylohexane-1-carboxylate
SYBR Green	asymmetrical cyanine dye
TAE buffer	tris-acetate-EDTA buffer
TCEP	tris(2-carboxyethyl)phosphine
TEM	transmission electron microscopy

Appendix

TEMED	tetramethylethylenediamine
TFA	trifluoroacetic acid
TGF-β	transforming growth factor beta
TLC	Thin-layer chromatography
TNF-α	tumor necrosis factor alpha
TNF-R	tumor necrosis factor receptor
Tricin	O-methylated flavone
Tris	tris(hydroxymethyl)aminomethane
TRIzol	guanidinium thiocyanate-phenol-chloroform extraction reagent
Tween 20	polyoxyethylene (20) sorbitan monolaurate (Polysorbate 20)
U87 MG	human gliloblastoma cell line
UC11	human astrocytoma cell line
UV	ultraviolet light or irradiation
VEGF	vascular endothelial growth factor

Curriculum vitae

Personal Data

Name:	Anika Veser
Date of birth:	19.10.1986
Place of birth:	Ravensburg, Germany

Work experience

Since 04/2017	Process Specialist, Sandoz GmbH, Schaftenau, Austria

Scientific education

11/2012 – 12/2016	PhD candidate, Department of Pharmaceutical Technology, University of Regensburg
05/2013 – 08/2012	Reasearch Assistant, Department of Biopolymer Chemistry, Technical University of Munich, Freising/ Weihenstephan
04/2010 – 05/2012	Master of Science in Molecular Biotechnology, Technical University of Munich, Freising/ Weihenstephan
10/2006 – 03/2010	Bachelor of Science in Molecular Biotechnology, Technical University of Munich, Freising/ Weihenstephan

School education

06/ 2006	General qualification for university entrance
09/2003 – 06/2006	Secondary school, Edith-Stein-Schule, Berufliches Gymnasium der dreijährigen Aufbauform mit biotechnologischer Richtung, Ravensburg
09/1997 – 07/2003	Secondary school, Theresia Gerhardinger Realschule, Ravensburg
09/1993 – 07/1997	Primary school, Grundschule St. Christina, Ravensburg

Acknowledgements

An dieser Stelle möchte ich mich herzlich bei allen bedanken, die mich in den letzten Jahren unterstützt und damit maßgeblich zum erfolgreichen Abschluss dieser Arbeit beigetragen haben.

Mein besonderer Dank gilt Herrn Prof. Dr. Achim Göpferich, der diese Arbeit erst ermöglicht hat und mich bei deren Umsetzung unterstützte, insbesondere durch interessante Diskussionen und hilfreiches Feedback. Besonders bedanken möchte ich mich für die gewährten Freiheiten im Laufe meines Forschungsprojektes und für die Möglichkeit die erzielten Ergebnisse auf nationalen und internationalen Konferenzen vorstellen zu dürfen.

Für die Einführung in die Zellkulturarbeit danke ich Frau Renate Liebl ganz herzlich. Auch allen anderen technischen Mitarbeitern und Mitarbeiterinnen des Lehrstuhls danke ich für ihre stetige Hilfsbereitschaft.

Meinen besonderen Dank möchte ich Dr. Robert Hennig aussprechen für die interressanten fachlichen Diskussionen rund um die Themen Calciumassays und Quantenpunkte.

Ein herzlicher Dank gilt natürlich allen aktuellen und ehemaligen Kollegen für die schöne und unvergessliche Zeit am Lehrstuhl. Vorallem danke ich meinen beiden Kollegen Dr. Johanna Lempp und Ali Rami für die nette Atmosphäre im gemeinsamen Labor.

In schöner Erinnerung habe ich die lustigen gemeinsamen Grillabende mit allen Doktoranden und Doktorandinnen des Lehrstuhls und insbesondere die Zeit beim Klettern und Bouldern mit Johanna, Michael, Vanessa und Sebastian.

Natürlich möchte ich auch meiner Familie für ihre stetige Unterstützung und Ermutigung während meines Studiums und der Promotion danken.

Einen herzlichen Dank möchte ich auch Thomas für seine seelische Unterstützung in den letzten Zügen dieser Arbeit aussprechen.